

**Synthesis of Derivatizable Semiconductor
Nanocrystals Through Rational Ligand Design, and
Applications Thereof**

by

José Manuel Cordero Hernández

B.S., Chemistry, University of Puerto Rico, Mayagüez (2009)

Submitted to the Department of Chemistry
in partial fulfillment of the requirements for the degree of

Doctor of Philosophy

at the

MASSACHUSETTS INSTITUTE OF TECHNOLOGY

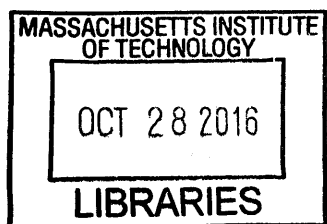
September 2016

© Massachusetts Institute of Technology 2016. All rights reserved.

Author **Signature redacted**
Department of Chemistry
August 9, 2016

Certified by **Signature redacted**
Moungi G. Bawendi
Lester Wolfe Professor of Chemistry
Thesis Supervisor

Accepted by **Signature redacted**
Robert W. Field
Haslam and Dewey Professor of Chemistry



ARCHIVES

Synthesis of Derivatizable Semiconductor Nanocrystals Through Rational Ligand Design, and Applications Thereof

by

José Manuel Cordero Hernández

Submitted to the Department of Chemistry
on August 9, 2016, in partial fulfillment of the
requirements for the degree of
Doctor of Philosophy

Abstract

Over the last decade, the synthesis methods of colloidal nanocrystals have advanced at an astonishing rate, producing particles that are chemically stable, monodisperse, and, in the case of semiconductor quantum dots (QDs), immensely bright. Inorganic nanocrystals linked to functional organic or biological molecules have recently emerged as a new class of nanomaterials for generating highly efficient devices, and sensing agents for a broad range of advanced applications. A key step in the synthesis of these constructs involves transforming the chemistry of the surface from that generated by the nanocrystals synthesis conditions (high boiling-point and hydrophobic solvent environment) to one possessing the appropriate functional groups for derivatization and that is compatible with the intended final application. Here, we describe the synthesis of a series of organic ligands that modify the surface in that manner. The first ligand exhibits a norbornene functional group and binds strongly to the surface of colloidal nanocrystallites during particle synthesis, eliminating the need for ligand exchange and enabling large-scale production of high quality derivatizable nanomaterials. This ligand is compatible with state-of-the-art synthesis methods of a large variety of semiconductor nanocrystallites, including PbS, CdSe/CdS, and InAs/CdSe/CdS core/shell nanoparticles. Applications that make use of the norbornene click-chemistry functionality will be presented, along with efforts to preserve the high quantum yield and colloidal stability in water. We also introduce a bidentate carboxylate-based ligand as part of an effort to enhance the quality of QDs through the chelate effect. This ligand enhances the PLQY at high temperature, as a result of surface-related trap state passivation. Finally, we describe the synthesis of a new functional group for generating derivatizable-QDs that can be easily copolymerized with the polyimidazole ligand (PIL), and that is reactive with tetrazine and, upon thermal activation, with thiols to form stable bioconjugates.

Thesis Supervisor: Mounqi G. Bawendi
Title: Lester Wolfe Professor of Chemistry

This doctoral thesis has been examined by a Committee of the
Department of Chemistry as follows:

Professor Alice Y. Ting
Signature redacted
Chairman, Thesis Committee
Ellen Swallow Richards Professor of Chemistry

Professor Mounji G. Bawendi....
Signature redacted
Thesis Supervisor
Lester Wolfe Professor of Chemistry

Professor Keith A. Nelson....
Signature redacted
Member, Thesis Committee
Haslam and Dewey Professor of Chemistry

Contents

1 The Organic Ligands, and Their Role in the Synthesis and Biological Applications of Quantum Dots	11
1.1 Organic Ligands in QD Synthesis	11
1.2 X-, L-, and Z-Type Ligands	12
1.3 The Ligand Exchange	14
1.4 Water Soluble QDs for Biological Applications	18
1.4.1 Encapsulation	19
1.4.2 Ligand Exchange	21
1.5 QD Bioconjugates for Biological Applications	23
2 The Norbornene Carboxylate Ligand, and the Synthesis of “Click” Ready Quantum Dots	25
2.1 Background and Motivation	25
2.2 Results and Discussion	26
2.2.1 Monodentate Ligand Synthesis and Design	26
2.2.2 Water-Soluble CdSe-CdS: The High Temperature Case	29
2.2.3 Water-Soluble PbS: The Low Reaction Temperature Case	35
2.2.4 The Traditional Ligand Exchange	36
2.2.5 The NB-Bidentate Ligand Synthesis and Design	36
2.3 Conclusion	38
2.4 Chapter-Specific Acknowledgements	38
2.5 Experimental Details	39

2.6	Appendix: ^1H NMR, $^{13}\text{C}\{^1\text{H}\}$ NMR, and DART/FT-MS Spectra of Chemical Compounds	49
3	The Bidentate Carboxylate Ligand: A Strong Grip to Enhance the Photoluminescence Quantum Yield at High Temperature	67
3.1	Background and Motivation	67
3.2	Results and Discussion	68
3.2.1	Quantum Dot Stock Solution	68
3.2.2	Binding Isotherms	68
3.2.3	Fluorescence Lifetimes	76
3.3	Conclusion	80
3.4	Chapter-Specific Acknowledgement	80
3.5	Experimental Details	81
3.6	Appendix I: Tables	84
3.7	Appendix II: ^1H NMR, $^{13}\text{C}\{^1\text{H}\}$ NMR, and DART/FT-MS Spectra of Chemical Compounds	88
4	The Furan Maleimide Adduct: A New Functional Group for the Polymeric Imidazole Ligand	91
4.1	Background and Motivation	91
4.2	Results and Discussion	92
4.2.1	The Furan-Maleimide Adduct Functional Group	92
4.2.2	Synthesis of the BromoFMA Monomer	94
4.2.3	Synthesis and Characterization of the BromoFMA Homopolymer	97
4.2.4	The rDA Reaction Kinetics	98
4.2.5	Derivatization of FMA-coated QDs	99
4.3	Conclusion	106
4.4	Chapter-Specific Acknowledgements	106
4.5	Experimental Details	107
4.6	Appendix I: Tables	112

4.7 Appendix II: ^1H NMR, $^{13}\text{C}\{^1\text{H}\}$ NMR, and DART/FT-MS Spectra of Chemical Compounds	113
---	-----

Chapter 1

The Organic Ligands, and Their Role in the Synthesis and Biological Applications of Quantum Dots

1.1 Organic Ligands in QD Synthesis

High-quality QDs are synthesized at high temperature (typically above 300°C for wurtzite-CdSe), in the presence of hydrophobic coordinating solvents, i.e. trioctylphosphine (TOP), and trioctylphosphine oxide (TOPO), or non-coordinating solvents, i.e. 1-octadecene (ODE), and organic ligands. [1–4] In most cases, the organic ligands are surfactant molecules containing long aliphatic chains, and bearing a phosphonic acid, an amine or a carboxylic acid head group. Apart from providing colloidal stability, the organic ligands play a crucial role during synthesis in controlling the growth kinetics, and defining the shape and size of the final nanocrystals. Nanoparticles resembling rods [3, 5], tetrapods [6], and, more recently, platelets [7] have been successfully synthesized by carefully selecting the appropriate ligand, and controlling its corresponding concentration during synthesis. A study published by Yu and Peng [8], and which now serves as the basis of some of the most commonly used synthesis methods [3, 9], described the effect of ligand concentration on monomer reactivity and the

temporal evolution of nanocrystal size. Their work, using oleic acid (OA) in ODE, demonstrated that the reactivity of “cationic monomers”, which are defined as metal complexes in solution that are not in the form of nanocrystals, increases with decreasing ligand concentration. Thus, the initial ligand concentration can be tuned to control the number of nanocrystal nuclei formed after precursor injection, and, in turn, the final QD size; the number of nuclei formed being inversely proportional to the final size of the nanocrystal.

In addition to influencing the physical characteristics of QDs, organic ligands bound to the surface can alter the electronic and optical properties, and can profoundly affect the PLQY and carrier dynamics of their hosts. [10–17] In part, this effect is the result of interactions between surface electronic states and the organic ligands. Therefore, preparing QDs for biological and device applications usually involves the substitution of their original ligands for others that are engineered to impart new, or enhance existing, physical, optical, or electronic features. [18–20] This process is known as ligand exchange, and will be discussed in section 1.3.

1.2 X-, L-, and Z-Type Ligands

Three different types of ligands have been recognized to bind to the surface of nanocrystals. A short description of each using an extension of the covalent model as developed by M. L. H. Green [21] follows below. [22] Figure 1-1 provides a schematic representation of all three types of ligands, their respective mode of bonding to the surface of QDs, and their reactivity towards ligand exchange.

- **X-Type:** In the covalent model, these ligands are regarded as capable of forming one-electron radical bonds to neutral metal centers. They are anionic species forming normal covalent bonds. Some examples of X-type ligands commonly used to passivate the surface of QDs include alkylphosphonates, alkylcarboxylates, and alkylthiolates. X-type ligands bound to a metal center give rise to a Z-type ligand (*vide infra*).

- **L-Type:** These are neutral ligands, which form two-electron dative covalent bonds. They are generally Lewis bases capable of donating an electron lone pair to a metal center. Some examples of L-type ligands include alkylamines, alkylthiols, alkylphosphines, and alkylphosphine oxides.
- **Z-Type:** These are two-electron acceptor ligands. They are generally Lewis acids containing an empty orbital which accepts the donation of an electron pair from a chalcogen center on the surface. Z-type ligands appear as metal carboxylate, or phosphonate complexes possessing an empty orbital at the metal center. For a divalent metal (M), such as Cd, Zn, and Pb, the ligand takes the form of $M(O_2CR)_2$, or $M(O_2(OH)PR)_2$.

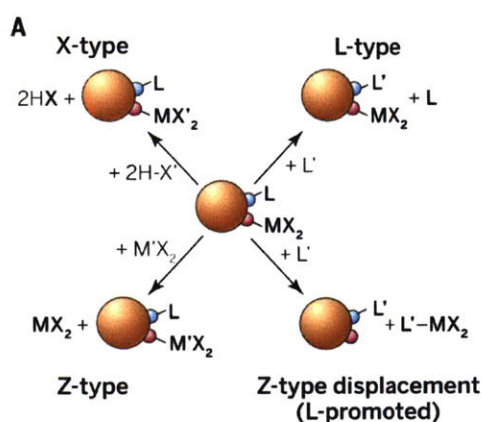
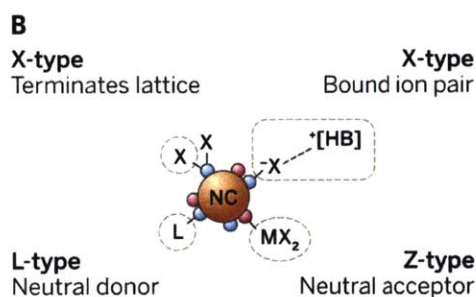


Figure 1-1: (A) Some examples of ligand exchange reactions are shown. (B) A schematic representation of the modes of coordination of all three types of organic ligands to the surface of QDs is presented. R represents an alkyl group, and Bu represents a n-Butyl group. Image reproduced from [23]. Copyright © 2015, American Association for the Advancement of Science



M = Cd, Pb, etc. ●	X = O_2CR , Cl, SR, etc.
E = S, Se ●	L = PR_3 , NH_2R , etc.
MX_2 = $Cd(O_2CR)_2$, $CdCl_2$, $Pb(SCN)_2$, etc.	
$[X]^- [HB]^+$ = $[Cl]^- [HPBu_3]^+$, $[S]^{2-} 2[H_4N]^+$, $[In_2Se_4]^{2-} 2[N_2H_5]^+$, etc.	

1.3 The Ligand Exchange

The last 20 years have witnessed the development of new, and refined synthesis methods that produce QDs with superb physical, and optical properties. A good example is found in a report from Chen, et al. [4] from our group, that described the synthesis of CdSe-CdS (core-shell) nanocrystals exhibiting suppressed blinking behavior, and ensemble fluorescent linewidths approaching those of single particle emitters; an indication of perfect control over the particle growth kinetics. Scientific advancements, such as this one, have transformed the nanocrystal synthesis field, but as nanoparticles of increasingly higher quality are sought for ever more complex applications, new research on the chemistry of ligand coordination is expected to be a fresh source of innovation in nanotechnology. [23] A summary of some of the work that have shed new light into the chemical behavior of ligands, their role in improving the optical and electronic features of nanocrystals, and the dynamics of ligand exchange is presented below.

Until now, most of the work aimed at understanding the interactions between organic ligands and nanocrystals utilize CdSe cores as the host material. [24–28] Considering that CdSe-CdS core-shell nanostructures are the material-of-choice for the two main applications of QDs: lighting of electronic displays, and labelling of biological systems —both of which have successfully taken products into the market— a study focused on cores alone may seem too simplistic. In reality, there are two good reasons in favor of this selection. The first is a historical reason. That is, high quality CdSe cores have been studied for longer time, and in greater detail than any other nanoparticle system, which makes possible the unambiguous characterization of the effects of ligand exchange and ligand coverage on the properties of QDs. The second, and more relevant reason, is that high-quality zincblende-CdSe can be prepared in ODE, and in the presence of carboxylic acids (i.e. OA or myristic acid) as the one and only organic ligand, which offers a clean, and controllable system for the study of X-type interactions, or others, after ligand exchange.

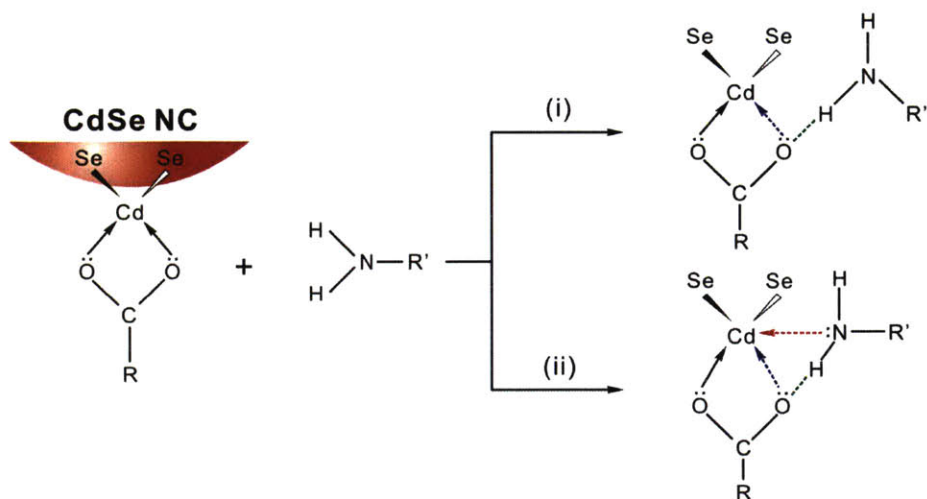
Nanocrystals passivated with X-type ligands are necessarily cadmium enriched.

Elemental analysis have repeatedly demonstrated that they exhibit a non-stoichiometric—that is to say, a greater than one— cadmium-to-selenium (Cd:Se) ratio, which suggests that at least some of the crystal facets terminate in Cd ions, and form coordination complexes with negatively charged ligands (i.e. X-type, ionic model). [25, 26] Nevertheless, it is important to point out that the level of cation enrichment can vary with synthesis and purification methods, [29] and that the size of the nanocrystal can alter the surface-area-to-volume ratio, and, consequently, the fraction of Cd ions at the surface. X-type ligand exchange has been shown to be a process that is dependent on the relative binding affinity of the ligands involved. Recently, Fritzing, et al. [26] reported that isolated samples of zincblende-CdSe QDs coated with alkylcarboxylate groups, and devoid of excess organic ligands show no evidence of adsorption/desorption dynamics, for neither X- (oleate), or Z-type (cadmium oleate) ligands. However, when excess OA was added in solution, self-exchange occurred rapidly, and reached equilibrium at room temperature. These results suggest that Coulomb interactions keep X-type ligands tightly bound to the surface, and that the ligand exchange process must conserve charge-balance in order to take place; in this particular example, involving a proton transfer event. In a similar report, Owen, et al. [24] utilized chlorotrimethylsilane, and bis(trimethylsilyl)selenide to exchange the original alkylphosphonate ligands in wurtzite-CdSe for chloride, and selenide atoms, respectively. This exchange produced *O,O'*-bis(trimethylsilyl)alkylphosphonic acid, and nanocrystals that precipitate out of solution. Additionally, work published by Gomes, et al. [30] using wurtzite-CdSe showed that OA is incapable of replacing alkylphosphonate groups under normal conditions. Instead, partial exchange occurs only after heating to 100°C for prolonged periods of time, which suggests that alkylphosphonate ligands bind more strongly to Cd ions than their carboxylate counterparts.

An altogether different story unfolds for the L-type ligands, which exhibit very fast adsorption/desorption dynamics. Here, NMR spectroscopy has been unable to distinguish between the ligands bound to the surface and those that are free in solution [31], in sharp contrast to the behavior of X-type ligands, which appear to bind more strongly to QDs. As shown in figure 3-2, and elsewhere [26, 28], nanocrystals

coated with oleate groups display two different peaks in the vinyl region, corresponding to the bound (oleate) and unbound (OA) ligands. This difference in binding dynamics between the X and L, is routinely employed in the purification of wurtzite-CdSe cores that are synthesized in a mixture of alkylphosphonic acids, TOP, and TOPO; resulting in nanoparticles that are exclusively passivated by alkylphosphonate groups (X-type). [25] X-, and L-type ligands have been shown to bind jointly, and to coexist on the surface of nanocrystals, with important consequences for the PLQY. Primary amines, such as oleyl amine (OAm), are the most frequently studied L-type ligand in QD systems, and their influence on the optical properties of nanocrystals is well characterized. At low concentrations, primary amines quench the PLQY of zincblende-CdSe cores. [27, 28] The current model suggests that this is the result of Z-type ligand destabilization, as shown in scheme 1.1. [27] Upon coordination, the amine donates electron density to the Z-ligand as a whole, which in turn, decreases the oxidation state of the metal center. Theoretical studies on PbS QDs, show that the adsorption of “metallic” Pb^0 to the surface of nanocrystals introduces filled electronic states within the band gap, but that these states are removed when the same atoms are converted to Pb^{2+} , and coordinated by X-type ligands (MX_2 , Z-type) [32] Similarly, our own work shows that mid-bandgap states resulting from ligand exchange procedures are directly linked to the formation of Pb^0 sites, and that this states can be removed by oxidizing the Pb atoms with benzoquinone. [33] Together, these results suggest that the empty orbitals in Z-type ligands play a crucial role in the passivation of chalcogen-derived filled electronic states on the surface of QDs. However, at elevated temperature, or increased ligand concentration, primary amines enhance the PLQY of zincblende-CdSe QDs, as they efficiently remove the cadmium oleate (MX_2) from the surface, and reduce the cadmium-to-selenium ratio to approximately one [27, 28]. Anderson et al. [28] studied the PLQY of nanocrystals after ligand exchange with various amine-containing ligands (including 1°, 2°, 3°, and aromatic amines), and showed that, although all amines were able to remove cadmium oleate from the surface, only primary amines improved the original PLQY. The same work also found that, in general, the PLQY is proportional to the number

of Z-ligands bound to the surface (surface coverage), but that this relationship is not linear, and exhibits a threshold ($\sim 3 \text{ MX}_2$ per nm^2), below which the PLQY drops rapidly to $\leq 2\%$.



Scheme 1.1: Some of the possible surface configurations in zincblende-CdSe nanocrystals after the adsorption of primary amines are shown. Configuration **ii** is expected to introduce the highest amount of electron density into the metal center. Image reproduced from [27]. Copyright © 2011, American Chemical Society.

In summary, alkylcarboxylate, and alkylphosphonate groups are the main organic ligands covering the surface of as-synthesized zincblende-, and wurtzite-CdSe QDs, respectively. The binding of primary amines to nanocrystals is a complex process. At low concentration it resembles physisorption. At high concentration, however, it enhances ligand exchange, and releases cadmium carboxylate or cadmium phosphonate from the surface. Thiols (e.g. cysteine, $-\text{SH}$ $\text{pK}_a = \sim 8.4$) bind as L-type ligands but, in the presence of a base, they bind as thiolates (X-type). [24] Finally, our own work, as will be revealed in chapters 2 and 3, and that of others, has shown that the principles described here may be extended to other nanocrystal systems, including the CdSe-CdS core-shell QDs. [28, 34]

1.4 Water Soluble QDs for Biological Applications

QDs are bright inorganic fluorophores with emission tunable from the visible to the near-infrared (NIR) regions of the spectrum. [1, 4, 35] In recent years, they have emerged as powerful tools for advanced biological imaging. Their unique optical and physical properties have enabled the study of living systems in ways that were previously difficult using conventional organic fluorophores. [18, 19, 36] QDs emitting in the visible have narrow fluorescence spectra, and PLQY in excess of 75%. Their excitation band is broad, but their emission band is narrow and symmetric. A size series of QDs can cover a wide range of emission wavelengths and be excited with the same light source—an ideal feature for multiplexed tracking studies. [19] Additionally, their two-photon absorption cross-section is up to three orders of magnitude higher than those of conventional fluorescent dyes. [37] This means that QD probes are particularly well suited to *in vivo* and *intravital* deep tissue imaging using two-photon fluorescent microscopy. [38] Furthermore, their emission wavelength can be easily tuned to match the NIR transparent windows, where there is minimal absorbance from blood, tissue, and water, (i.e. NIR-I 0.75-0.9 μm and NIR-II 1.1-1.4 μm). QDs emitting in the NIR have been used to extend the penetration depth of *intravital* microscopy, and to image large anatomical structures in animals through their skin. [39, 40] Finally, QDs are exceptionally stable towards sustained irradiation over long periods of time and high excitation fluences, when compared to organic fluorescent dyes, which photo-bleach rapidly and are susceptible to oxidative degradation. [36, 41] As a result, QDs have been successfully employed to study the motion of single receptors and other transport processes in cells. [42–45] Moreover, well-passivated QDs have been shown to be sufficiently stable during *in vivo* experiments for their emission to be detected on time scales of days or even months. [42, 46]

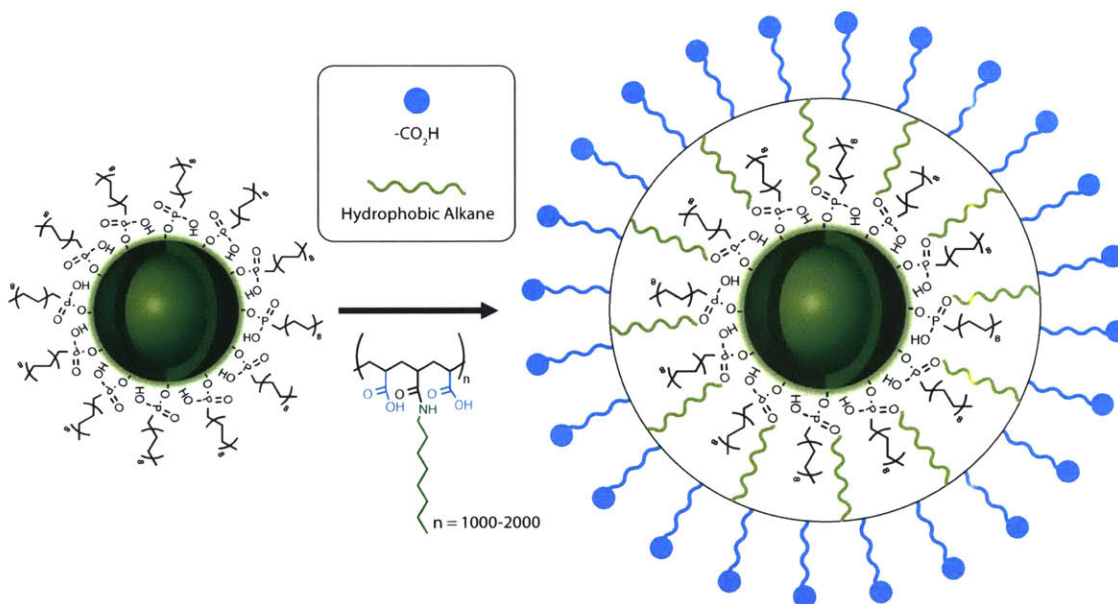
Over the years, many different strategies have been developed to transform the as-synthesized QDs into useful probes for biological applications. At the center of these transformations, there is always a new—or, sometimes, a slightly improved—organic coating that has been designed to adhere to the surface of QDs and to provide water

solubility. [19] This organic coating must also display several key features, so as to produce QD probes that are suitable for biological applications. First, the organic coating must be compact, in order to maintain the small size of the nanocrystal. Second, it must not interact with the electronic structure of the QD, so that the PLQY is preserved. Third, it must minimize non-specific binding. In this respect, organic coatings that are positively charged, which are known to bind non-discriminately to the surface of cells, should be avoided. [47] Fourth, it must exhibit functional groups for facile derivatization. Well-passivated QDs are biologically inert. Thus, for some of the most complex applications they rely on biologically active molecules to do the targeting or the sensing. [18,48] For example, immunoglobulin G (IgG), an antibody whose hydrodynamic diameter ($HD = \sim 11\text{nm}$) is comparable to that of QDs, is the most commonly used molecule for biological targeting. Nanocrystals that have been chemically attached to IgG act as bright fluorescent labels that can be used to pinpoint the location of molecules of interest, usually cell-surface receptors, *in vitro* and *in vivo*. [41,49] A long list of organic coatings that fulfill the aforementioned requirements have been synthesized and reported, each with a particular set of strengths and weaknesses. They can be effectively divided into two groups based on their mode of binding: encapsulation, and ligand exchange. A quick overview of these groups, and their constituents follows below.

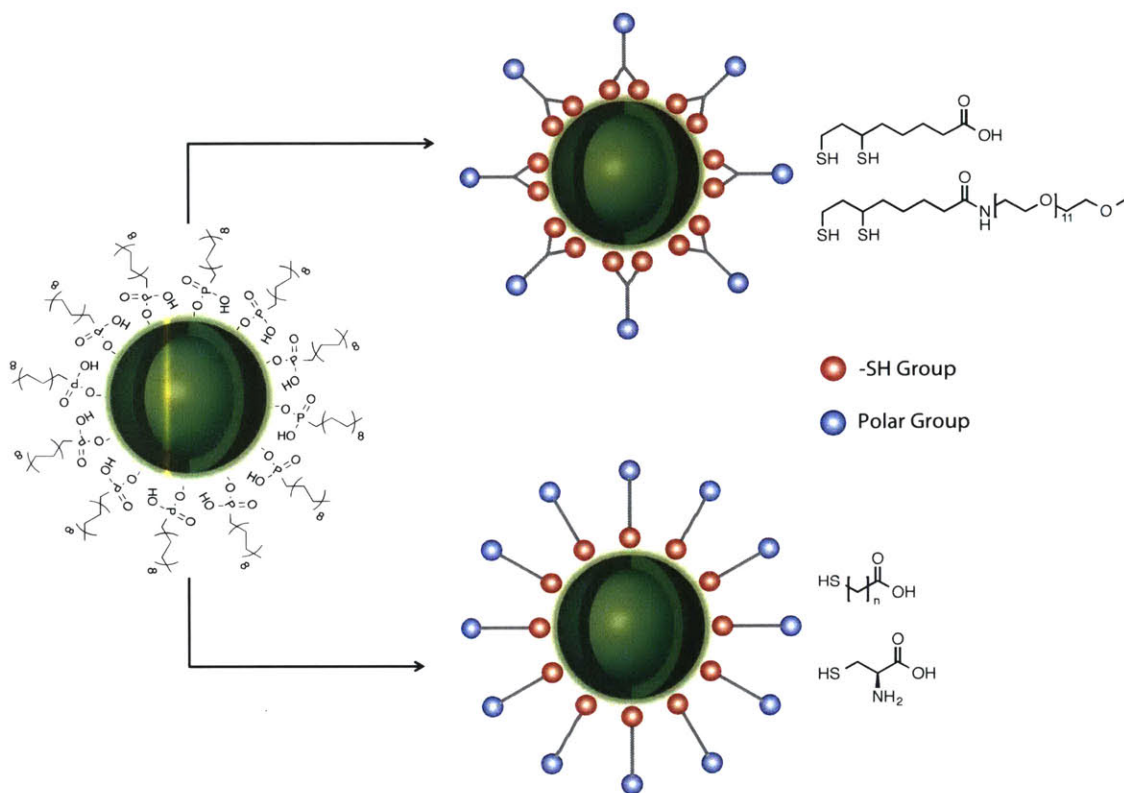
1.4.1 Encapsulation

Amphiphilic polymers are a common type of organic coating based on partially modified polyacrylic acid, presenting long hydrophobic alkyl side chains and negatively charged carboxylate groups. [19,41,42] The hydrophobic effect and van der Waals interactions between the alkyl residues of the polymer and the native ligands on the surface of the QD drive a self-assembly process that encapsulates the nanocrystal. The charged groups in the polymer are then left exposed, which provides water solubility. Scheme 1.2 depicts the encapsulation process, and the final structure of water-soluble QDs that is achieved through this method. Encapsulated QDs are highly stable in water and, because the amphiphilic coating does not perturb the inorganic surface

atoms, the optical properties are also well preserved. However, the size of these constructs is typically large ($HD = \sim 20\text{-}30\text{nm}$), and hinders their utility for biological applications. Probes of this size, especially when conjugated to large biomolecules, such as IgG, have been shown to alter the diffusion of labelled proteins and to impair the normal traffic of cell-surface receptors. [42] Furthermore, heavily charged QDs, like those generated using this technique, exhibit a high level of non-specific binding that results from electrostatic interactions between the polymer and charged surfaces already present in the cellular environment. Non-specific binding increases the amount of background noise, which decreases image quality. Incorporating PEG groups (PEGylation) into the organic coating have been shown to reduce non-specific binding but it adds to the size of an already large construct. [50]



Scheme 1.2: The synthesis of water-soluble QDs using amphiphilic polymers and nanocrystal encapsulation. Image adapted from the thesis of Wenhao Liu. Copyright © 2010, Massachusetts Institute of Technology.



Scheme 1.3: The synthesis of water-soluble QDs using thiol-containing molecules and ligand exchange. Image adapted from the thesis of Wenhao Liu. Copyright © 2010, Massachusetts Institute of Technology.

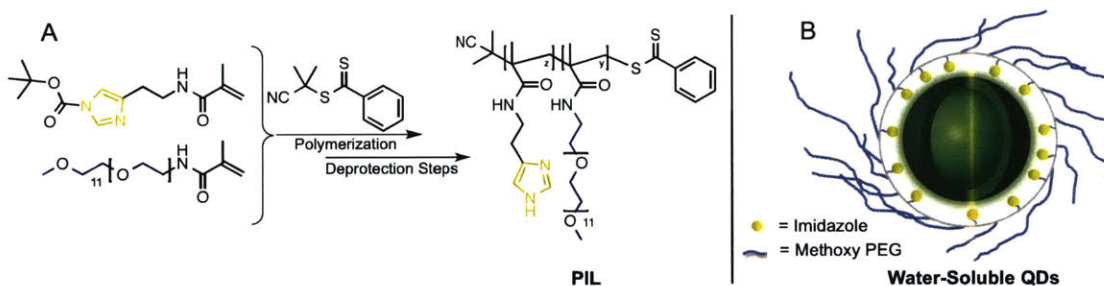
1.4.2 Ligand Exchange

The Thiol Ligands

Compact biocompatible QDs can be prepared by substituting the native hydrophobic ligands with molecules containing both a hydrophilic and a surface-anchoring moiety. Thiol groups are known to form strong complexes with metals, which they bind as either L-type or X-type ligands. [21, 22] The cysteine molecule is arguably one of the simplest and most extensively used thiol-containing ligands. In nature, it is an integral part of several metal-binding protein motifs, where it has been shown to bind to metals such as, Cu, Zn and Cd, among many others. As an organic ligand for QDs, it displays a single thiol for binding to the surface and a zwitterionic amino-acid group for water solubility. QDs with HD below 5nm can be synthesized using cysteine

as the organic coating. These nanocrystals are sufficiently tiny to effectively enter the renal system of rats and exit the body as urine. [51] Unfortunately, QDs coated with thiol-containing ligands are not stable, as this functional group is susceptible to oxidation. [52] The oxidation product is usually a dimer containing a disulfide bond, which lacks the capacity to form complexes with metals. Although freshly prepared samples can be used for some biological applications, these QD constructs are not suitable for experiments lasting long periods of time, as they slowly aggregate. Organic molecules possessing two thiol residues in close proximity to each other have been synthesized to improve the stability of water-soluble QDs through the chelate effect. Some commonly used bidentate ligands are dihydrolipoic acid (DHLLA) and PEGylated DHLLA, both of which are considered to be a significant improvement over single-thiol coatings. [48, 53–56] Recent studies, however, have demonstrated that DHLLA-coated QDs continue to exhibit signs of degradation during storage under dark and refrigerated conditions, which limits their utility for complex biological applications. [47] A schematic representation of the ligand exchange process and some examples of thiol-based ligands are shown in scheme 1.3.

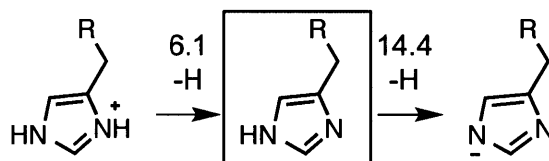
The Poly-Imidazole Ligands



Scheme 1.4: (A) The synthesis of PIL through RAFT polymerization. (B) A schematic representation of PIL-coated QDs.

More recently, our laboratory has developed the poly-imidazole ligand (PIL) coating, a random polyacrylamide graft copolymer containing multiple imidazole groups for surface binding and PEG domains for water solubility. [47] Scheme 1.4 shows the

structure of the polymer and a representation of the final QD construct. On average, each polymer exhibits between seven and ten imidazole groups, whose collective action results in highly stable water-soluble constructs. As shown in scheme 1.5 the imidazole group binds the surface of QDs as a neutral L-type aromatic amine ligand. The size of water-soluble QDs coated with PIL is usually small (HD = 10-15nm)—a desirable feature for tracking studies. The polymeric nature of PIL is modular, which means that the polymer structure can be tailored to the specific needs of each particular biological application. New monomers with extra features can be inserted into the backbone of the polymer with relative ease and then linked to the QD after ligand exchange. For example, monomers containing functional groups, such as primary amines and biotin, have been successfully added to PIL to make derivatizable QDs. QD-Bioconjugates have been successfully prepared using these functionalities and have been used for imaging of cells, both *in vivo* and *in vitro*. [49, 57–59] In 4, we introduce a monomer with a new functional group for derivatization that can be activated to expose one of two possible distinct chemical states, each capable of performing a unique set of reactions reactions that are orthogonal to the other’s. Thus, the same monomer can be used to couple two distinct families of molecules to the QD depending on the final state of the monomer.

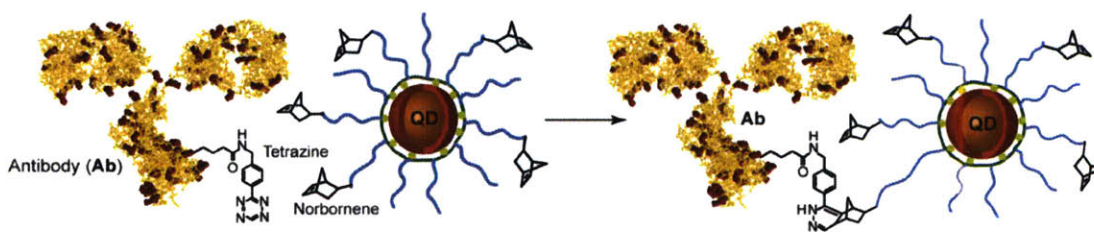


Scheme 1.5: The different ionization states of the histidine side-chain. The equilibrium constants are noted in pK_a values for each of the reactions. In biologically relevant media, the imidazole group binds the surface of the nanocrystal as a neutral, L-type, ligand (middle structure) through the sp^2 nitrogen in position 3

1.5 QD Bioconjugates for Biological Applications

As already mentioned in the previous section, intrinsically insensitive nanocrystals can be converted into targeting agents with the aid of antibodies with known affinities

for specific cell-surface receptors. Additionally, QD can be transformed into powerful sensors by covalently attaching environmentally responsive dyes to their surface. In this way, a large number of different analytes have been detected both *in vitro* and *in vivo*, including pH [58, 60–62], O₂ concentration [62–64], and glucose concentration [62]. Traditionally, QD-bioconjugates were prepared using amide coupling, which resulted in low reaction yields and positively charged QDs—a by-product of unreacted amine functional groups on the surface. In recent years, new synthesis techniques have been developed to solve this problem. “Click” chemistry represents a series of new biocompatible coupling reactions that are highly efficient and proceed at very rapid rates. [65–67] As an example, scheme 1.6 shows the “click” reaction between norbornene (NB) functionalized QDs and tetrazine (Tz) functionalized antibodies, which was used to synthesize IgG-QD complexes, which were later successfully employed to locate hematopoietic stem cells within their native environment (the bone marrow) *in vivo*. [59]



Scheme 1.6: The synthesis of QD-antibody probes using the “click” reaction between tetrazine-functionalized IgG and norbornene-coated QDs. Image reproduced from [49]

Chapter 2

The Norbornene Carboxylate Ligand, and the Synthesis of “Click” Ready Quantum Dots

2.1 Background and Motivation

The last several years have witnessed tremendous progress in our understanding of the synthesis of high-quality colloidal nanocrystals. This has led to new and refined methods for making QDs with better physical, optical and electronic properties for applications in biological imaging, photovoltaic systems and light emitting devices. Nanocrystals of different sizes and shapes are now easier to produce—in many cases, revealing unique features that depend on the dimensionality of these structures. Additionally, the number of new chemical species reaching the nanoscale grows each year—adding to a large and constantly expanding library of nanomaterials. Despite all these advances, only a very small subset of nanoparticles, namely spherical CdSe-CdS, InAs-CdSe, and CdSe-Cd_xZn_{1-x}S, can be consistently prepared to meet the requirements for biological applications. As mentioned in Section 1.4, the main challenge lies in substituting the native organic ligands for water-soluble coatings without disrupting the critical features that make QDs useful in the first place, which include

their small size and high PLQY. Furthermore, this ligand exchange often affects the electronic structure of QDs in negative ways, as previously discussed in Section 1.3. Thus, it is not surprising that, for the most part, this process has been limited to Type I core-shell structures like those mentioned above, which confine the exciton to the core and away from surface-related electronic trap states, thereby reducing the amount of fluorescent quenching. Many nanomaterials with superb characteristics, including PbS QDs, cannot form reliable Type I structures, and consequently, their utility has been limited to applications in the solid state. A new process capable of producing water-soluble and derivatizable QDs without ligand exchange is expected to radically expand the number of nanocrystal probes available for biology and unlock new applications.

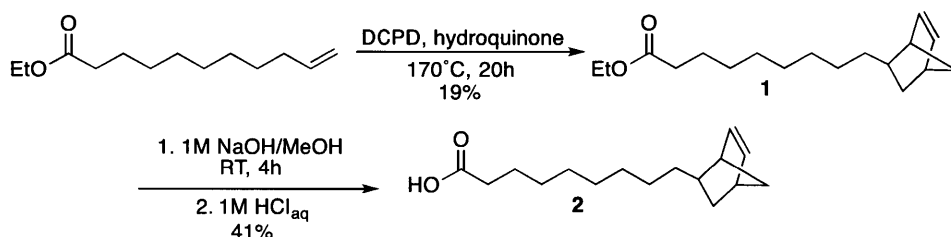
This chapter describes such a method using a new organic ligand that binds effectively to the surface of QDs during synthesis, and which also exhibits a functional group for facile derivatization. The resulting organic coating can then be PEGylated using “click” chemistry to render the nanoparticles soluble in water.

2.2 Results and Discussion

2.2.1 Monodentate Ligand Synthesis and Design

As mentioned in Section 1.3, OA forms strong coordination complexes with cations on the surface of QDs that withstand the purification and dilution steps following synthesis. Moreover, OA is commonly used to generate metal precursors for QD synthesis (e.g. cadmium oleate), which are safer alternatives to many pyrophoric organometallic compounds. Hence, in our effort to eliminate the ligand exchange process, we chose to develop a ligand with many of the chemical attributes of OA, and in particular, a ligand that is capable of binding to QDs during synthesis. This new ligand possesses a carboxylic acid group for surface-anchoring and a norbornene moiety for derivatization. The latter functional group was selected based on its very high specificity towards tetrazine with few potential side-reactions, as previously dis-

cussed in Section 1.5. Additionally, its utility in QD systems has been already tested, as described in a report from Han *et al.* in which IgG antibodies are successfully conjugated to CdSe-CdS after ligand exchange with a norbornene-containing water-soluble polymer. The norbornene group, a hydrophobic cyclic aliphatic compound, is also compatible with the organic solvents used during synthesis. Scheme 2.1 describes the strategy that was used to prepare this new ligand, hereinafter referred to as the NB-Monodentate ligand.



Scheme 2.1: The synthesis of the NB-Monodentate ligand (**2**).

Apart from being able to bind to the surface, an effective synthesis ligand must also tolerate the high reaction temperatures used to make QDs. We used ^1H NMR spectroscopy to measure the thermostability of the NB-Monodentate ligand and to characterize the main chemical pathways leading to its thermal decomposition. As shown in Figure 2-1, the NB-Monodentate ligand is stable up to 200°C , but beyond that point, the norbornene moiety undergoes a retro-Diels-Alder reaction decomposing into the starting materials (i.e. 10-undecenoic acid and cyclopentadiene). Thus, it follows that the maximum temperature compatible with the ligand falls short of that required for the synthesis of some of the most important and commonly used nanocrystals, including CdSe (360°C). In order to make the ligand accessible to QDs with high reaction temperatures, we have developed two strategies for functionalization. The first, for syntheses with reaction temperatures below 200°C , as is the case for PbS, [9,68,69] and perovskites nanocrystals, [70–74], the NB-Monodentate ligand can be simply added as a substitute for OA, without altering the overall synthetic procedure. The second, for reaction temperatures that exceed 200°C , the NB-Monodentate ligand is added to the growth solution as a final step during synthesis once the tem-

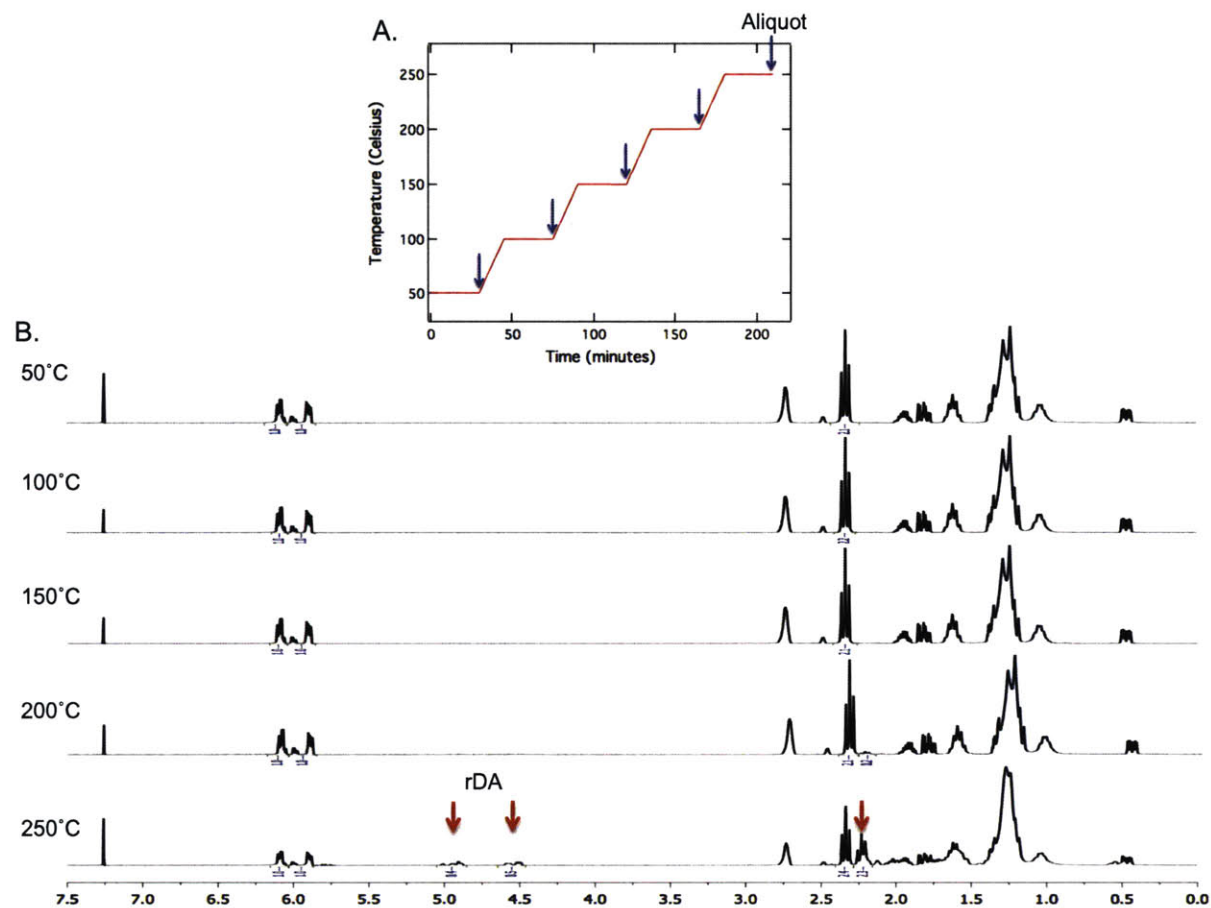


Figure 2-1: (A) A graphical representation of the heating ramp used to measure the thermostability of the NB-Monodentate ligand. (B) The ^1H NMR spectra of NB-monodentate. Each spectrum corresponds to an aliquot that was incubated up to a particular temperature, as shown in the *top* panel. Signs of the retro-DA reaction start to become evident at temperatures above 200°C.

perature reaches 200°C or less during the cool-down stage. A detailed description of these methods is included in section 2.5.

2.2.2 Water-Soluble CdSe-CdS: The High Temperature Case

The NB-Monodentate Ligand Binding

As mentioned above, one of the strategies for obtaining derivatizable nanocrystals involves the addition of NB-Monodentate to the growth solution during synthesis, where it competes with the native ligands for binding until the system reaches equilibrium. Our ability to design an effective and reliable method for functionalization relies on our understanding of the conditions that drive this exchange reaction to completion. We focused our efforts on studying the extent of the NB-Monodentate binding to CdSe-CdS QDs after incubating at various temperatures and immediately after the CdS shell growth. We used ^1H NMR spectroscopy to characterize the ligands bound to the surface and determine the degree of functionalization on QD samples that have been purified using tangential flow filtration. As shown in figure 2-2, the amount of NB-Monodentate ligand on the QD, expressed as a fraction of the total number of carboxylate ligands on the surface, reaches equilibrium—that is to say, the ratio of NB-Monodentate to OA on the surface matches the ratio in solution—when the new ligand is added at 100°C or a higher temperature and is allowed to react for one hour. We also noticed that the binding of the NB-Monodentate ligand is favored over that of OA at high temperatures, as indicated by a surface ligand ratio of NB-Monodentate to OA that is higher than that in solution. We believe that this is due to a tighter packing and, thus, a higher level of self-attraction between NB-Monodentate as compared to OA, whose *cis* configuration limits its ability to form dense structures. Using these results as guidelines, we developed a method to functionalize QDs with high reaction temperatures that employs an incubation temperature of 150°C for one hour and can be used to prepare water-soluble CdSe-CdS, as will be discussed below. A complete description of this method can also be found in section 2.5. Finally, we found that adding the NB-Monodentate ligand to the growth solution does not alter

the size, the shape, nor the size-distribution of the QDs obtained after synthesis, as shown in figure 2-3.

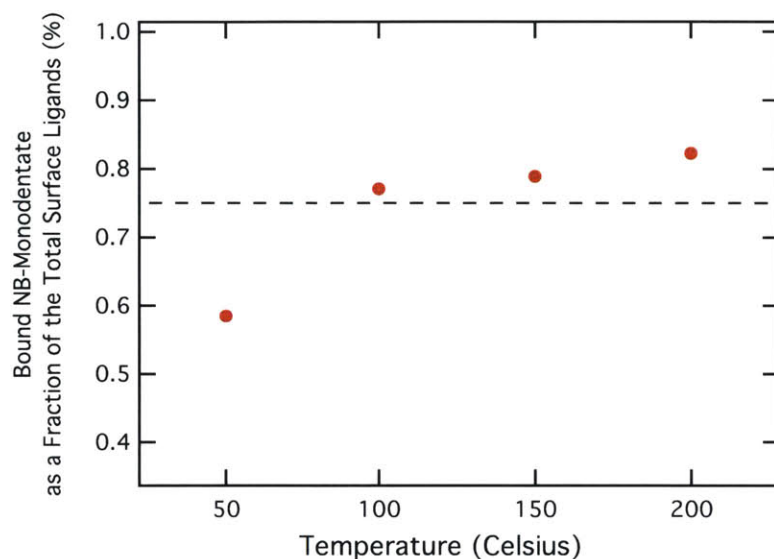


Figure 2-2: The total number of NB-Monodentate ligands bound to QDs as a fraction of the total carboxylate ligands on the surface after incubation for 1 hour at various temperatures. The dash line (- -) represents the fraction in solution, which is equivalent to a NB-Monodentate to OA ratio of 3:1.

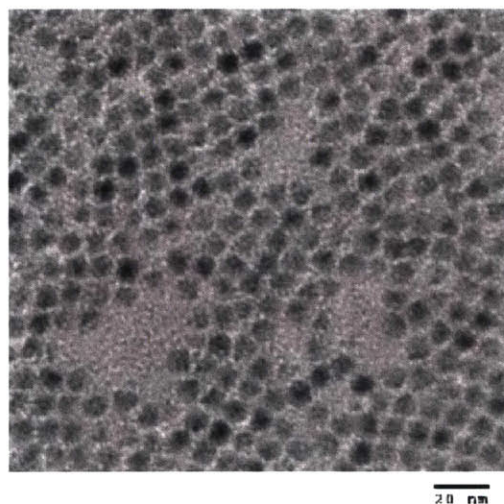
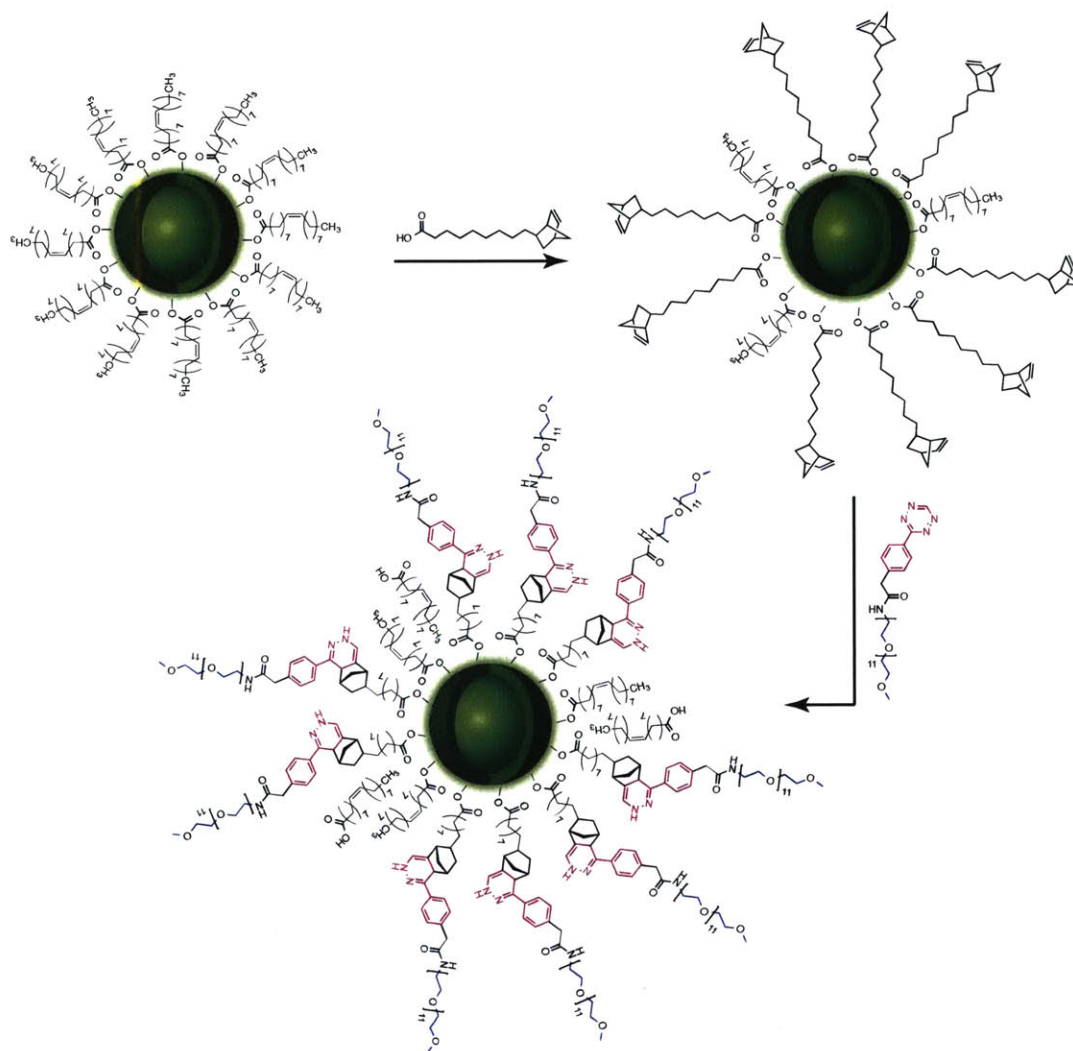


Figure 2-3: TEM image of QDs coated with the NB-Monodentate ligand showing spherical nanoparticles with low polydispersity and no signs of aggregation. The sample was drop-casted onto a copper grid from a solution in hexanes.

Water Solubilization and Characterization of Hydrophilic QDs

Water-soluble CdSe-CdS QDs were prepared by derivatizing the NB-Monodentate-coated surface with PEG₅₀₀ using the tetrazine-norbornene “click” reaction. A schematic representation of this process is presented in scheme 2.2. The QDs were transferred into water using a modified procedure based on the work of Liu *et al.* [47].



Scheme 2.2: The synthesis of water-soluble QDs using the NB-Monodentate ligand and Tz-PEG. In the first step, NB-Monodentate binds to the surface of QDs during synthesis. In the second step, Tetrazine-PEG reacts with the organic coating to produce hydrophilic QDs.

Figure 2-4 displays the absorption and emission spectra of a representative QD sample coated with NB-Monodentate, before and after reacting with Tetrazine-PEG (Tz-PEG) and dispersing in water. The absorption spectra show no significant differences between the two samples, but the emission intensity decreases when the QDs are transferred into water. We found that, on average, the QDs in water retain 70% of their original PLQY (typically $\geq 90\%$ in hexanes), and achieve stupendous levels of brightness on par with the best ligand exchange techniques to date. Unlike other ligand exchange procedures, however, our method does not remove the hydrophobic coatings that result from synthesis. Instead, it builds upon them, endowing the nanocrystals with new and desirable characteristics, including hydrophilicity, as we have demonstrated here. Additionally, figure 2-4B shows that the final constructs exhibit a hydrodynamic size that is compact. Moreover, using the results from DLS and those collected using TEM, we estimate that the organic coating contributes four nanometers, on average, to the total hydrodynamic diameter.

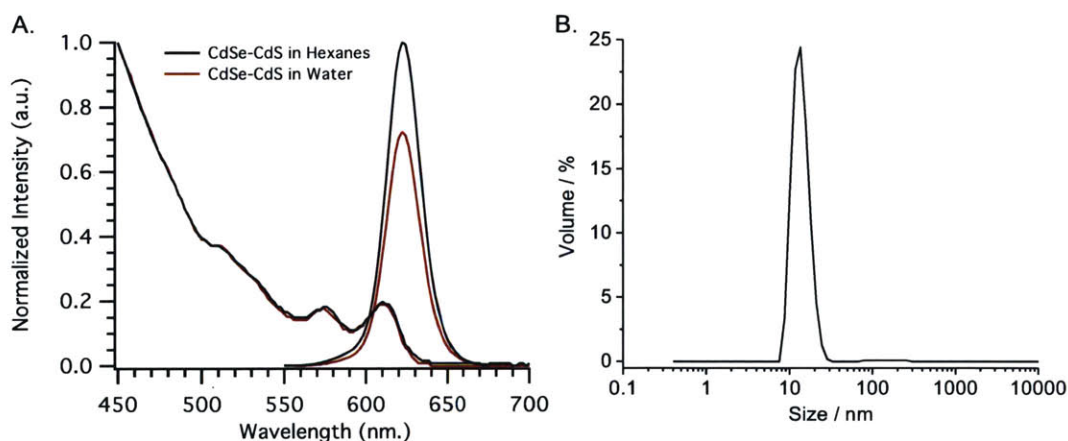


Figure 2-4: (A) Absorption and emission spectra of NB-Monodentate-coated CdSe-CdS QDs in hexanes (black) and in water (red). Water-soluble QDs were prepared by coupling Tz-PEG₅₀₀ to their surface. The PLQY decreases slightly after moving from an organic to an aqueous media. (B) Representative dynamic light scattering histogram of water-soluble NB-coated QDs with sizes averaging 11nm in HD.

Finally, we examined the stability of QDs in aqueous solutions with different pHs. As shown in figure 2-5, the QDs appear to be stable at neutral pHs, however, at high

concentrations of hydrogen or hydroxide ions the PLQY falls rapidly in response to a less passivated surface.

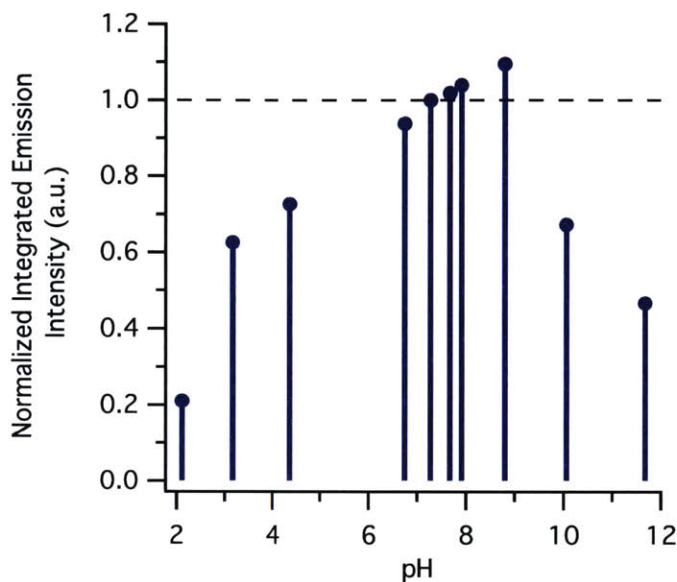


Figure 2-5: Stability of the NB-Monodentate-coated QDs in aqueous solutions at different pHs after incubation at RT for 4 hours. The graph shows that the QDs are stable at neutral and biologically relevant pHs.

Ligand Exchange of OA- Vs. Phosphonic Acid-Coated QDs

The CdS inorganic shell described above was synthesized following a procedure described by Chen *et al.* [4], which utilizes OA as the main surface ligand. Under those conditions, the NB-Monodentate binds effectively to the surface of QDs through a ligand exchange process between identical functional groups ($R-COO^-$). We wanted to test whether the NB-Monodentate ligand would also be effective at functionalizing QDs whose surfaces were not covered with OA. We prepared a water-soluble CdSe-CdS QD sample using the aforementioned procedure (**A**) and compared it against a similar sample derived from a more traditional synthesis method [55], which employs *n*-hexylphosphonic acid as the principal surface ligand (**B**). In both cases, an equivalent amount of NB-Monodentate was added to the growth solution and allowed to react for one hour. As shown in figure 2-6, however, after conjugating Tz-PEG to the

QDs, only **A** was capable of producing QDs that were stable in water. These results suggest that the exchange does not work to the same extent in QDs coated with phosphonic acids as it does in QDs with OA—without sufficient NB-Monodentate ligand on the surface the PEGylation step does not yield nanoparticles that are soluble in water. We believe that this is yet another example of a general trend that was first recognized by Gomes *et al.* [30], which declares that alkylphosphonate groups bind more strongly to Cd ions on the surface than their alkylcarboxylate counterparts, as previously discussed in section 1.3. It follows that the NB-Monodentate ligand is only suitable for QDs that have been prepared using alkylcarboxylates as the sole X-type ligand during synthesis. Fortunately, the recent discovery of new metal-carboxylate-based precursors has led to an explosion in the number of methods that utilize alkylcarboxylate ligands, to the point that today they are the most commonly used surface coatings in the field.



Figure 2-6: A photograph of two NB-Monodentate-coated CdSe-CdS samples under UV-illumination displaying different levels of stability in water; each of them represents a particular CdS shell synthesis method. (A) Stable CdSe-CdS QDs derived from a method described by Chen *et al.* [4] and using OA as the main surface ligand. (B) Aggregated CdSe-CdS QDs derived from a method described by Liu *et al.* [55] and using *n*-hexylphosphonic acid as the main surface ligand.

2.2.3 Water-Soluble PbS: The Low Reaction Temperature Case

The NB-Monodentate ligand is particularly suited for nanocrystal syntheses with reaction temperatures below 200°C, where it is thermostable. In this regime, derivatizable QDs can be prepared simply by including the NB-Monodentate ligand during the synthetic procedure, as a direct substitute for OA. We employed this method to generate bright water-soluble PbS QDs emitting in the NIR and exhibiting PLQY values that were comparable to those encountered in water-soluble InAs-CdSe-CdS QDs. Figure 2-7 shows the absorption and emission spectra of two representative PbS samples of different sizes, before and after dispersing in water. The data demonstrates that the water solubilization process keeps the main optical features in the spectra mostly intact. As discussed in sections 2.1 and 1.3, high-quality water-soluble PbS QDs are difficult to obtain using the traditional ligand exchange approach, which alters the chemistry of the surface and introduces surface-related trap states. We believe that this method succeeds where others have failed due to its unique ability to generate a functional ligand coating, while maintaining the chemical structure of the surface unchanged.

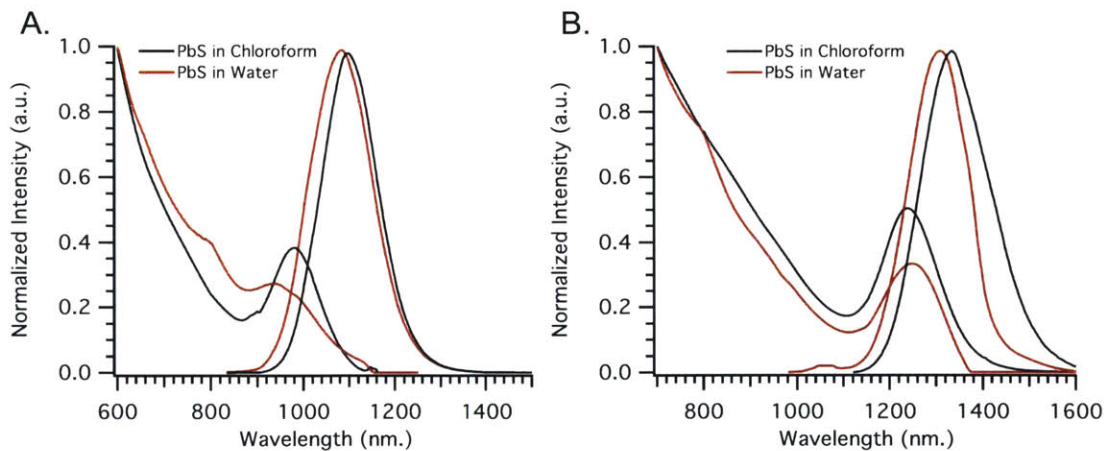


Figure 2-7: Absorption and emission spectra of two different NB-Monodentate-coated PbS QDs samples in chloroform (black) and in water (red). (A) PbS sample with emission peak (λ_{\max}) at 1074nm and PLQY of 15% in water. (B) PbS sample with emission peak (λ_{\max}) at 1309nm and PLQY of 6% in water.

Another example that illustrates the utility of this method involves the synthesis

of CsPbBr₃ perovskite QDs. Here, the metal-carboxylate-based precursor, cesium oleate, was replaced by a NB-Monodentate-containing precursor (cesium 10-(norborn-2-en-5-yl)decanoate), which was then used to prepare the nanocrystals. Figure 2-8 shows the absorption and emission spectra of the resulting nanoparticles in hexanes, which resembles those obtained using OA. The perovskite inorganic structure readily dissolves in water, which destroys the material. Hence, we did not attempt to transfer these QDs into water.

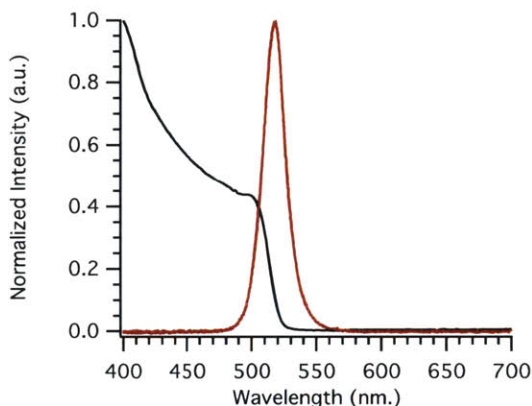


Figure 2-8: Absorption (black) and emission (red) spectra of NB-Monodentate-coated CsPbBr₃ perovskite nanocrystals in hexanes.

2.2.4 The Traditional Ligand Exchange

Nanocrystals that have been previously purified and isolated from the mother liquor can also be functionalized using the NB-Monodentate ligand. Typically, a separate ligand exchange step is performed in a hydrophobic solvent, and the resulting QDs are then transferred into water with help from Tz-PEG. Figure 2-9 presents the absorption and emission spectra of a representative InAs-CdSe-CdS sample before and after water solubilization using this particular method.

2.2.5 The NB-Bidentate Ligand Synthesis and Design

The NB-Monodentate ligand works well for functionalizing the surface of a broad range of nanocrystals and for dispersing them in water. Notwithstanding, the stability

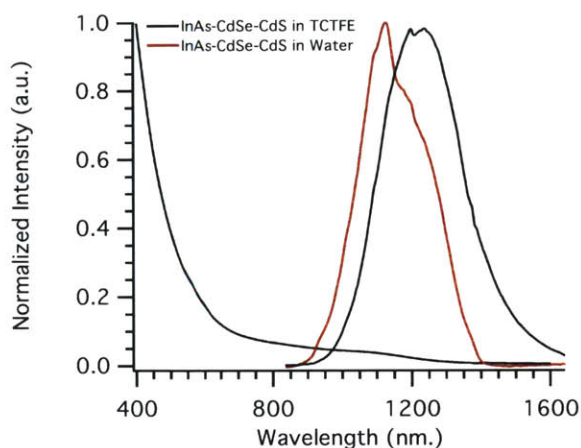
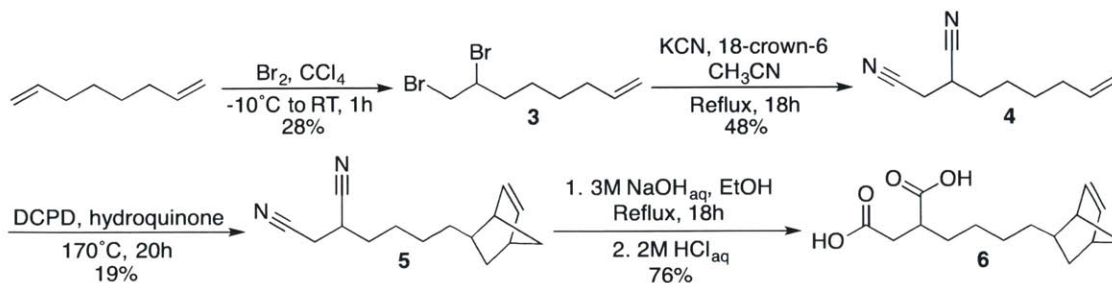


Figure 2-9: Absorption and emission spectra of NB-Monodentate-coated InAs-CdSe-CdS QDs in trichlorotrifluoroethane (TCTFE) (black) and in water (red). As-synthesized QDs exhibit a PLQY of 21% in organic solvents; this value drops to 4% in water.

of the water-soluble QDs hinges on the binding affinity of a single carboxylic acid anchoring group per ligand. This metal-ligand complex, although relatively strong when compared to those composed of L-type ligands, decays in solutions with high salt concentration and in the presence of organic molecules that compete for binding to the surface. Therefore, water-soluble QDs obtained through this method are not suitable for biological applications, which typically involve cellular media. In order to increase the stability of the metalorganic complex, we developed a new ligand that possess two carboxylic acid groups in close proximity, for maximum chelate effect. Scheme 2.3 describes the synthesis of this NB-Bidentate ligand.



Scheme 2.3: The synthesis of the NB-Bidentate ligand.

As will be discussed in chapter 3, a bidentate carboxylate domain greatly enhances

the optical properties of QDs in organic solutions. Whether the new NB-Bidentate or a subsequent version of the ligand is capable of producing water-soluble QDs that fulfill the requirements for biological applications remains a subject of intense research and investigation.

2.3 Conclusion

We successfully developed a new organic ligand that exhibits a norbornene functional group and binds strongly to the surface of colloidal nanocrystals during particle synthesis, eliminating the need for a dedicated ligand exchange step and enabling the large-scale production of high-quality derivatizable nanomaterials. The molecule is compatible with state-of-the-art synthesis methods of a large variety of semiconductor QDs that make use of OA as the principal surface ligand. Furthermore, we conjugated Tz-PEG to QDs coated with NB-Monodentate, and have rendered the particles soluble in water. We expect this technology to enable new and exciting applications that were previously impossible due to a lack of QDs with the appropriate functional groups for derivatization.

2.4 Chapter-Specific Acknowledgements

Yue Chen performed some of the synthesis and characterization of CdSe-CdS QDs. Francesca Freyra, Daniel Franke and Odin Achorn performed the synthesis and characterization of PbS, InAs-CdSe-CdS, and CsPbBr₃ nanocrystals, respectively.

2.5 Experimental Details

Materials and Instrumentation:

All chemicals unless otherwise noted were obtained from Sigma Aldrich and used as received. All solvents were spectrophotometric grade and purchased from EMD Millipore. Absolute ethanol (200° Proof) was purchased from Koptec. Flash column chromatography was performed using a Teledyne Isco CombiFlash Companion. ^1H NMR spectra, and ^{13}C NMR spectra with complete proton decoupling were recorded on a Bruker DRX 400 NMR spectrometer. Chemical shifts are reported in ppm from tetramethylsilane, and using the solvent resonance as the internal standard (CDCl_3 : ^1H NMR δ 7.26, ^{13}C NMR δ 77.16). UV-Vis-NIR absorbance spectra were collected using a Cary 5000 spectrophotometer. UV-Vis absorbance spectra were taken using an HP 8453 diode array spectrophotometer or a BioTek Synergy 4 Microplate Reader, on which some emission spectra were also recorded. The rest of the emission spectra in the visible were collected using a Fluoromax-3 spectrofluorometer and in the NIR using an calibrated InGaAs array detector. pH measurements were collected using an Orion PerpHecT model 310 LogR Meter operating a Orion PerpHecT Ag/AgCl electrode.

ethyl 10-(norborn-2-en-5-yl)decanoate (**1**)

Caution! This reaction involves the use of a pressure vessel. The use of a blast shield is recommended. Dicyclopentadiene (15.73g 0.119mol), ethyl undecylenoate (30.30g, 0.143mol) and hydroquinone (39.3mg, 0.36mmol) were added to a 65mL pressure vessel equipped with a Teflon valve. The temperature was raised to 170°C and the sample was left to react for 20h under constant stirring. After cooling to room temperature, the solution was distilled under vacuum (200mTorr). A fraction containing **1** with vapor temperature of 120-130°C was collected, and set aside for 4 hours to allow for a solid side-product to precipitate, which was then filtered out of solution using a fritted glass filter funnel. The filtrate was collected and stored at 4°C overnight to induce a second precipitation event. Another filtration step yields **1** as a clear oil. (7.69g, 0.028mol, 19% yield): mixture of exo and endo (2:8, respectively)

¹H NMR (400MHz, CDCl₃) MAJOR ISOMER (endo) δ (ppm) 6.09 (m, 1H), 5.89 (m, 1H), 4.11 (q, $J = 7.6$ Hz, 2H), 2.73 (m, 2H), 2.27 (t, $J = 7.4$ Hz, 2H), 1.94 (m, 1H), 1.81 (m, 1H), 1.60 (m, 2H), 1.38–1.22 (br, 11H), 1.24 (t, $J = 7.1$ Hz, 3H), 1.19 (d, $J = 8.0$ Hz, 1H), 1.03 (m, 2H), 0.47 (m, 1H); ¹³C{¹H} (100MHz, CDCl₃) δ (ppm) 174.0, 137.0, 132.6, 60.3, 49.7, 45.5, 42.6, 38.9, 34.9, 34.5, 32.6, 30.0, 29.6, 29.4, 29.3, 28.7, 25.1, 14.4; HRMS (DART/FT-MS): m/z [M + H]⁺ Calcd for C₁₈H₃₁O₂ 279.2319; Found 279.2310

10-norborn-2-en-5-yl)decanoic Acid (2)

Compound **1** (6.81g, 0.024mol) was added dropwise to a 1M NaOH solution in methanol (105mL), and stirred at room temperature for 4 hours. The solution was transferred into a separation funnel and washed with hexanes (150mL, 3X) to remove any unreacted material. The methanol phase was then acidified to pH 3 using a 1M HCl aqueous solution, and the product was extracted into hexanes (150mL, 3X). The combined organic layers were dried over Na₂SO₄, and the solvent was evaporated under reduced pressure to obtain **2** as a white solid. (2.82g, 0.011mol, 47% yield): mixture of exo and endo (2:8, respectively) ¹H NMR (400MHz, CDCl₃) MAJOR ISOMER (endo) δ (ppm) 11.53 (br, 1H), 6.10 (m, 1H), 5.90 (m, 1H), 2.74 (m, 2H), 2.34 (t, $J = 7.4$ Hz, 2H), 1.96 (m, 1H), 1.82 (m, 1H), 1.63 (m, 2H), 1.39–1.23 (br, 11H), 1.20 (d, $J = 8.0$ Hz, 1H), 1.04 (m, 2H), 0.48 (m, 1H); ¹³C{¹H} (100MHz, CDCl₃) δ (ppm) 180.5, 137.0, 132.6, 49.7, 45.5, 42.7, 38.9, 34.9, 34.2, 32.6, 30.0, 29.6, 29.4, 29.2, 28.8, 24.8; HRMS (DART/FT-MS): m/z [M - H]⁻ Calcd for C₁₆H₂₅O₂ 249.1860; Found 249.1856

We have successfully performed the synthesis of **1** and **2** at six times the scale described above and have obtained similar reaction yields.

7,8-dibromooct-1-ene (3)

1,7-octadiene (100g, 0.907mol) and CCl₄ (600mL, 1.51M) were mixed in a 2000mL round bottom flask equipped with an addition funnel, and cooled to -10°C using an ice-salt bath. A solution of bromine (42.0mL, 130.3g, 0.815mol, 0.9eq) in CCl₄ (110mL, 7.4M) was added drop-wise, and with care to not allow the temperature to rise above -5°C. The sample was protected from light, and stirred for an additional

hour. The solvent was evaporated *in vacuo*, and the resulting oil was distilled under vacuum (300mTorr) to obtain **3** with vapor temperature of 41-44°C as a clear, light-yellow oil. (69.19g, 0.256mol, 28% yield) [Note: This product is sensitive to ambient conditions, and may darken over time.] ¹H NMR (400MHz, CDCl₃) δ (ppm) 5.81 (m, 1H), 5.02 (ddt, $J_d = 17.1$ Hz, $J_d = 2.1$ Hz, $J_t = 1.6$ Hz, 1H), 4.96 (ddt, $J_d = 10.2$ Hz, $J_d = 2.1$ Hz, $J_t = 1.2$ Hz, 1H), 4.16 (m, 1H), 3.85 (dd, $J_1 = 10.2$ Hz, $J_2 = 4.4$ Hz, 1H), 3.63 (dd, $J_1 = J_2 = 10.0$ Hz, 1H), 2.19–2.06 (br, 3H), 1.79 (m, 1H), 1.62–1.39 (br, 4H); ¹³C{¹H} (100MHz, CDCl₃) δ (ppm) 138.6, 114.9, 53.1, 36.4, 36.0, 33.6, 28.2, 26.3; HRMS (DART/FT-MS): m/z [M + H]⁺ Calcd for C₈H₁₅Br₂ 270.9518; Found 270.9520

7,8-dicyanoct-1-ene (**4**)

Caution! This reaction makes use of cyanide salts, which can produce highly toxic hydrogen cyanide gas. The use of a well-ventilated fume hood, and personal protective equipment is required. Compound **3** (60.79g, 0.225mol), 18-crown-6 (59.47g, 0.225mol), finely ground potassium cyanide (30.84g, 0.476mol), and anhydrous acetonitrile (325mL, 0.69M) were combined in a 2000mL round bottom flask equipped with a condenser, and stirred at reflux for 36 hours. After cooling to room temperature, the solution was filtered through silica gel (~1 inch thick in a 150mL fritted glass filter funnel). The silica gel was then washed thrice with DCM (75mL), the combined filtrates were collected, and the solvent was evaporated *in vacuo*. The resulting oil was distilled under vacuum (200mTorr), and a fraction with vapor temperature of 100-120°C, containing a mixture of 18-crown-6 and **4**, was collected. Excess 18-crown-6 was precipitated out of solution by adding the mixture into 400mL of cold acetonitrile (-5°C) drop-wise. The newly formed crystals were filtered using a fritted glass filter funnel, and washed with excess cold acetonitrile. The filtrate was collected, and the solvent was evaporated under reduced pressure. This process was repeated a second time to precipitate more 18-crown-6 out of solution. The resulting oil was then purified using silica gel chromatography (hexanes/ethyl acetate, 2:3) to obtain **4** as clear oil. (17.44g, 0.107mol, 48% yield) ¹H NMR (400MHz, CDCl₃) δ (ppm) 5.78 (m, 1H), 5.02 (ddt, $J_d = 17.1$ Hz, $J_d = 2.0$ Hz, $J_t = 1.6$ Hz, 1H), 4.98 (ddt, $J_d =$

10.2 Hz, $J_d = 2.0$ Hz, $J_t = 1.2$ Hz, 1H), 2.90 (m, 1H), 2.75 (dd, $J_1 = 16.9$ Hz, $J_2 = 6.2$ Hz, 1H), 2.69 (dd, $J_1 = 16.9$ Hz, $J_2 = 7.2$ Hz, 1H), 2.09 (q, $J = 6.8$ Hz, 2H), 1.78 (m, 2H), 1.64–1.41 (br, 4H); $^{13}\text{C}\{^1\text{H}\}$ (100MHz, CDCl_3) δ (ppm) 138.0, 119.0, 115.7, 115.3, 33.3, 31.4, 28.5, 28.1, 26.1, 21.1; HRMS (DART/FT-MS): m/z $[\text{M} + \text{H}]^+$ Calcd for $\text{C}_{10}\text{H}_{15}\text{N}_2$ 163.1230; Found 163.1233

5-(5,6-dicyanohexyl)norborn-2-ene (5)

Dicyclopentadiene (11.33g 0.086mol), **4** (16.65g, 0.103mol) and hydroquinone (28.1mg, 0.26mmol) were added to a 65mL pressure vessel. The temperature was raised to 170°C, and the sample was left to react for 20 hours under constant stirring. The solution was cooled to room temperature, transferred to a round bottom flask equipped with a secondary liquid N_2 cold trap, and heated to 120°C under vacuum to remove any volatile side product. The resulting oil was then purified using silica gel chromatography (hexanes/ethyl acetate gradient 9:1 to 1:1, v/v), to obtain a fraction containing the desired product mixed with **4**. Compound **5** was obtained through vacuum distillation (0.6 mTorr) with vapor temperature of 145°C as a clear, colorless and viscous oil (4.51g, 0.019mol, 19% yield): mixture of exo and endo (2:9, respectively) ^1H NMR (400MHz, CDCl_3) MAJOR ISOMER (endo) δ (ppm) 6.10 (m, 1H), 5.88 (m, 1H), 2.89 (m, 1H), 2.74 (m, 2H), 2.73 (dd, $J_1 = 16.9$ Hz, $J_2 = 6.3$ Hz, 1H), 2.68 (dd, $J_1 = 16.9$ Hz, $J_2 = 7.1$ Hz, 1H), 1.95 (m, 1H), 1.82 (m, 1H), 1.73 (m, 2H), 1.58–1.25 (br, 5H), 1.20 (d, $J = 8.0$ Hz, 1H), 1.07 (m, 2H), 0.47 (m, 1H); $^{13}\text{C}\{^1\text{H}\}$ (100MHz, CDCl_3) δ (ppm) 137.2, 132.2, 119.1, 115.8, 49.6, 45.4, 42.5, 38.6, 34.4, 32.4, 31.5, 28.5, 27.9, 27.0, 21.1; HRMS (DART/FT-MS): m/z $[\text{M} + \text{H}]^+$ Calcd for $\text{C}_{15}\text{H}_{21}\text{N}_2$ 229.1699; Found 229.1704

5-(5,6-dicarboxyhexyl)norborn-2-ene (6)

Compound **5** (4.25g, 0.019mol) was dissolved in a 3M NaOH solution (100mL) and ethanol (110mL) in a 500mL round bottom flask equipped with a condenser. The solution was heated to reflux, and kept under constant stirring for 18 hours. After cooling to room temperature, TLC was used to confirm that all the starting material had reacted. The solvent was evaporated under reduced pressure and the resulting solid was re-dissolved in deionized H_2O (100mL). The solution was transferred into a

separation funnel and washed with diethyl ether (75mL, 3X). The aqueous layer was transferred into an Erlenmeyer flask, combined with diethyl ether (75mL), and kept under vigorous stirring. The resulting mixture was acidified to pH 2 using a 2M HCl solution. [Note: We found that adding diethyl ether during the neutralization step removes the diprotic acid from the aqueous phase as soon as it is fully neutralized, and prevents the formation of an ethyl monoester side product.] The mixture was transferred into a separation funnel, and the product was extracted into diethyl ether (75mL, 3X). The combined organic layers were dried over Na₂SO₄, and the solvent evaporated under reduced pressure. The resulting solid was then purified using silica gel chromatography (dichloromethane/methanol gradient 95:5 to 85:15, v/v) to obtain **6** as a white solid. (3.75g, 0.014mol, 76% yield): mixture of exo and endo (2:9, respectively) ¹H NMR (400MHz, CDCl₃) MAJOR ISOMER (endo) δ (ppm) 11.96 (br, 2H), 6.10 (m, 1H), 5.90 (m, 1H), 2.83 (m, 1H), 2.74 (m, 2H), 2.72 (dd, *J*₁ = 17.0 Hz, *J*₂ = 10.8 Hz, 1H), 2.50 (dd, *J*₁ = 17.0 Hz, *J*₂ = 3.6 Hz, 1H), 1.95 (m, 1H), 1.82 (m, 1H), 1.68 (m, 1H), 1.54 (m, 1H), 1.39–1.24 (br, 5H), 1.20 (d, *J* = 8.0 Hz, 1H), 1.07 (m, 2H), 0.47 (m, 1H); ¹³C{¹H} (100MHz, CDCl₃) δ (ppm) 181.9, 178.9, 137.1, 132.5, 49.7, 45.5, 42.7, 41.2, 38.8, 35.8, 34.6, 32.5, 31.8, 28.5, 27.2; HRMS (DART/FT-MS): *m/z* [M - H]⁻ Calcd for C₁₅H₂₁O₄ 265.1445; Found 265.1469

2-(4-(1,2,4,5-tetrazin-3-yl)phenyl)acetic acid (**7**)

The amine-reactive tetrazine was prepared according to the method described by Yang *et al.* [75]. We found it very difficult to completely wash away the Ni(OTf)₂ catalyst—a powerful quencher of QD fluorescence—from the final product, thus, we omitted it from the synthesis.

Tetrazine-PEG₅₀₀ (Tz-PEG) Compound 7 (0.50g, 2.33mmol), DCC (0.58g, 2.79mmol), and NHS (0.32g, 2.79mmol) were dissolved in DCM (40mL) and the resulting solution was allowed to react at room temperature for two hour under constant stirring. The mixture was filtered using a 0.45μm PTFE syringe filter and added to a solution containing *O*-(2-Aminoethyl)-*O'*-methylpolyethylene glycol (1.0g, 1.94mmol) in DCM (5mL), which was kept at room temperature under constant stirring for 12 hours. The organic phase was then washed thrice with water (20mL) and dried over

Na₂SO₄. The solvent was evaporated *in vacuo* and the resulting solid was purified using silica gel chromatography (dichloromethane/methanol gradient 92:8 to 90:10, v/v), to obtain Tz-PEG as a pink solid.

Cadmium Selenide Core Nanocrystals

Wurtzite-CdSe nanocrystals were synthesized using the method described by Carbone, et al. [3]

Cadmium Oleate

Cadmium oxide (2.57g 0.020mol), and oleic acid (40.0mL, 0.127mol) were combined in a three-necked round-bottomed flask equipped with a Hempel column, and a thermocouple that was connected to a heating circuit and a heating mantle for precise temperature control. The solution was degassed under vacuum (<200mTorr), with constant stirring, and at high temperature according to the following heating ramp: room temperature for 10 minutes, 80°C for 1 hour, 120°C for 1.5 hour, and 150°C for 10 minutes. The reaction flask was then filled with N₂ gas, and the temperature was raised to 160°C and held constant until the solution became clear, and colorless. The temperature was then lowered to 120°C, and ODE (60mL) was swiftly injected into the mixture. The temperature was lowered to 80°C, and the solution was placed under vacuum to degas for one hour. The hot solution was cannula-transferred to a dry Erlenmeyer flask equipped with a rubber septum seal. The cadmium oleate was stored at room temperature as a white soft solid, and was melted before use by partially immersing in a hot oil bath (80°C).

The Synthesis of Cadmium Selenide - Cadmium Sulfide Core-Shell Nanocrystals Coated with NB-Monodentate Using Metal-Carboxylate Precursors

The epitaxial growth of CdS followed a modified procedure described by Chen, *et al.* [4] A solution of ODE (3mL) and OAm (3mL) was prepared in a 100mL four-necked round-bottomed flask equipped with a Hempel column, and a thermocouple that was connected to a heating circuit and a heating mantle for precise temperature control. A solution of CdSe cores (30nmols) in hexanes was injected into the mixture, and the resulting reaction solution was degassed under vacuum (<200mTorr) for one

hour at room temperature, and constant stirring. The temperature was raised to 120°C, and degassed for an additional 20 minutes to completely remove the hexanes, and any trace of water and oxygen. The reaction flask was filled with N₂ gas, and the temperature was raised to 310°C and held constant throughout the infusion of the CdS precursor materials. During the heating step, and when the temperature reached 240°C, the infusion of cadmium and sulfur precursor solutions was initiated using a syringe pump, and set to proceed at a rate such that the total material required for four monolayers was injected in two hours. Once the infusion was completed, the temperature was reduced to 150°C and a solution of **2** (2.0g, 7.8mmol in 3mL of ODE) was swiftly injected. The ligand exchange reaction was allowed to proceed for one hour. The heating mantle was removed and the reaction flask was rapidly cooled to room temperature with the aid of an air blower. The nanocrystals were precipitated from the growth solution using acetone, and separated from the mother liquor using centrifugation (7,500 RPM, 5 minutes). The resulting near-colorless supernatant was discarded. The nanocrystals were further purified through a second precipitation event using hexanes (solvent), and acetone (anti-solvent). Finally, the nanocrystals were dispersed in hexanes and stored at room temperature.

Precursor Solutions

A cadmium precursor solution was prepared by diluting the appropriate amount of cadmium oleate solution that is required to grow four epitaxial monolayers of CdS with ODE to a final concentration of 0.143M. A sulfur precursor solution was prepared by dissolving 1-octanethiol (1.2x molar excess relative to cadmium oleate) in ODE for a final concentration of 0.171M.

The Synthesis of Cadmium Selenide - Cadmium Sulfide Core-Shell Nanocrystals Coated with NB-Monodentate Using Organometallic Precursors

CdSe-CdS QDs were synthesized using the traditional organometallic according to a procedure described in the literature [55]. Once the precursor infusion was completed, the temperature was held at 130°C a solution of **2** (2.0g, 7.8mmol in 3mL of ODE) was swiftly injected and the ligand exchange reaction was allowed to proceed

for one hour. Afterwards, the reaction flask was rapidly cooled to room temperature with the aid of an air blower. The nanocrystals were isolated from the growth solution using the same protocol described in the synthesis of CdSe-CdS nanocrystals using metal-carboxylate precursors.

Lead Sulfide Nanocrystals Coated with NB-Monodentate

Derivatizable PbS QDs were synthesized according to a modified procedure described by Hines *et al.* and Zhang *et al.* [?,76], in which OA was partially substituted for compound **2**. QDs of different sizes were prepared by adjusting the molar ratio of the carboxylic acid ligands (OA and **2**) to lead, and to sulfur precursors. We found empirically that large QDs require a lower level of OA substitution (between 25 to 75%) in order to be colloidally stable. As mentioned in section 2.2.2, a high amount of tightly packed NB-Monodentate on the surface can decrease the number of interaction between the QD and the solvent and change the solubility of the final construct. After synthesis, the nanocrystals were precipitated from the growth solution using acetone, and separated from the mother liquor using centrifugation. The resulting supernatant was discarded. The QDs were further purified through a second precipitation event using hexanes (solvent), and acetone (anti-solvent). Finally, the functionalized nanocrystals were dispersed in hexanes and stored at room temperature under N₂ atmosphere.

cesium 10-(norborn-2-en-5-yl)decanoate (8**)**

Cs₂CO₃ (0.407g, 2.5mmol), **2** (1.01g, 3.9mmol) and ODE (20mL) were combined in a three-necked round-bottomed flask equipped with a Hempel column, and a thermocouple that was connected to a heating circuit and a heating mantle for precise temperature control. The solution was degassed under vacuum (<100mTorr), at constant stirring, and at 120°C for one hour. The reaction flask was filled with N₂ gas and the temperature was raised to 150°C and held constant until the solution ceases to evolve CO₂. The heating mantle was removed and the reaction flask was cooled to room temperature. The final solution was stored under N₂ atmosphere.

Cesium Lead Bromide Nanocrystals Coated with NB-Monodentate

Derivatizable CsPbBr₃ QDs were synthesized according to a modified method

published by Protesescu *et al.* [71], in which cesium-oleate and OA were completely substituted for **8** and **2**, respectively.

Indium Arsenide - Cadmium Selenide - Cadmium Sulfide Core-Shell-Shell Nanocrystals Coated with NB-Monodentate

InAs-CdSe-CdS QDs were synthesized using the method described by Franke *et al.* [77]. Purified InAs-CdSe-CdS (10-20nmols) and **2** (~50-100mg), were dissolved in ODE (0.5mL) and OAm (0.5mL) in a three-necked round-bottomed flask. The temperature was raised to 150°C and held constant for one hour. After synthesis, the nanocrystals were precipitated from the growth solution using acetone, and separated from the mother liquor using centrifugation. The resulting supernatant was discarded. The QDs were further purified through a second precipitation event using hexanes (solvent), and acetone (anti-solvent). Finally, the functionalized nanocrystals were dispersed in hexanes and stored at room temperature.

Conjugation of Tetrazine-PEG₅₀₀ and Water Solubilization

QDs (2nmols) and Tz-PEG (~5mg) were dissolved in CHCl₃ and the resulting solution was allowed to react at room temperature for one hour under constant stirring. Ethanol (50μL) and hexanes (~5mL) were added sequentially in order to precipitate the newly formed hydrophilic constructs. The QDs were separated from the reaction mixture using centrifugation and collected into a pellet, which was then redissolve into CHCl₃. The precipitation process was repeated three times or until the supernatant was completely colorless. The final pellet was dissolved in water, dialyzed three times using a Millipore Amicon Ultra with a 30kDa cut-off filter and filtered using a 0.02μm HT Tuffryn syringe filter before storing at room temperature.

Dynamic Light Scattering Measurement

The hydrodynamic size was measured on a Malvern Instruments ZetaSizer ZS90. The instrument's software was used fit the autocorrelation functions and calculate a volume weighted size distribution taking the average of three sets of data, each consisting of 25-50 individual measurements.

Photoluminescence Quantum Yield (PLQY) Measurement

The PLQY was measured using a Labsphere integrating sphere, a chopper working

at 210 Hz in association with a Stanford Research Systems lock-in amplifier, and a 5 mW, 405 nm laser and a calibrated Si for QDs emitting in the visible or a 25 mW, 785 nm laser and a calibrated InGaAs detector for QDs emitting in the NIR. A glass filter was also used to spectrally separate the photoluminescence from the excitation source.

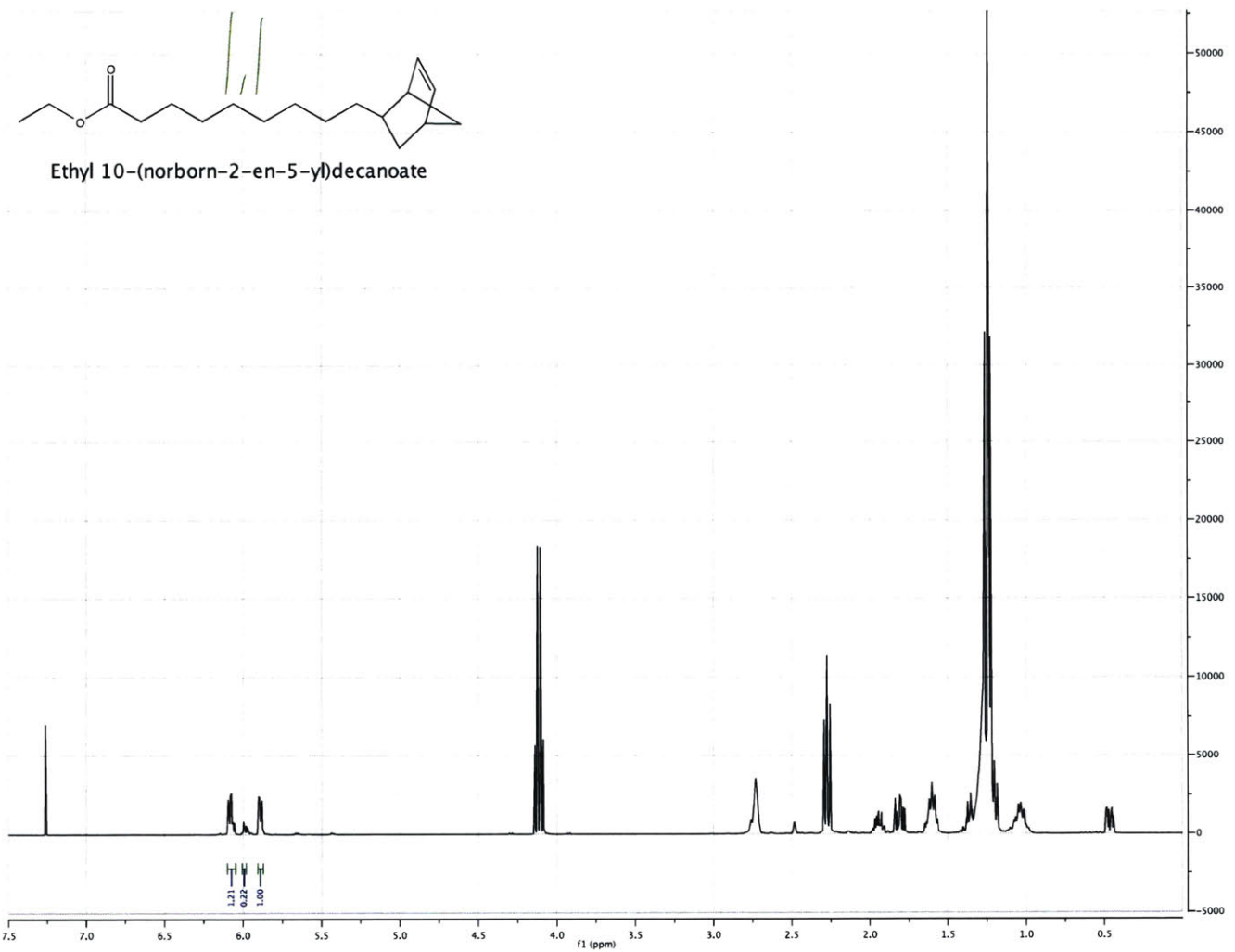
Transmission Electron Microscopy (TEM)

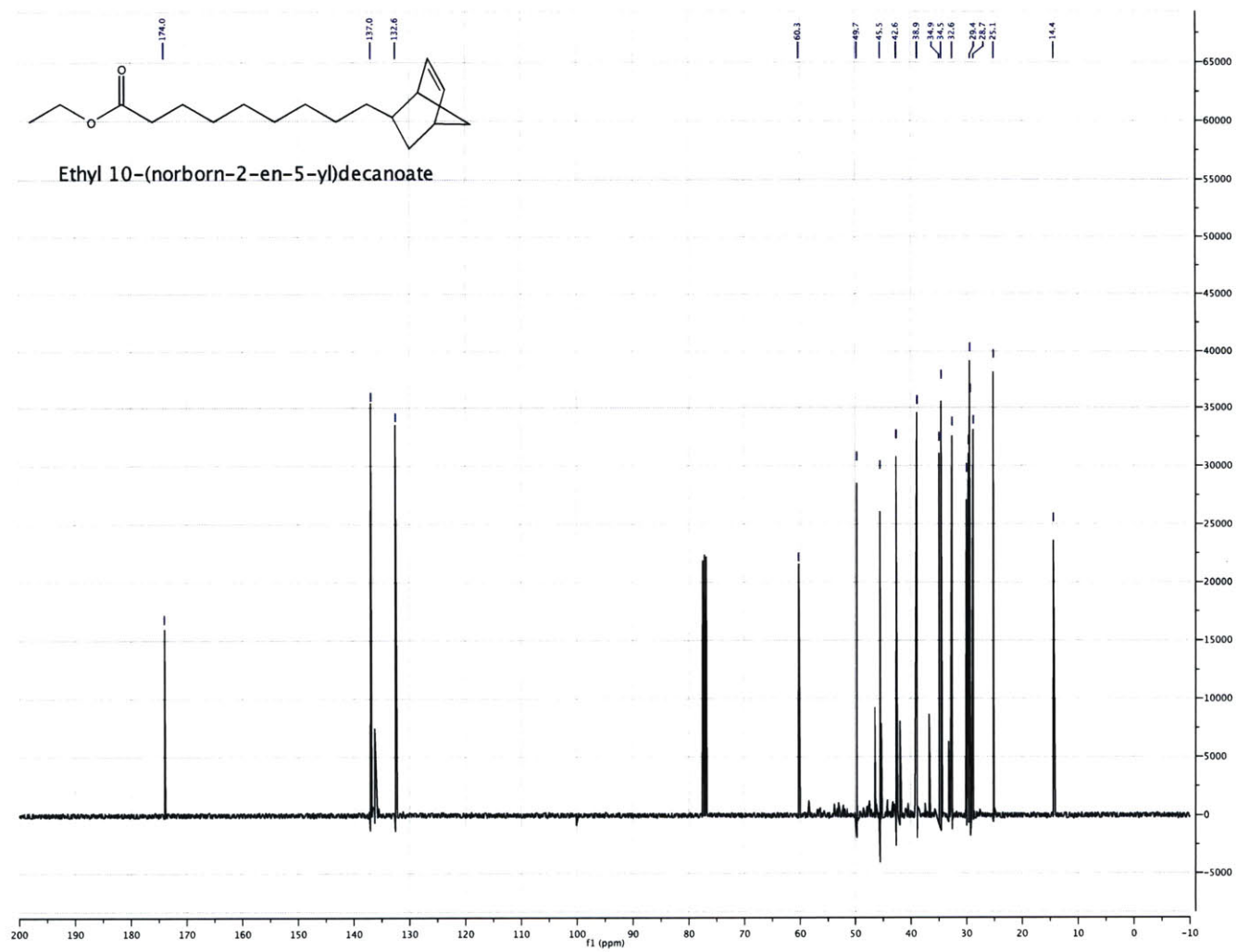
TEM micrographs were taken using a JEOL 2010 Advanced High Performance TEM operating at 200 kV.

pH Stability Measurement

A water-soluble CdSe-CdS QD stock solution was diluted to a concentration of 100nM using various aqueous solutions ranging from pH 2 to pH 12. The samples were incubated at room temperature for four hours, and their relative fluorescence intensity was measured using a BioTek Synergy 4 Microplate Reader.

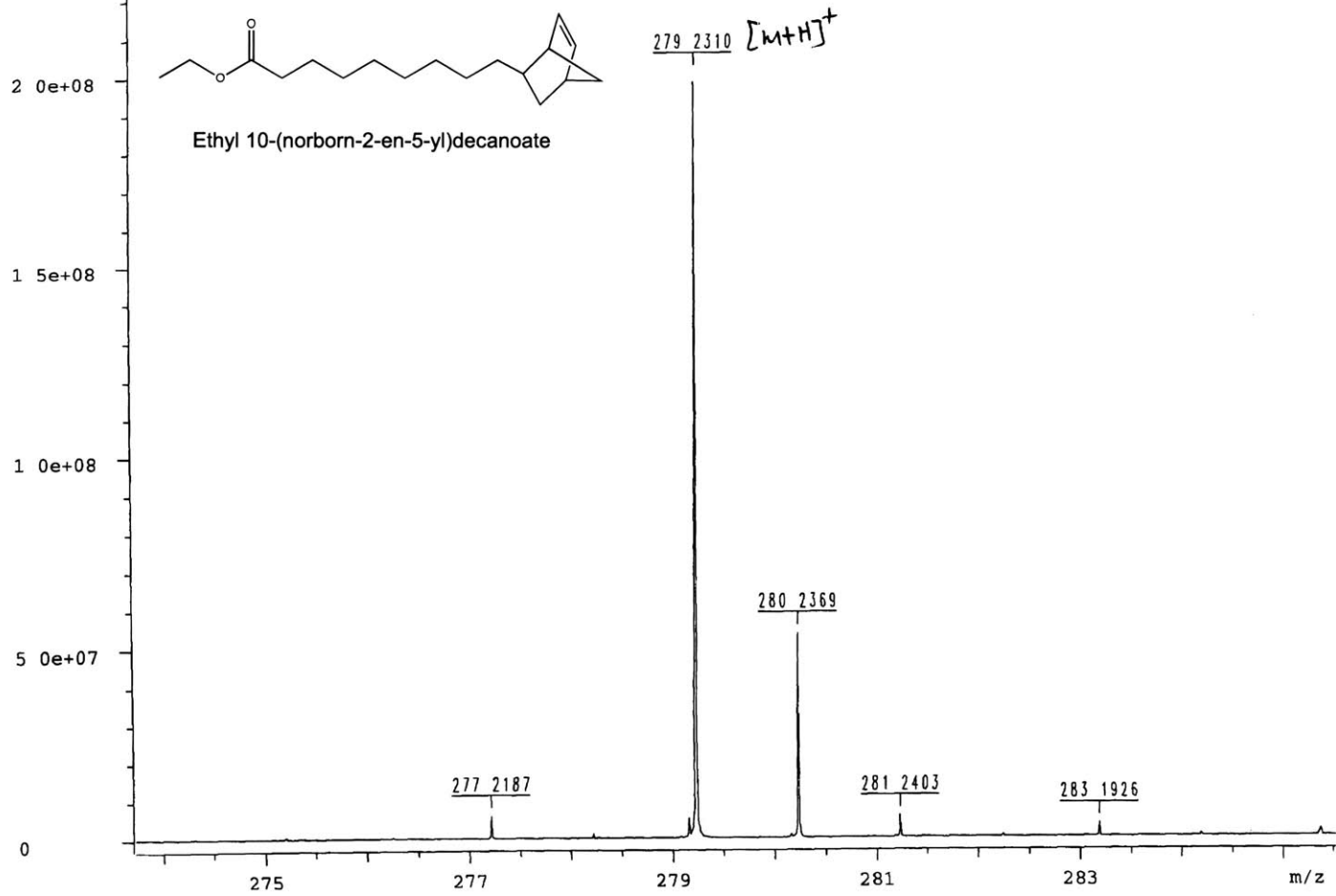
2.6 Appendix: ^1H NMR, $^{13}\text{C}\{^1\text{H}\}$ NMR, and DART/FT-MS Spectra of Chemical Compounds

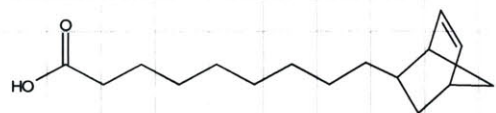




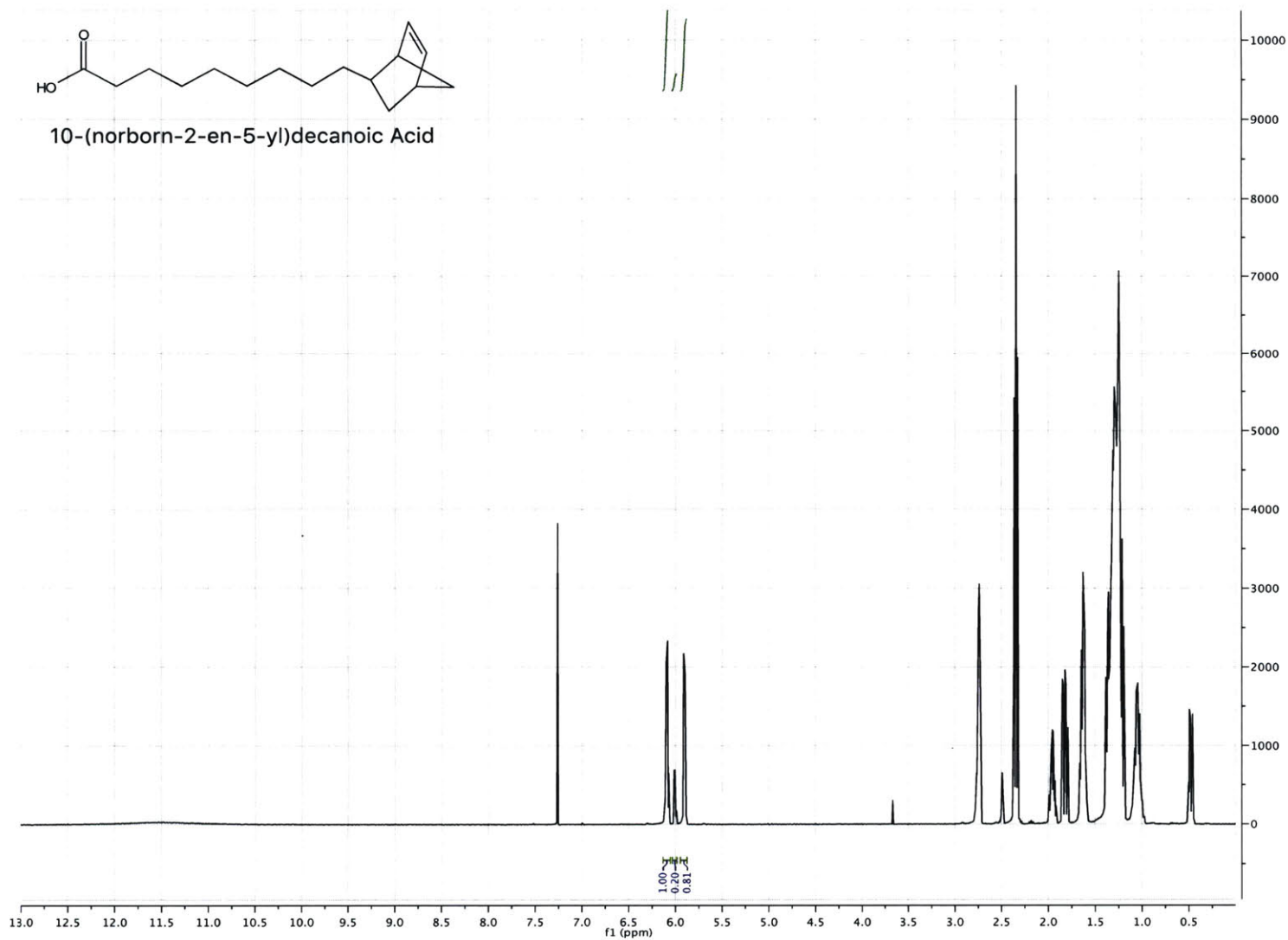
a i

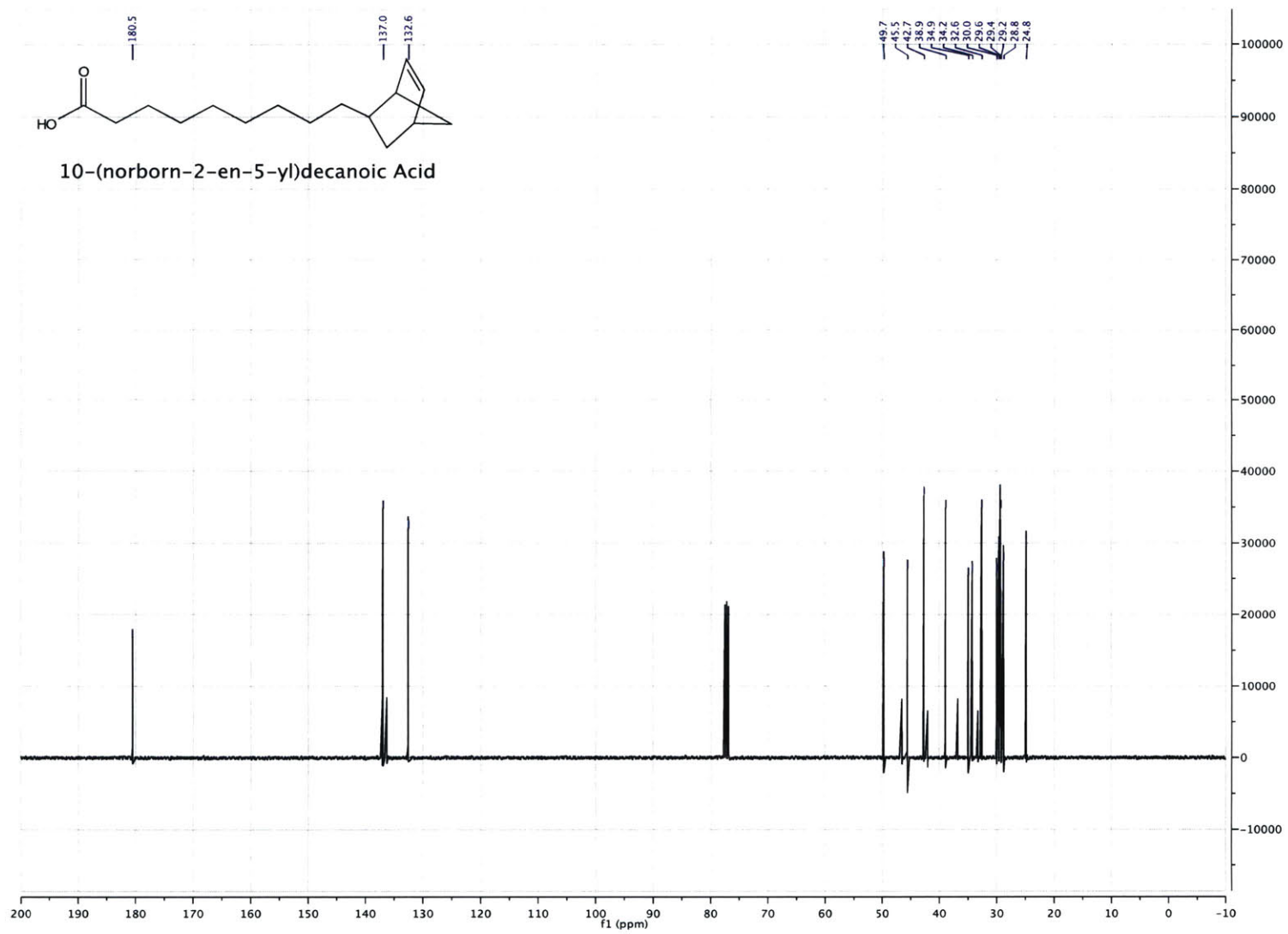
Sample ID JC 1113 06
C18H30O2 Theoretical Mass [M+H]⁺ 279 2319





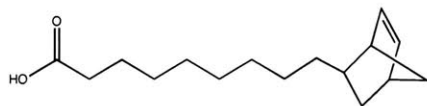
10-(norborn-2-en-5-yl)decanoic Acid



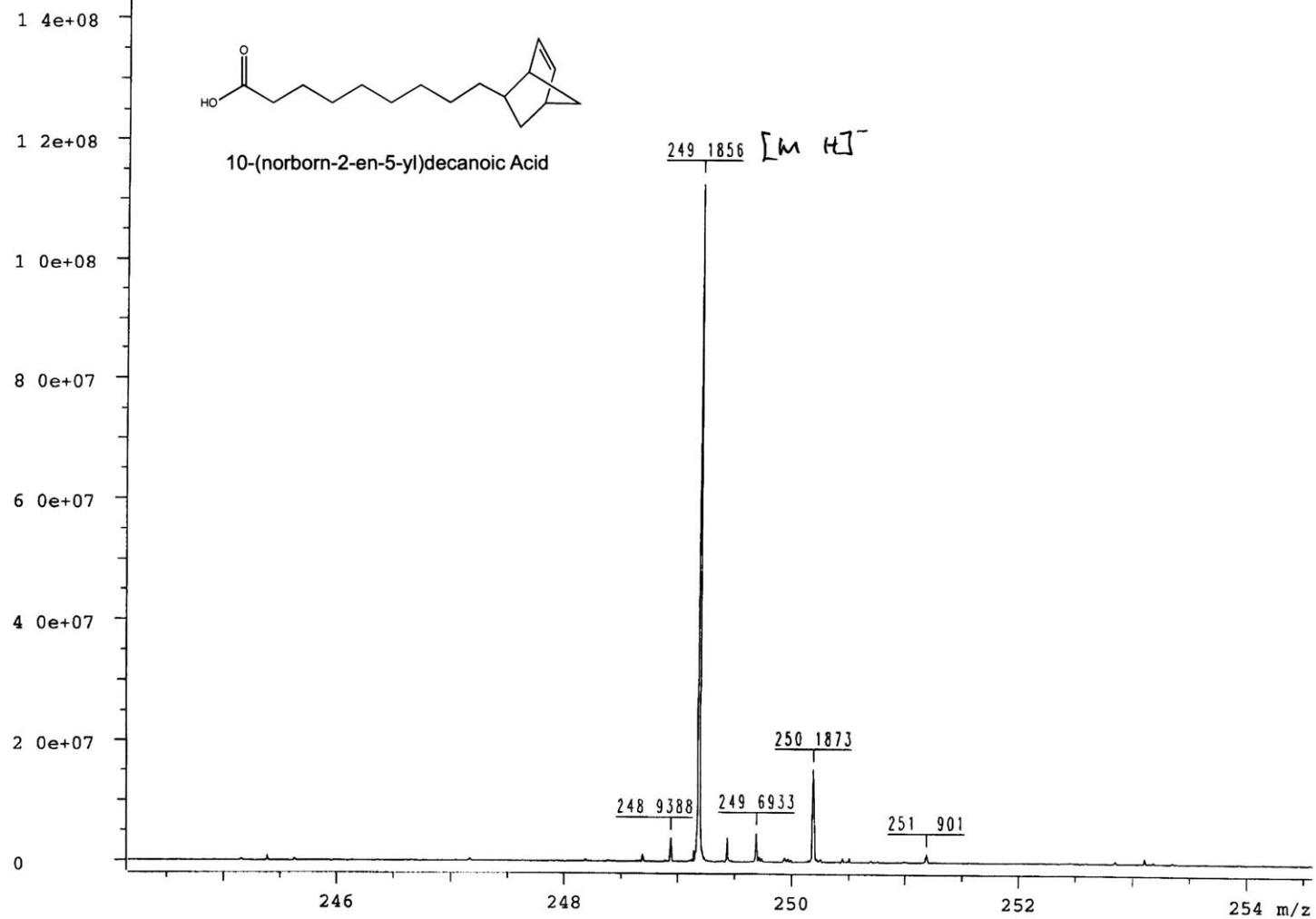


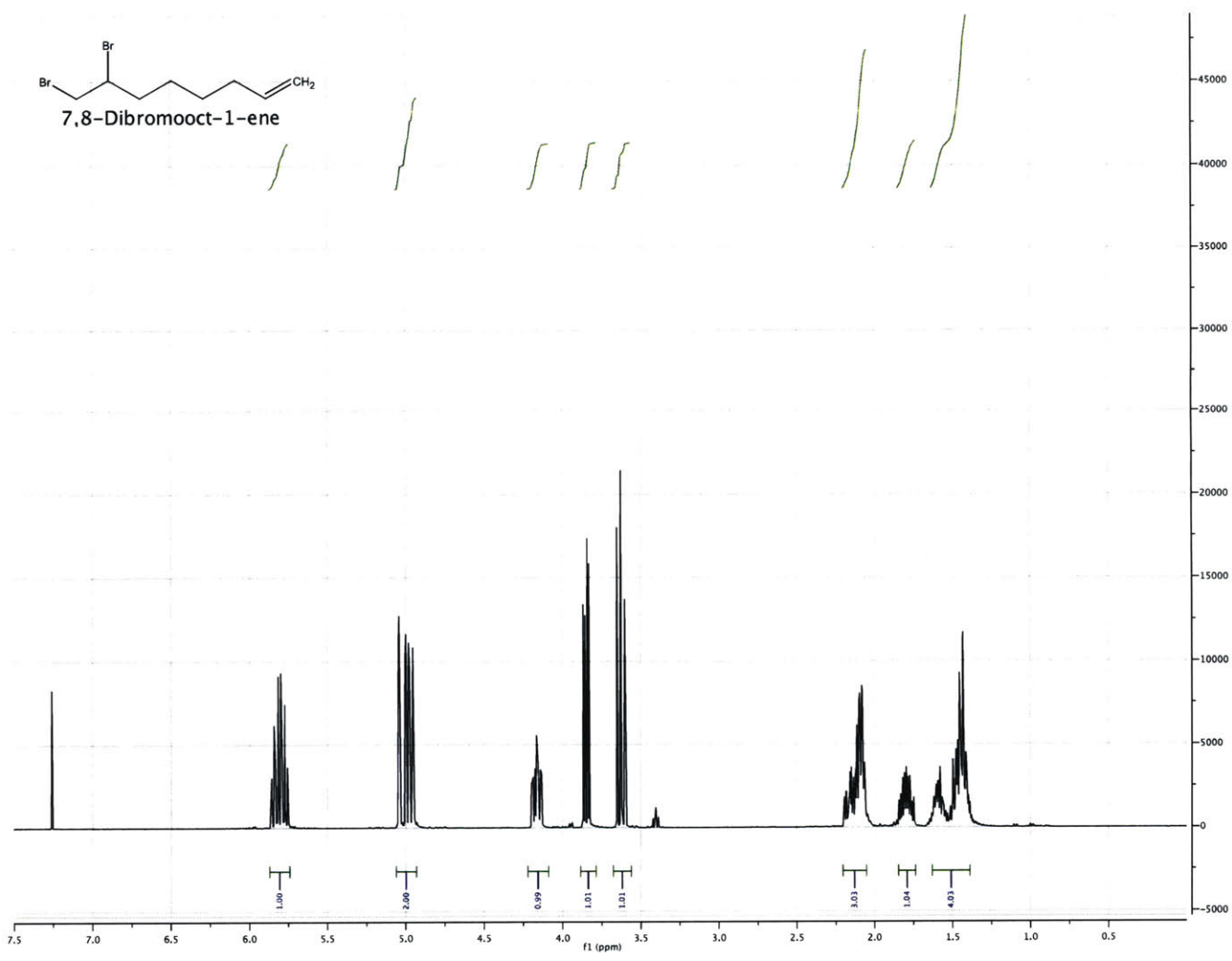
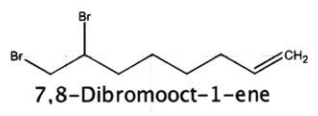
a i

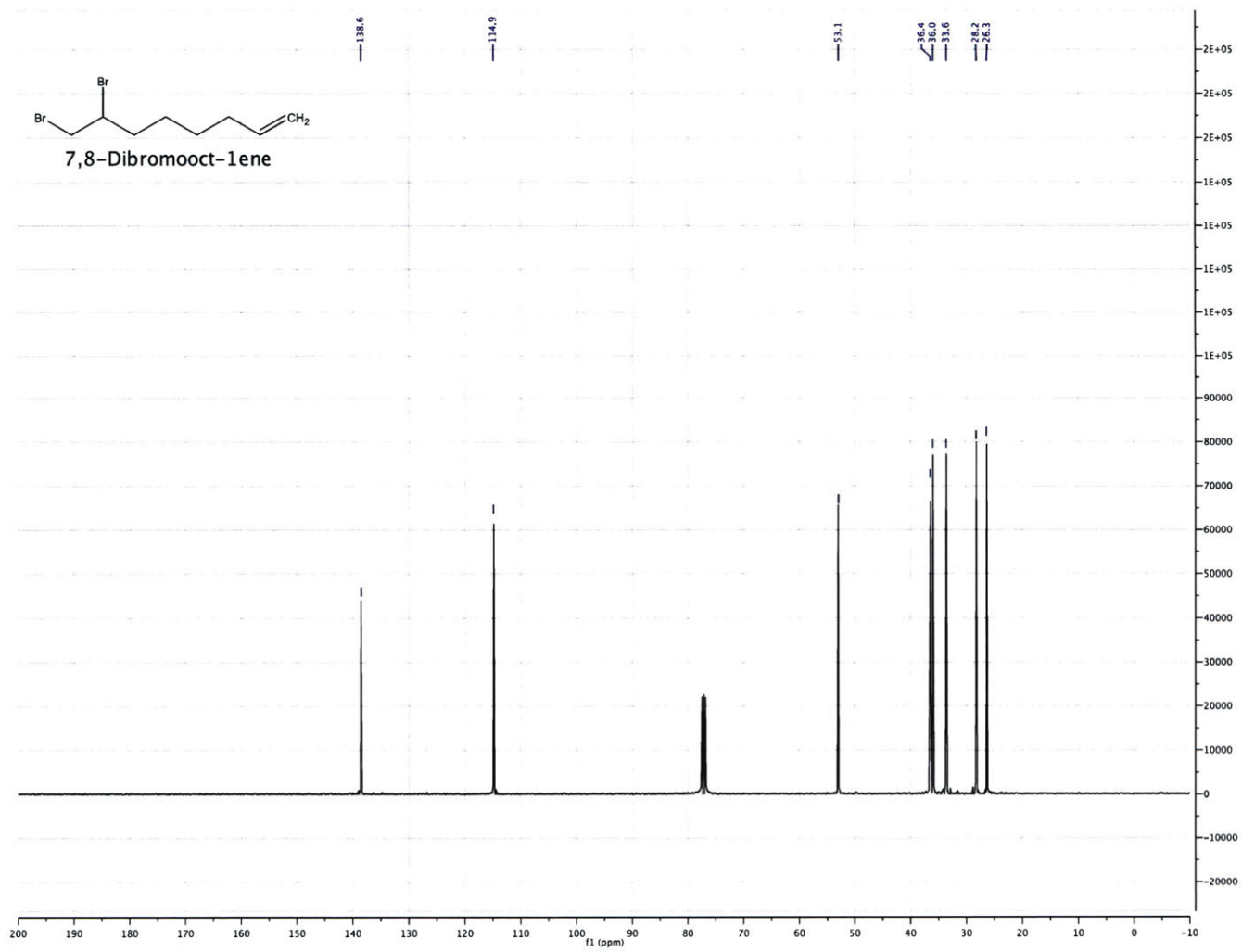
Sample ID JC 1113 07)
C16H26O2 Theoretical Mass [M H] 249 1860

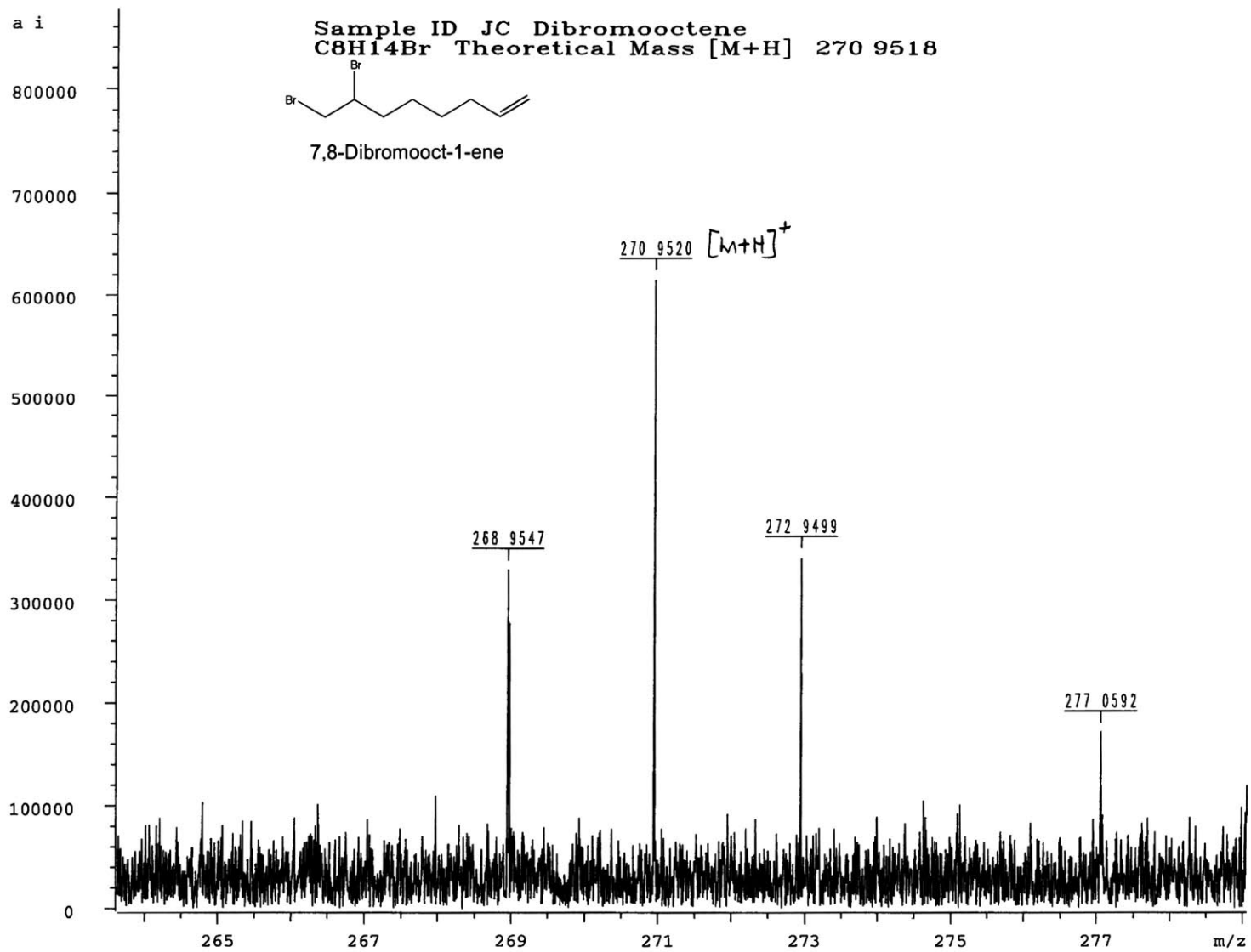


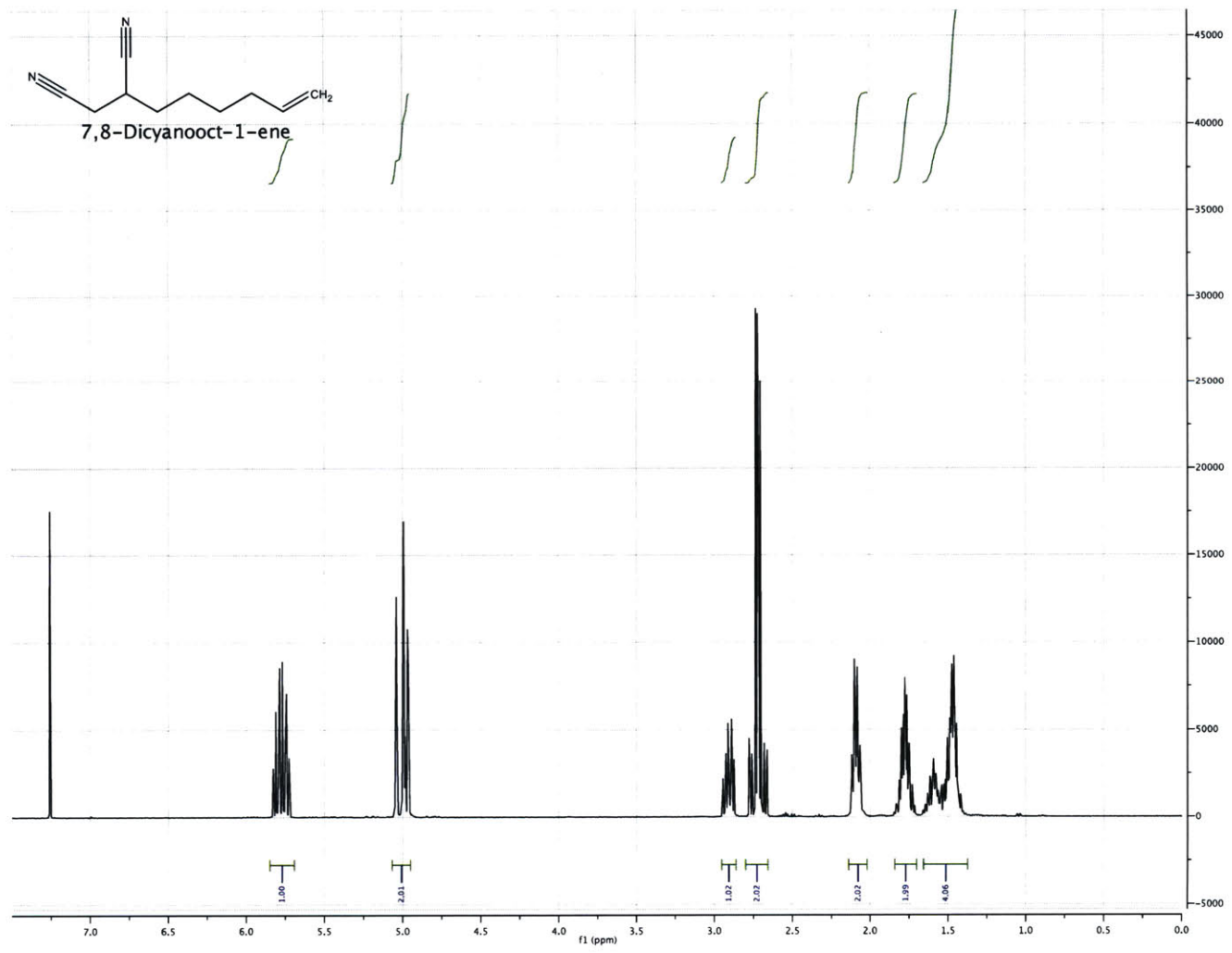
10-(norborn-2-en-5-yl)decanoic Acid

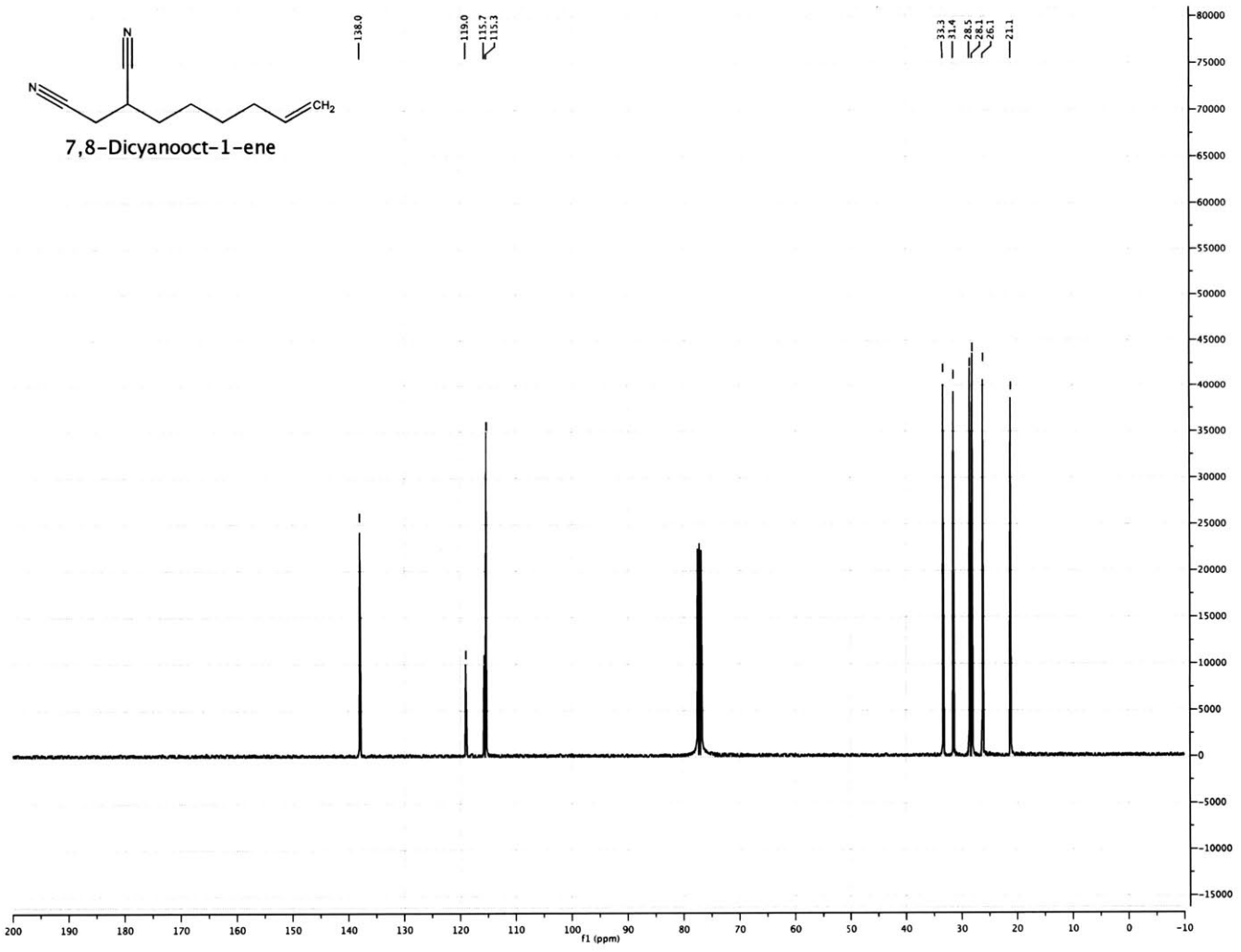
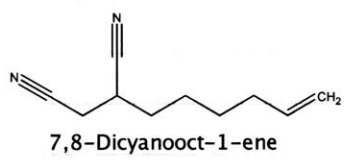


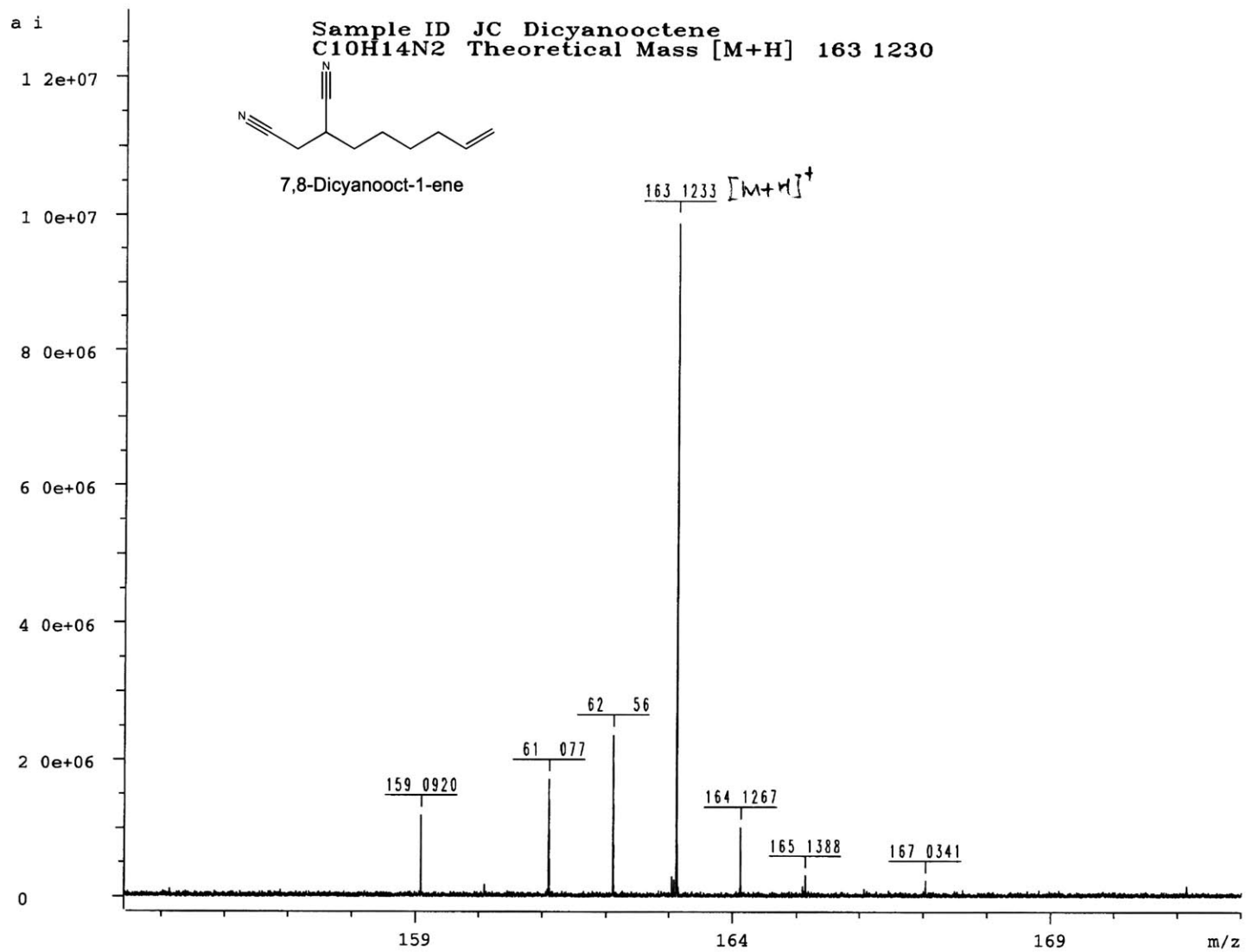


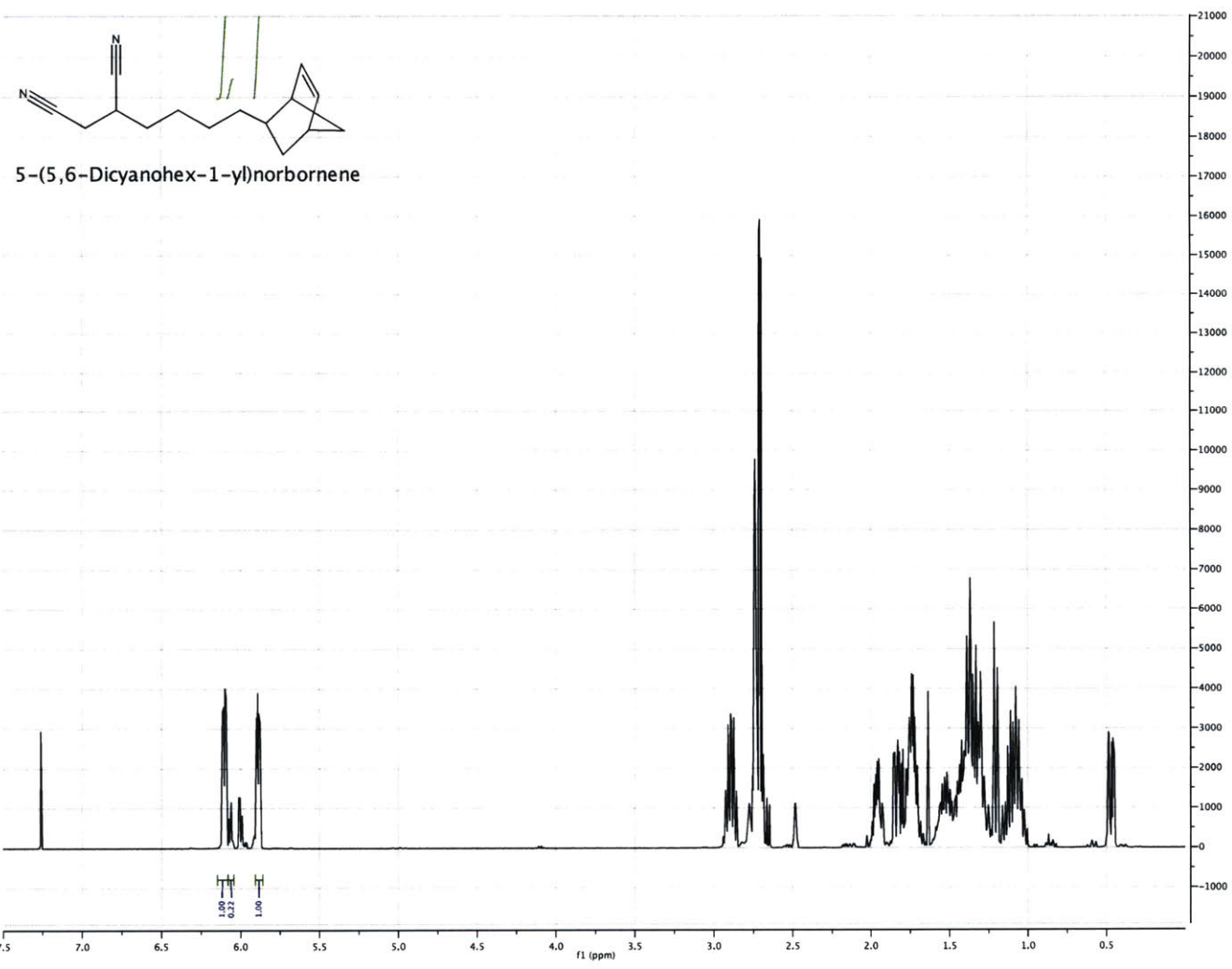


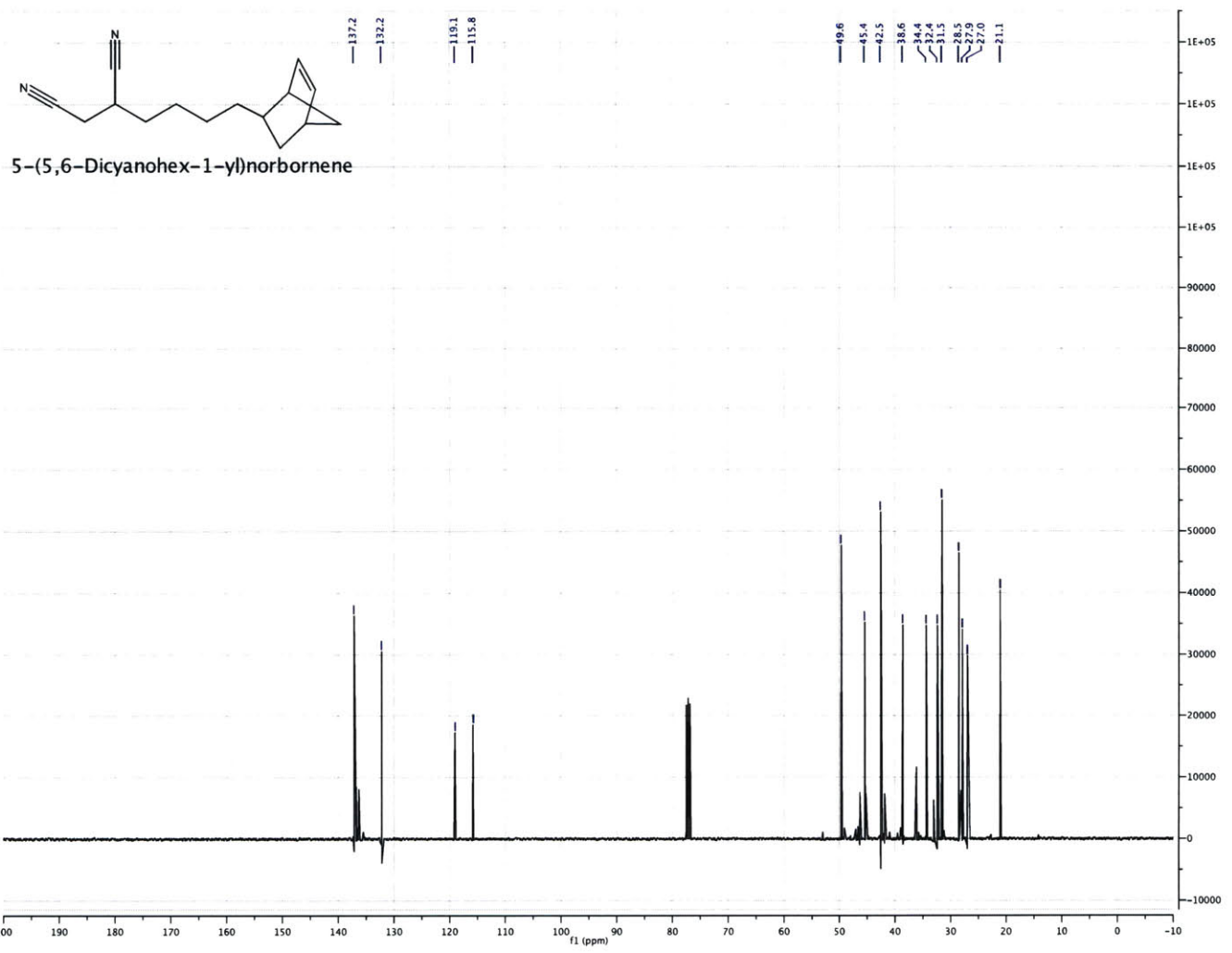


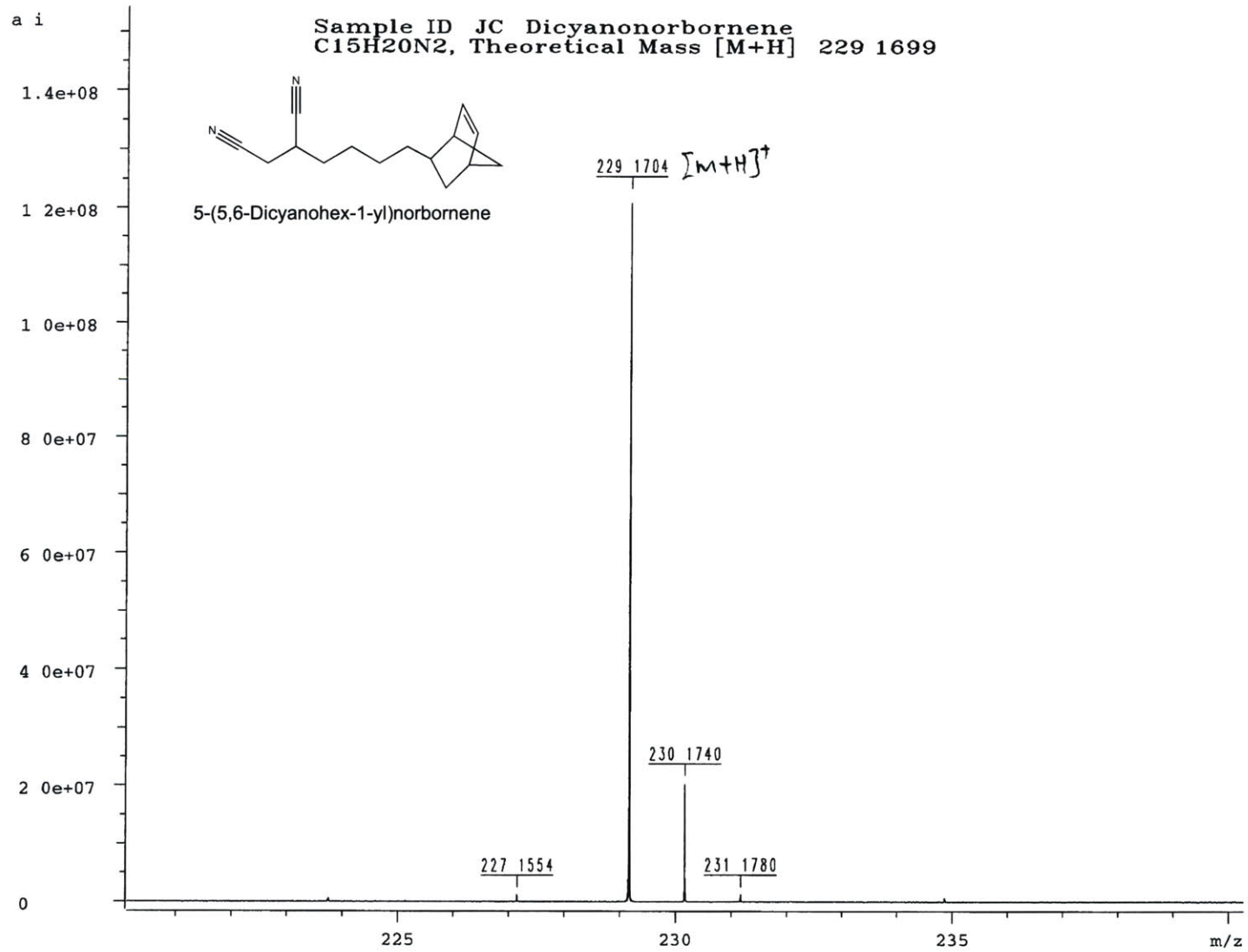


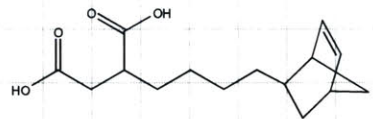




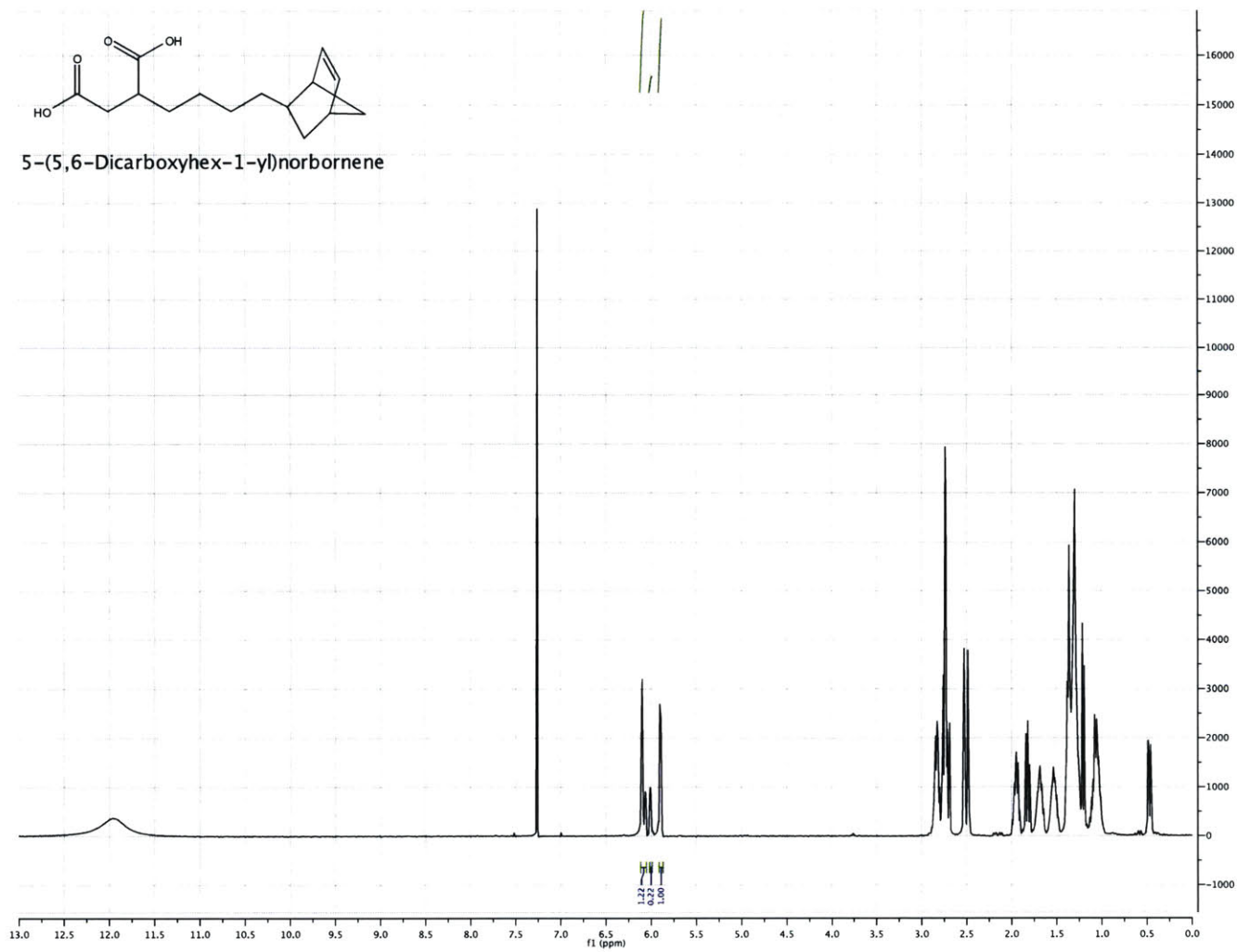


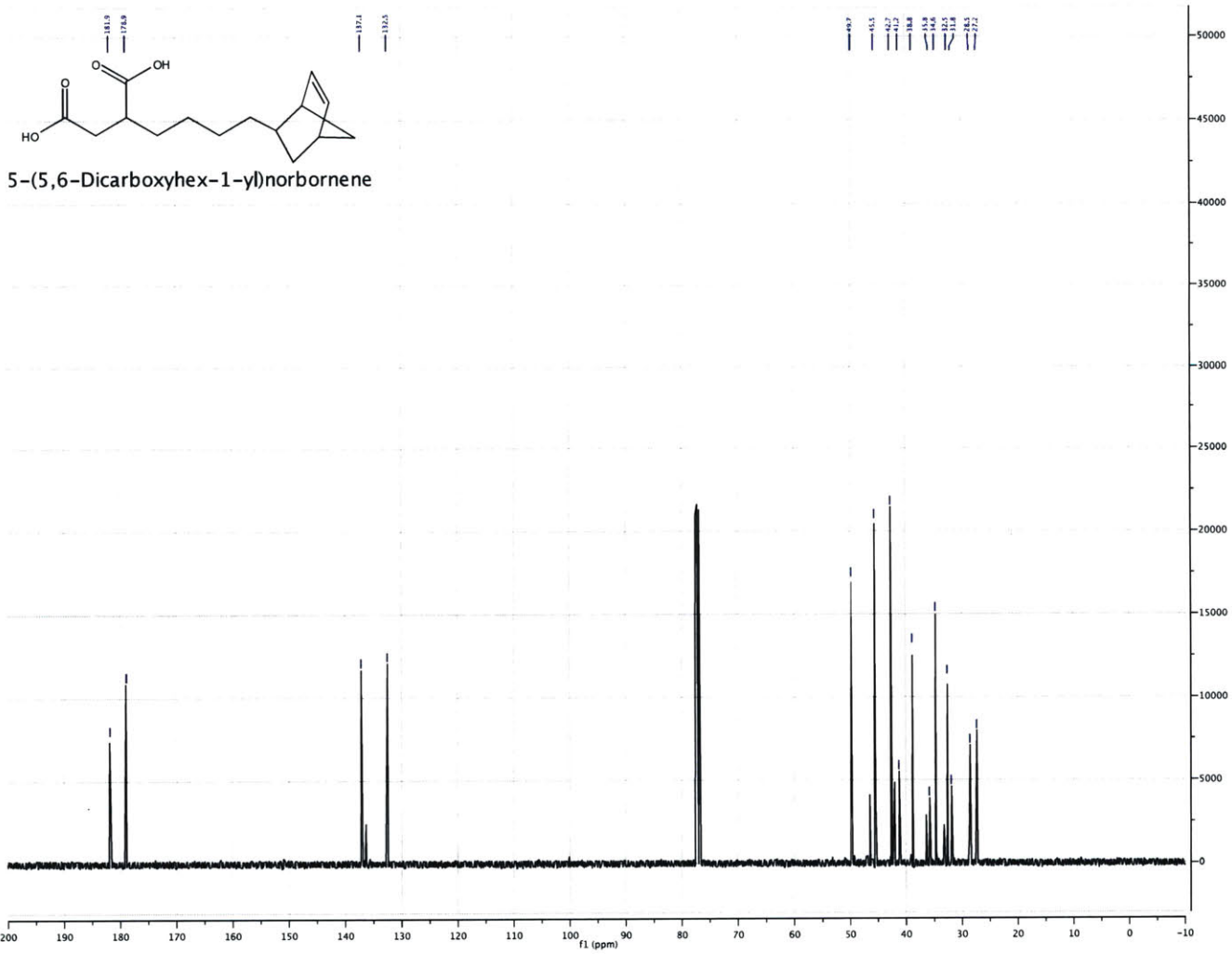


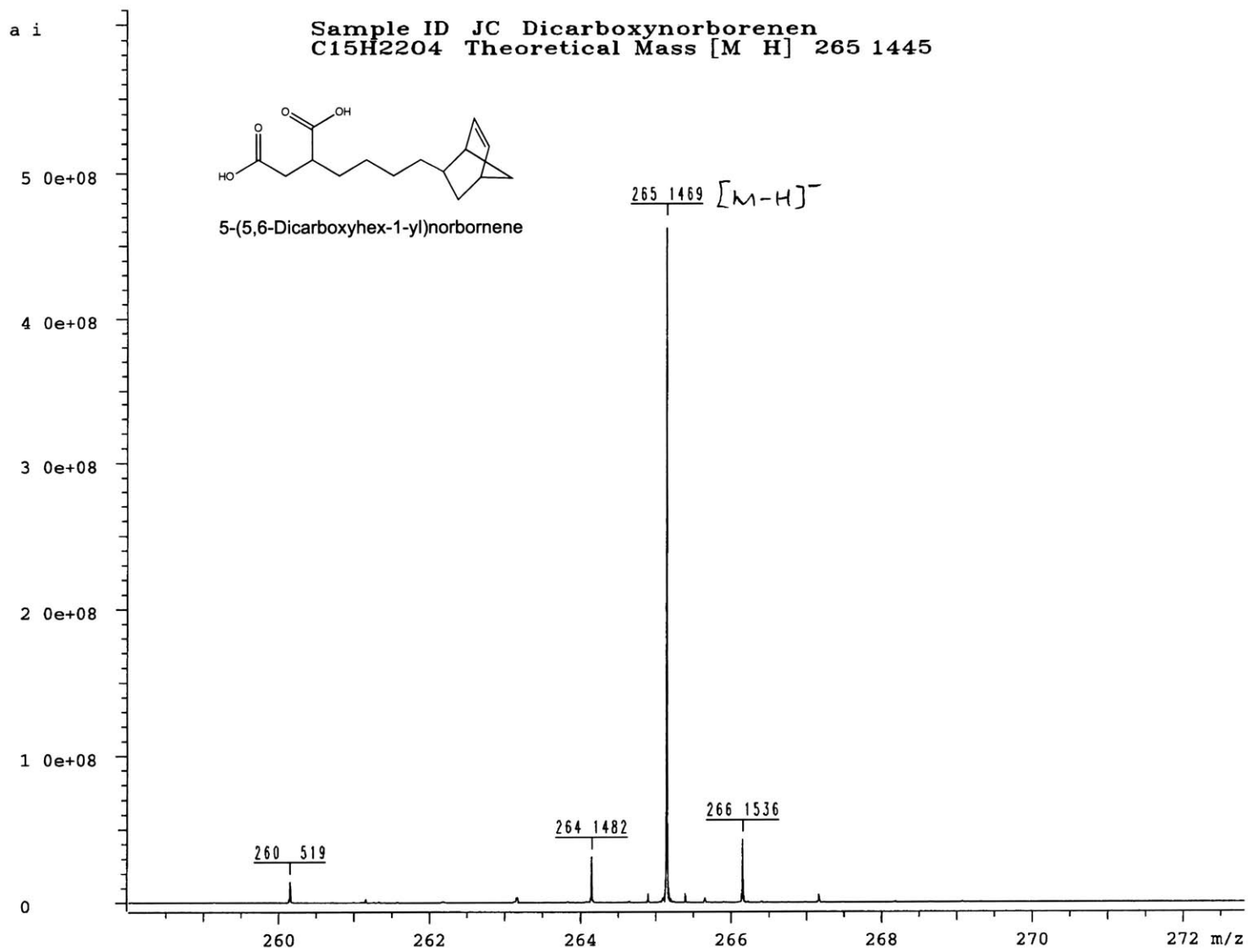




5-(5,6-Dicarboxyhex-1-yl)norbornene







Chapter 3

The Bidentate Carboxylate Ligand: A Strong Grip to Enhance the Photoluminescence Quantum Yield at High Temperature

3.1 Background and Motivation

In the previous chapter, we introduced the NB-Bidentate ligand as part of an effort to enhance the quality of colloidal QDs in water. Here, we will expand on the previous work by examining the role of ligand denticity as a means to achieve greater colloidal stability. We will base our work on a comparative study of the optical properties of QDs after ligand exchange using two model ligands, both with the same core structure but one of them possessing an extra coordinating site, as shown in figure 3-1. Also, we will discuss differences in the binding dynamics between these two ligands that arise from the chelate effect. We hope that this work will help us gain a more complete understanding of the connection between ligand structure and function and to establishing new guiding principles for the design and synthesis of better organic ligands for QDs.

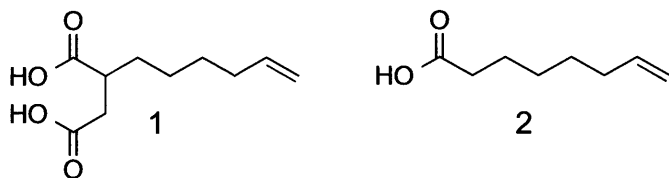


Figure 3-1: The Bidentate (BD) **1** and Monodentate (MD) **2** Ligands

3.2 Results and Discussion

3.2.1 Quantum Dot Stock Solution

All experiments were performed using one batch of CdSe-CdS (core-shell) nanocrystals that was prepared according to a procedure described by Chen *et al.* [4]. The QDs were isolated from the mother liquor and purified using tangential flow filtration. The level of purity was determined using ^1NMR spectroscopy by quantifying the relative ratio of bound to unbound ligand in solution. As shown in figure 3-2, our sample was chiefly composed of anionic (X-type) bound oleate ligands, but also contained small amount of free OA, representing only $\sim 13\%$ of the total (Oleate + OA).

A stock solution was prepared in toluene at a concentration of $6.375 \times 10^{-8}\text{M}$ —calculated according to method described by Leatherdale *et al.* [78]—and kept under refrigeration before use.

3.2.2 Binding Isotherms

A series of BD and MD ligand solutions were prepared with concentrations ranging from $2.63 \times 10^{-2}\text{M}$ to $8.22 \times 10^{-4}\text{M}$ using the stock solution as solvent. As shown in table 3.6, the concentration of QDs was kept constant in all solutions. Each sample was heated up to 100°C in order to promote ligand exchange, and the entire process was monitored using the QDs' fluorescence signal. Figure 3-3 depicts changes in the integrated emission intensity as a function of ligand exchange reaction time for different ligand concentrations. We noticed that at high BD ligand concentrations, the total fluorescence intensity increases, but that at high MD ligand concentrations, the intensity decreases instead. In order to confirm that these changes are the result of

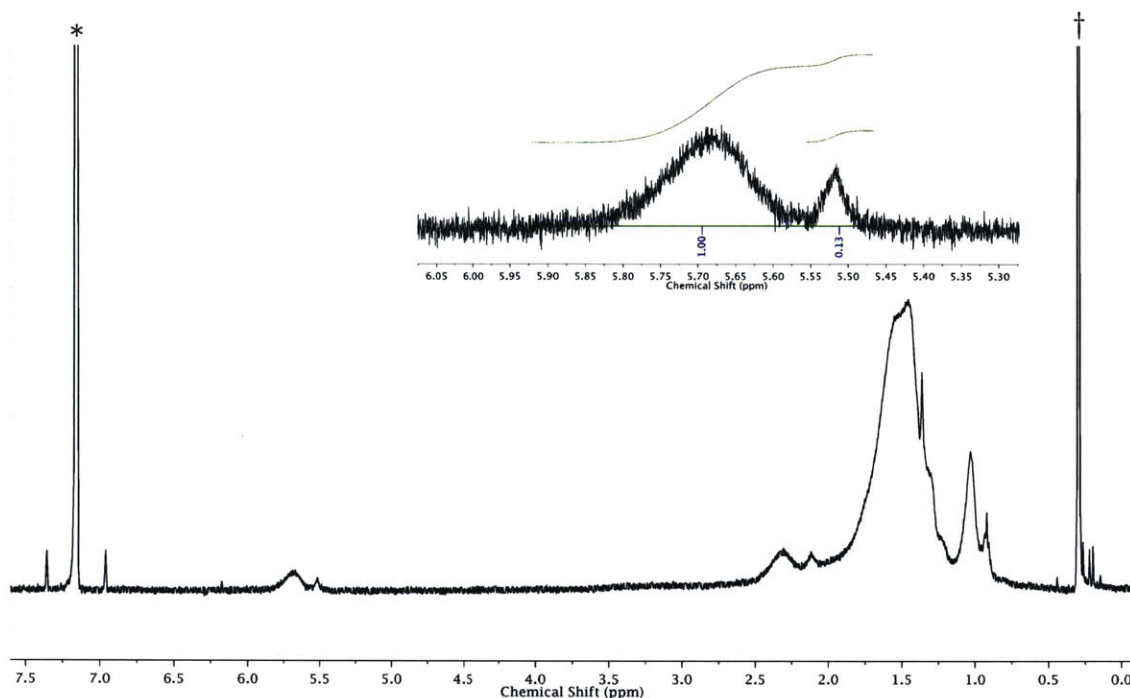


Figure 3-2: The ¹H NMR spectrum of the isolated CdSeCdS QDs. Inset: The vinylic region showing two resonance signals, each representing different OA species in close association with the QDs—the signals appear broad and downfield relative to free OA. The first peak at 5.69ppm (~87%) arises from oleate groups bound to the surface of QDs. The second peak at 5.52ppm (~13%) arises from free OA groups partially adsorbed to the surface of QDs. Residual solvent (*) C₆H₆ (†) H₂O.

ligand exchange processes and not an artifact of thermal degradation, we examined the absorption spectra for signs of Ostwald ripening (broadening of features) and of nanocrystal dissolution (intensity decay). Figure 3-5 demonstrates that the absorption spectra appears to be unchanged throughout the ligand exchange at 100°C, regardless of the type of ligand under examination. We also ruled out changes in the morphology of the QD using TEM imaging, as shown in figure 3-4. Based on these results, we conclude that changes in fluorescence intensity reflect changes in the level of surface passivation and in the number of surface-related trap states, which alter the QD's PLQY.

Figure 3-6 shows the evolution of the QD emission spectra as a function of the extent of the ligand exchange reaction with the BD ligand. The calculated PLQY for

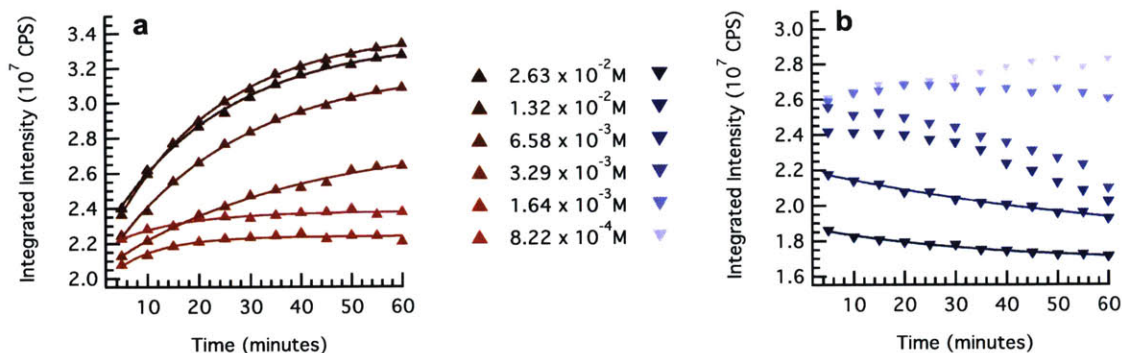


Figure 3-3: Ligand binding isotherms at 100°C at various concentration of (a) BD ligand and (b) MD ligand. Solid lines represent mono-exponential fits to the data.

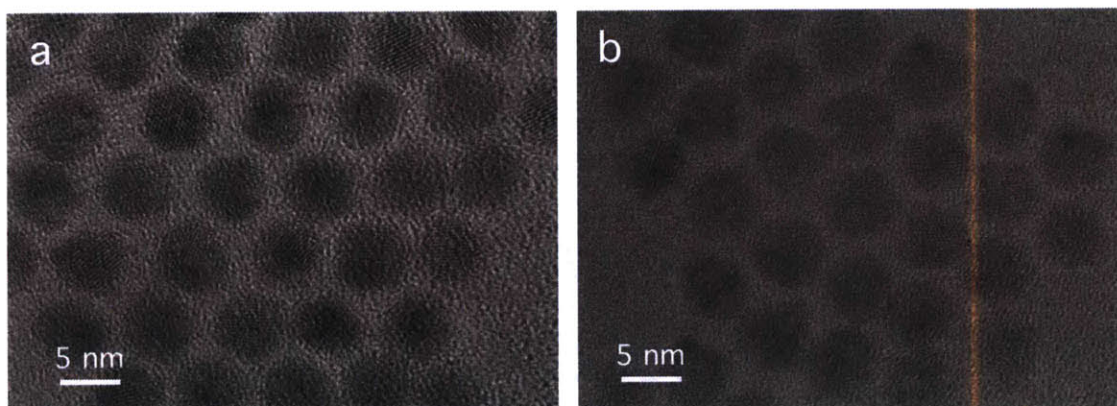


Figure 3-4: TEM micrograph of (a) As-synthesized oleate-coated QDs and (b) Ligand exchanged BD-coated QDs

this dataset is presented in table 3.2 and range from 68.8% after 5 minutes to 89.9% after 1 hour of reaction time. We noticed that the QD fluorescence spectrum appears to red-shift at high temperature (100°C), which we attribute to emission from defect states [79], and after cooling down, the spectrum reverts to its original position, as shown in figure 3-7 and table 3.4.

As shown in figure 3-8, we also analyzed other commonly used monodentate ligands such as OA and octylamine, and found that they too decrease the PLQY after binding to the surface of QDs.

A closer examination of the isotherm curves reveals that the PLQY responds to ligand exchange varies drastically, depending on the BD ligand concentration in so-

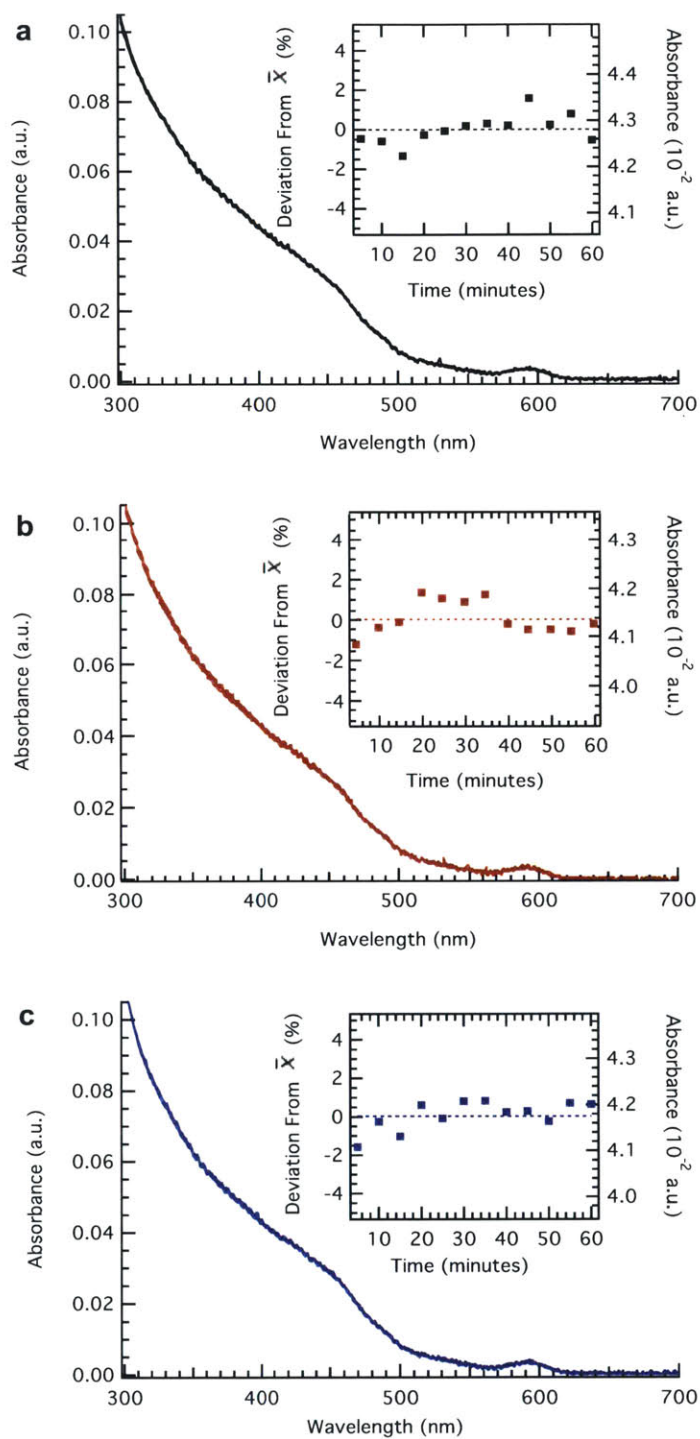


Figure 3-5: The absorption spectra of QDs incubated in toluene at 100°C with various ligands. (a) Control (No Ligand), (b) Bidentate Ligand (c) Monodentate Ligand. Inset: The QD absorption at 405nm stays constant as a function of reaction time.

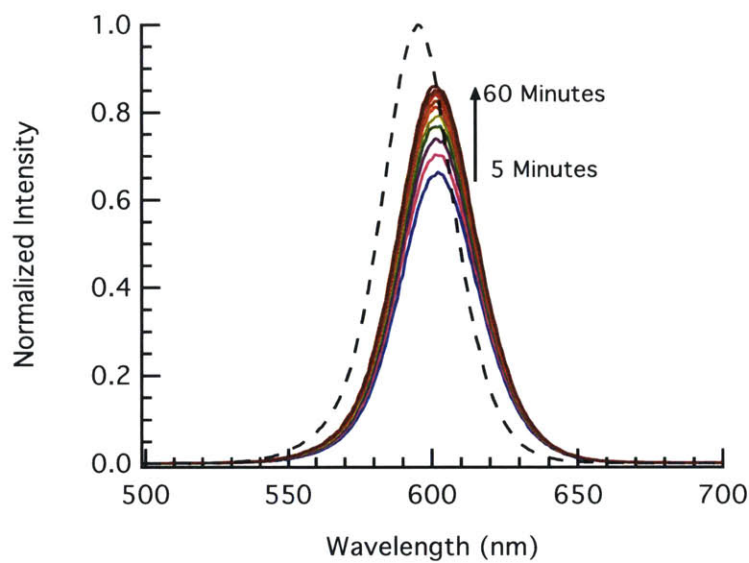


Figure 3-6: Normalized emission spectra at different points throughout the ligand exchange process. QDs were incubated at 100°C in a 2.63×10^{-2} M BD ligand solution. The dash-line (- - -) represents the emission spectrum of the stock solution at room temperature.

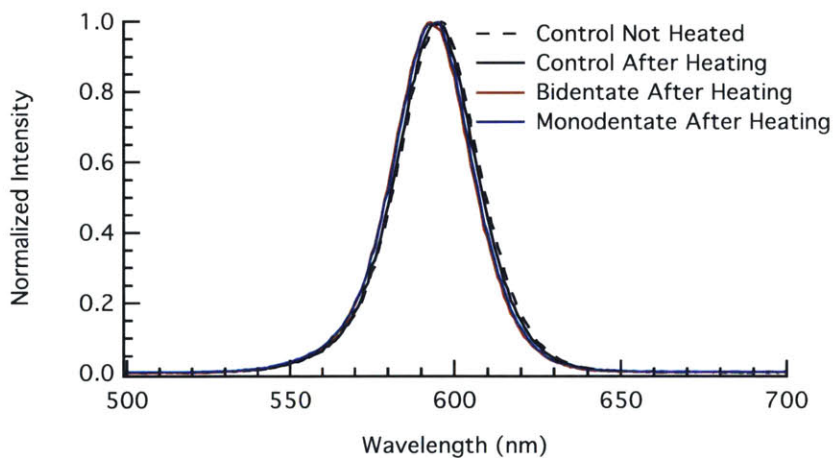


Figure 3-7: The emission spectra of QDs at room temperature after ligand exchange. No-Ligand (black), MD (blue) at 2.63×10^{-2} M, and MD (red) at 2.63×10^{-2} M. The dash-line (- - -) represents the emission spectrum of the stock solution at room temperature.

lution. At low concentrations of BD ligand ($\leq 1.64 \times 10^{-3}$ M) the emission intensity appears to decrease, relative to the starting point, and reaches equilibrium in a very short period of time (< 20 minutes). We attribute this fast component to the simple

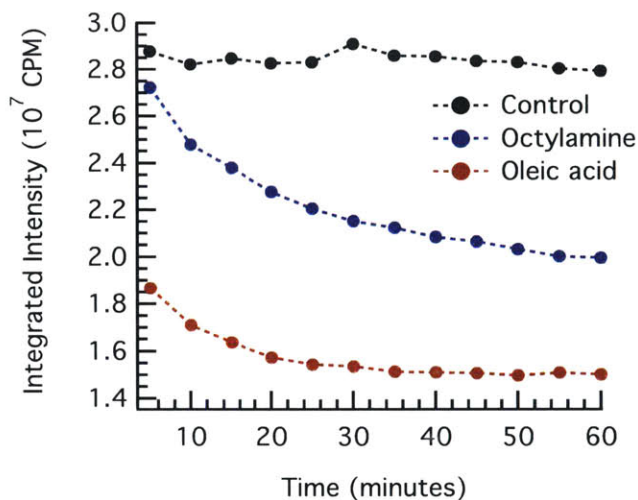
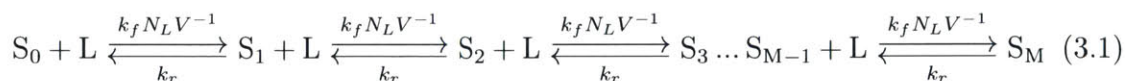


Figure 3-8: Ligand binding isotherms at 100°C for No-Ligand (black), Octylamine (blue) at 2.63×10^{-2} M, and OA (red) at 2.63×10^{-2} M.

exchange between free and adsorbed ligands, a process that is known to occur spontaneously at room temperature [26, 28, 80, 81], and that also appears to take place during the binding of OA. At higher concentrations, however, the emission intensity appears to increase slowly in response to a presumptive second binding event. We believe that the slow kinetic component is the result of a surface remodeling process to accommodate the two BD ligand binding motifs. In order to test the validity of this hypothesis, we fitted the BD ligand binding isotherms to mono-exponential functions, calculated the emission intensity at equilibrium, and plotted these values as a function of BD ligand concentration. As shown in figure 3-9, the slow binding process follows the Langmuir adsorption model at equilibrium.

Normally, the coordination state of a QD can be modeled using the following chemical equation, [82]



For a QD possessing M total number of binding sites, S_i represents a specific chemical state of the nanocrystal surface that is characterized by having i binding

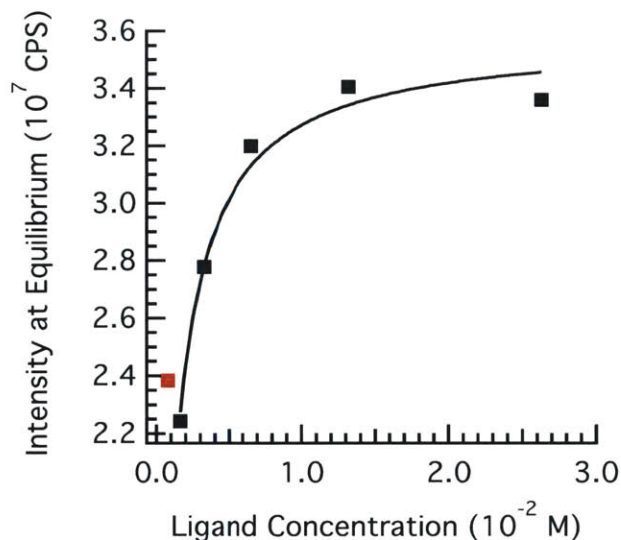


Figure 3-9: Langmuir adsorption isotherm for the BD ligand. The black squares represent our data and the solid line the fit to equation 3.5. The red square represents the data point with the lowest ligand concentration, 8.22×10^{-4} M, which deviates from the general trend.

sites that are each occupied by a ligand (L) and $M-i$ unoccupied binding sites having no ligands. Each surface state, S_i , may react with a ligand, L , to form a complex, denoted by the surface state S_{i+1} . The reaction is reversible, so S_i can break-up to produce a free organic ligand (L) and a corresponding unoccupied binding site, denoted by the surface state S_{i-1} . We assume that the reaction takes place in a solution of volume, V , and that the ligand molecules move uniformly throughout the whole volume. The rate at which an unoccupied site on the surface reacts with a free ligand to form a complex depends on the ligand density in solution, and is denoted by $k_f N_L V^{-1}$, where N_L represents the number of moles of ligand in solution. The reverse reaction occurs at a rate k_r .

The Langmuir adsorption model introduces the following three assumptions:

1. That each of the M binding sites are independent of each other, so that the binding event of a ligand to a particular unoccupied site on the surface of the nanocrystal is not influenced by the state of the other $(M - 1)$ binding sites.
2. That all of the binding sites are identical to each other, so that the rates of

binding and unbinding are the same for all M sites, and equal to $k_f N_L V^{-1}$, and k_r , respectively.

3. That the molar concentration of L in solution, as defined by $[L]=N_L V^{-1}$ does not change over time, and thus is defined by the constant L_0 .

These assumptions reduce the above chemical equation to simple two state model involving an unoccupied Z_U state and an occupied Z_O , shown below.



The dynamics of this system are in turn defined by the following rate equation,

$$\frac{\partial P_{Z_O}(t)}{\partial t} = k_f L_0 (1 - P_{Z_O}(t)) - k_r P_{Z_O}(t) \quad (3.3)$$

whose solution at equilibrium, when $t \rightarrow \infty$, results in the Langmuir adsorption isotherm, equation 3.4.

$$\Theta_A = \frac{L_0}{L_0 + K_D} \quad (3.4)$$

Due to the fact that our experiment does not quantify the number of occupied states directly, but instead relies on the ensemble PLQY, we must introduce a fourth assumption declaring that the PLQY and, consequently, the emission intensity reacts linearly to the number of ligands on the surface. It is important to recognize that all of these assumptions, which are put in place in order to simplify the system under consideration, do not capture all of the complexity of the ligand exchange process. The last one, in particular, has been shown to fail in very dilute regimes. [28, 83]. Nevertheless, after modifying equation 3.4 into equation 3.5, we found good agreement between our data and the model, and were able to extract a K_D value of $9.4(11) \times 10^{-4} \text{M}$ at 100°C (Figure 3-9. For comparison, other groups [80] have successfully measured K_D on the order of 10^{-6}M at 25°C for monodentate carboxylic acid ligands on CdS nanocrystals.

$$\bar{I}_{em} = \frac{L_0}{L_0 + K_D} * \alpha \quad (3.5)$$

Finally, in order to test the stability of the BD-coated QDs, we subjected the samples to three heating and cooling cycles (the first cycle accounting for the ligand exchange step), each consisting of a one hour of heating step up to 100°C followed by two hours of resting period at room temperature. As shown in figure 3-10, after the initial ligand exchange, BD-coated QDs retain a high PLQY in subsequent heating events.

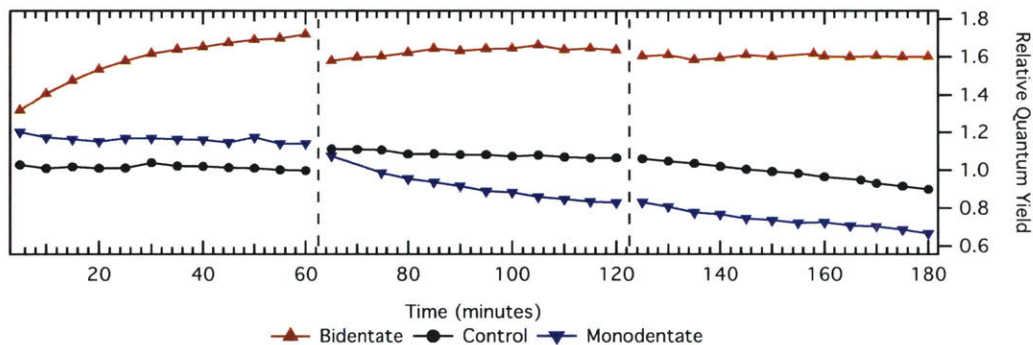


Figure 3-10: Heating Cooling Cycle. Ligand binding isotherms at 100°C for No-Ligand (black), BD (red) at $2.63 \times 10^{-2}M$, and MD (blue) at $2.63 \times 10^{-2}M$. The vertical dash-line represents a resting period of two hours at room temperature.

3.2.3 Fluorescence Lifetimes

In order to better understand the underlying electronic mechanism responsible for the enhancement in the QD's PLQY, we calculated the photoluminescence lifetimes as a function of the extent of the ligand exchange reaction. As demonstrated in 3-11, the photoluminescence lifetimes do not change during ligand exchange except in the BD ligand case, where it mimics the rise in the photoluminescence intensity discussed above. A detailed view of this trend is shown in Figure 3-12. We combined our previous photoluminescence emission data with the present lifetime results to extract the individual radiative and non-radiative decay rates. As shown in table 3.5, it appears that better surface passivation after BD ligand exchange decreases

the non-radiative decay rate, which in turn increases the overall PLQY. Finally, we include a close-up view of the fluorescence decay at 100°C after one hour of ligand exchange for various ligands (Figure 3-13 and Table 3.7), and after cooling down to room temperature (Figure 3-14 and Table 3.6).

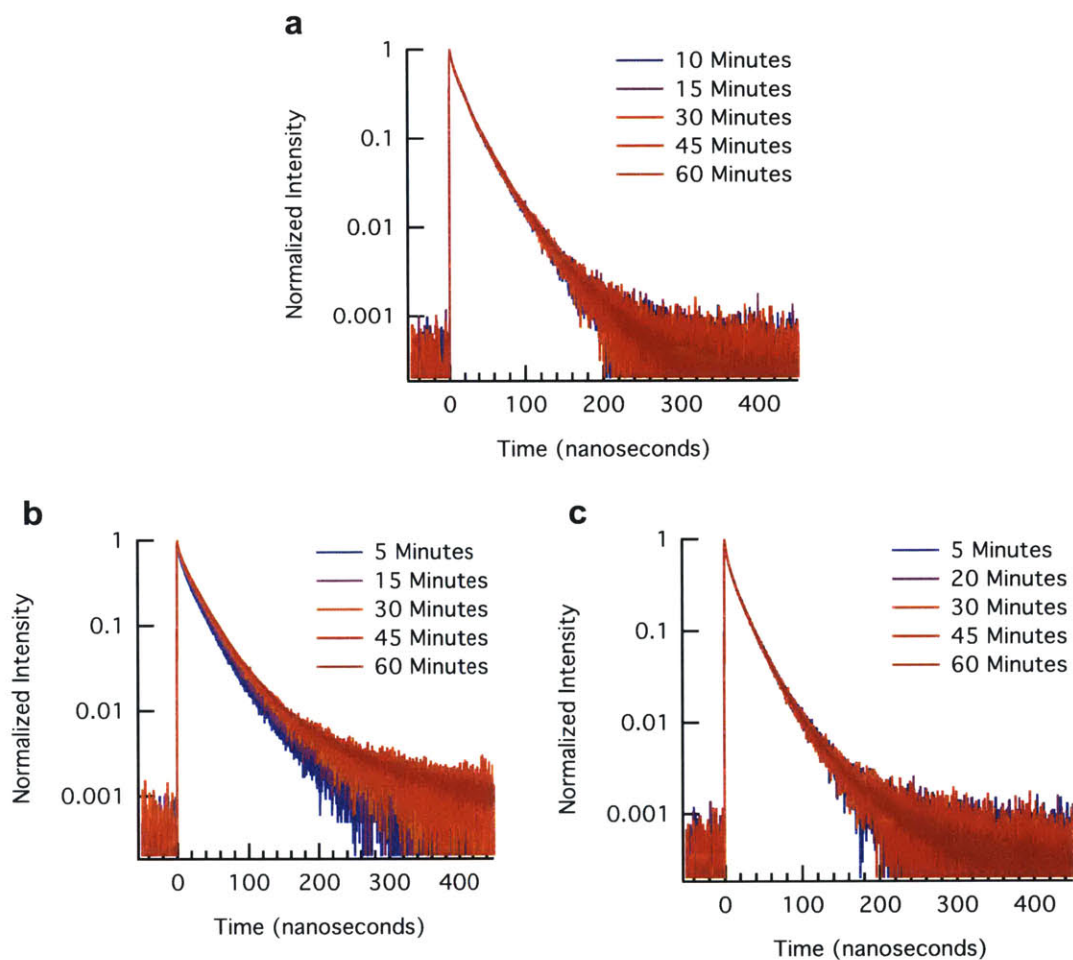


Figure 3-11: Normalized fluorescence decay curves during ligand exchange at 100°C for (a) No-Ligand, (b) BD ligand at $2.63 \times 10^{-2}M$, and (c) MD ligand at $2.63 \times 10^{-2}M$.

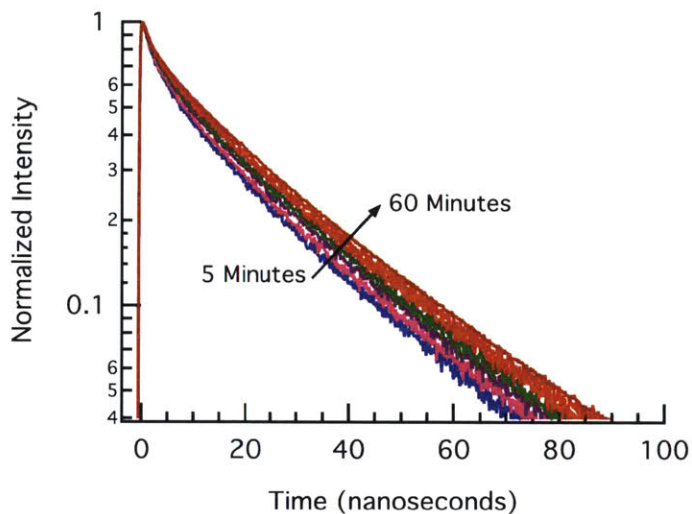


Figure 3-12: A close-up view of the fluorescence decay curves during ligand exchange at 100°C for the BD ligand at $2.63 \times 10^{-2}\text{M}$.

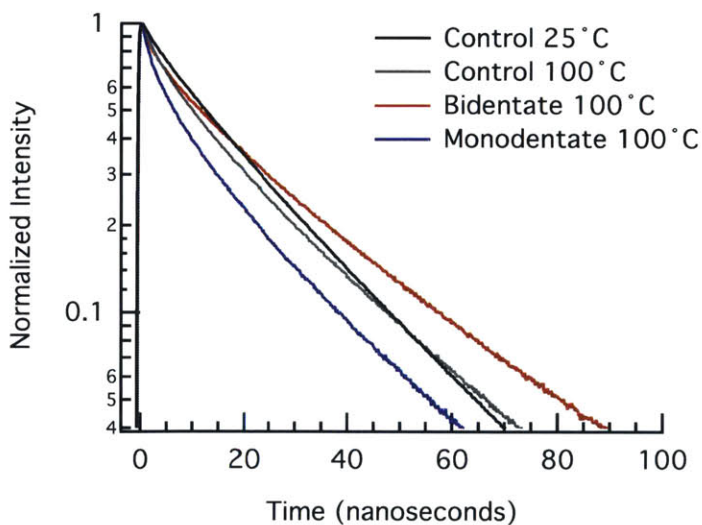


Figure 3-13: A close-up view of the fluorescence decay curves after one hour of ligand exchange at 100°C. No-Ligand (black), MD (blue) at $2.63 \times 10^{-2}\text{M}$, and BD (red) at $2.63 \times 10^{-2}\text{M}$. The (gray) line represents the fluorescence decay of the stock solution at room temperature.

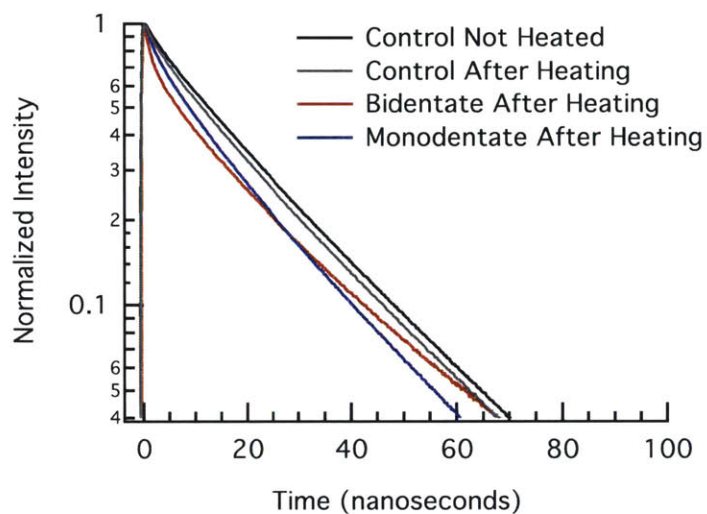


Figure 3-14: A close-up of the fluorescence decay curves at room temperature after ligand exchange. No-Ligand (black), MD (blue) at $2.63 \times 10^{-2}\text{M}$, and BD (red) at $2.63 \times 10^{-2}\text{M}$. The (gray) line represents the fluorescence decay of the stock solution at room temperature.

3.3 Conclusion

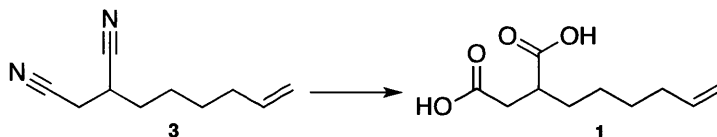
Using a systematic approach, we have successfully demonstrated that the denticity of a ligand can be used to dramatically enhance the thermal stability of colloidal QDs in solution by reducing the number of surface-related trap states. We also learned that the ligand exchange process for the BD ligand proceeds differently from that of the more traditional MD ligand, and appears to include a slow surface remodeling and passivation event, which raises the PLQY at high temperature. These results will help us design better ligands for the synthesis of more stable QDs for biological and device applications.

3.4 Chapter-Specific Acknowledgement

Dr. Lea Nienhaus performed the fluorescence lifetimes measurements and helped to design some of the other experiments.

3.5 Experimental Details

Materials and Instrumentation: All chemicals unless otherwise noted were obtained from Sigma Aldrich and used as received. All solvents were spectrophotometric grade and purchased from EMD Millipore. Absolute ethanol (200° Proof) was purchased from Koptec. Toluene ($\geq 99.5\%$), ACS reagent was purchased from Sigma Aldrich. ^1H NMR spectra, and ^{13}C NMR spectra with complete proton decoupling were recorded on a Bruker DRX 400 NMR spectrometer. Chemical shifts are reported in ppm from tetramethylsilane, and using the solvent resonance as the internal standard (CDCl_3 : ^1H NMR δ 7.26, ^{13}C NMR δ 77.16). UV-Vis absorbance spectra were collected using a Cary 5000 spectrophotometer. The emission spectra were collected using a Fluoromax-3 spectrofluorometer.



Scheme 3.1: Synthesis of the Bidentate Carboxylate Ligand (1)

2-(hex-5-en-1-yl)succinic acid (1) 7,8-dicyano-oct-1-ene (**3**) (17.44g, 0.107mol) was prepared according to the procedure described on section 2.5. It was dissolved in a 3M NaOH solution (500mL) and ethanol (400mL) in a 2000mL round bottom flask equipped with a condenser. The solution was heated to reflux, and kept under constant stirring for 18 hours. After cooling to room temperature, TLC was used to confirm that all the starting material had reacted. The solvent was evaporated *in vacuo* and the resulting solid was re-dissolved in deionized H₂O (300mL). The solution was transferred into a separation funnel and washed with diethyl ether (150mL, 3X). The aqueous layer was transferred into an Erlenmeyer flask, combined with diethyl ether (100mL), and kept under vigorous stirring. The resulting mixture was acidified to pH 2 using a 2M HCl solution. [Note: We found that adding diethyl ether during the neutralization step removes the diprotic acid from the aqueous phase as soon as it is fully neutralized, and prevents the formation of an ethyl monoester side product.]

The mixture was transferred into a separation funnel, and the product was extracted into diethyl ether (100mL, 3X). The combined organic layers were dried over Na₂SO₄, and the solvent evaporated under reduced pressure to obtain compound **1** as a white solid. (18.95g, 0.093mol, 88%) ¹H NMR (400MHz, CDCl₃) δ (ppm) 12.09 (br, 2H), 5.78 (m, 1H), 5.00 (ddt, $J_d = 17.1$ Hz, $J_d = 2.0$ Hz, $J_t = 1.6$ Hz, 1H), 4.94 (ddt, $J_d = 10.2$ Hz, $J_d = 2.1$ Hz, $J_t = 1.2$ Hz, 1H), 2.84 (m, 1H), 2.73 (dd, $J_1 = 17.1$ Hz, $J_2 = 10.8$ Hz, 1H), 2.51 (dd, $J_1 = 17.1$ Hz, $J_2 = 3.8$ Hz, 1H), 2.05 (q, $J = 6.9$ Hz, 2H), 1.71 (m, 1H), 1.56 (m, 1H), 1.45–1.33 (br, 4H); ¹³C{¹H} (100MHz, CDCl₃) δ (ppm) 181.7, 178.8, 138.6, 114.8, 41.1, 35.7, 33.5, 31.6, 28.7, 26.4; HRMS (DART/FT-MS): m/z [M + NH₄]⁺ Calcd for C₁₀H₂₀NO₄ 218.1387; Found 218.1388

Cadmium Selenide - Cadmium Sulfide Core-Shell Nanocrystals The epitaxial growth of CdS followed a modified procedure described by Chen, *et al.* [4] A solution of ODE (3mL) and OAm (3mL) was prepared in a 100mL four-necked round-bottomed flask equipped with a Hempel column, and a thermocouple that was connected to a heating circuit and a heating mantle for precise temperature control. A solution of CdSe cores (30nmols) in hexanes was injected into the mixture, and the resulting reaction solution was degassed under vacuum (<200mTorr) for one hour at room temperature, and constant stirring. The temperature was raised to 120°C, and degassed for an additional 20 minutes to completely remove the hexanes, and any trace of water and oxygen. The reaction flask was filled with N₂ gas, and the temperature was raised to 310°C and held constant throughout the infusion of the CdS precursor materials. During the heating step, and when the temperature reached 240°C, the infusion of cadmium and sulfur precursor solutions was initiated using a syringe pump, and set to proceed at a rate such that the total material required for four monolayers was injected in two hours. Once the infusion was completed, oleic acid (1mL) was swiftly injected into the mixture, and the solution left to anneal for one hour. The heating mantle was removed and the reaction flask was rapidly cooled to room temperature with the aid of an air blower. The nanocrystals were precipitated from the growth solution using acetone, and separated from the mother liquor using centrifugation (7,500 RPM, 5 minutes). The resulting near-colorless super-

natant was discarded. The nanocrystals were purified through a second precipitation event using hexanes (solvent), and acetone (anti-solvent). Finally, the nanocrystals were dispersed in hexanes and stored at room temperature.

High Temperature Experiments All high-temperature experiments were performed using a Type-54FL water jacketed fluorescence cell purchased from Firefly Sci. In order to heat up the sample, hot silicon oil was flowed through the cuvette in a circuit using a peristaltic pump. A thermocouple was periodically used during the course of an experiment to verify that the temperature was kept constant at 100°C.

Fluorescence Measurements All fluorescence measurements were performed using a 405 nm excitation, an entrance and exit slit of 1nm, and collecting from 450-700nm.

Photoluminescence Lifetimes Measurements The photoluminescence lifetimes are determined by time-correlated single-photon counting (TCSPC). To measure the lifetime decay dynamics, samples are excited at $\lambda=405$ nm, using the emission of a pulsed diode laser (PicoQuant LDH-C 400). For elevated temperature lifetimes, excitation occurs through a train of 100 ps FWHM pulses at a frequency of 1 Mhz, and an incident power of 100 nW over a 150 μ m spot size. This excitation power was chosen to ensure that the probability of detecting a photon during a single excitation pulse was ca. 1%, well below the 5% threshold above which pile-up artifacts cause inaccuracies. For room temperature lifetimes, the excitation power was adjusted to obtain a 5% count rate. The kinetics are effectively independent of incident power at the excitation powers used. Scattered excitation laser light was removed with a 425 nm long pass filter (Edmund Optics). Photon arrival times which result in the decay histogram were recorded with a PicoQuant PicoHarp 300.

Photoluminescence Quantum Yield (PLQY) Measurement The PLQY was measured using a Labsphere integrating sphere, a chopper working at 210 Hz in association with a Stanford Research Systems lock-in amplifier, and a 5 mW, 405 nm laser and a calibrated Si for QDs emitting in the visible or a 25 mW. A glass filter was also used to spectrally separate the photoluminescence from the excitation source.

3.6 Appendix I: Tables

Solution	[Ligands]	$\frac{[\text{Ligands}]}{[\text{NCs}]}$
1	$2.63 \times 10^{-2}\text{M}$	4.12×10^5
2	$1.32 \times 10^{-2}\text{M}$	2.06×10^5
3	$6.58 \times 10^{-3}\text{M}$	1.03×10^5
4	$3.29 \times 10^{-3}\text{M}$	5.15×10^4
5	$1.64 \times 10^{-3}\text{M}$	2.57×10^4
6	$8.22 \times 10^{-4}\text{M}$	1.28×10^4

Table 3.1: Characteristics of prepared xperimental samples following a two-fold serial dilution.

84

Time (Minutes)	Control	Bidentate											
	25°C	100°C											
		5	10	15	20	25	30	35	40	45	50	55	60
Relative Integrated Intensity	1.00	0.73	0.78	0.82	0.85	0.87	0.89	0.91	0.91	0.93	0.94	0.94	0.95
Quantum Yield	0.945	0.688	0.735	0.771	0.802	0.825	0.845	0.857	0.864	0.875	0.884	0.887	0.899

Table 3.2: Integrated emission intensity at different points throughout the ligand exchange process. Changes in PLQY were calculated after normalizing the data to the stock solution integrated emission intensity (Control 25°C). QDs were incubated at 100°C in a $2.63 \times 10^{-2}\text{M}$ BD ligand solution.

The FWHM was calculated by fitting the emission spectrum to a gaussian function and solving the following expression in

	Control		Monodentate	Bidentate
	25°C	100°C		
Emission Maxima (nm)	595	604	603	602
FWHM (nm)	21	24	23	24
Relative Integrated Intensity	1.00	0.55	0.63	0.95
Quantum Yield	0.945	0.520 [†]	0.595 [†]	0.898 [†]

Table 3.3: Integrated emission intensity after 60 minutes of ligand exchange. Changes in PLQY were calculated after normalizing the data to the stock solution integrated emission intensity (Control 25°C). QDs were incubated at 100°C in a 2.63×10^{-2} M BD or MD ligand solution.

terms of the standard deviation.

$$FWHM = 2\sqrt{2\ln 2}\sigma \quad (3.6)$$

	Control		Monodentate	Bidentate
	Not Heated	After Heating		
Emission Maxima (nm)	595	595	593	593
FWHM (nm)	21	21	21	21
Quantum Yield	0.945	0.865	0.805	0.800

Table 3.4: A description of the main emission features and the PLQY of QDs at room temperature after ligand exchange.

Time (Minutes)	Bidentate 100°C						
	5	10	15	20	30	45	60
Average fluorescence Lifetime $\bar{\tau}$ (ns)	24.3	25.3	26.1	26.8	27.6	28.6	29.2
Average Radiative Rate \bar{k}_r (ns ⁻¹)	0.0284	0.0291	0.0295	0.0299	0.0306	0.0306	0.0308
Average Non-Radiative Rate \bar{k}_{nr} (ns ⁻¹)	0.013	0.011	0.009	0.007	0.006	0.004	0.003

Table 3.5: Evolution of the photoluminescence lifetime as a function of ligand exchange reaction time at 100°C for the BD ligand at 2.63×10^{-2} M

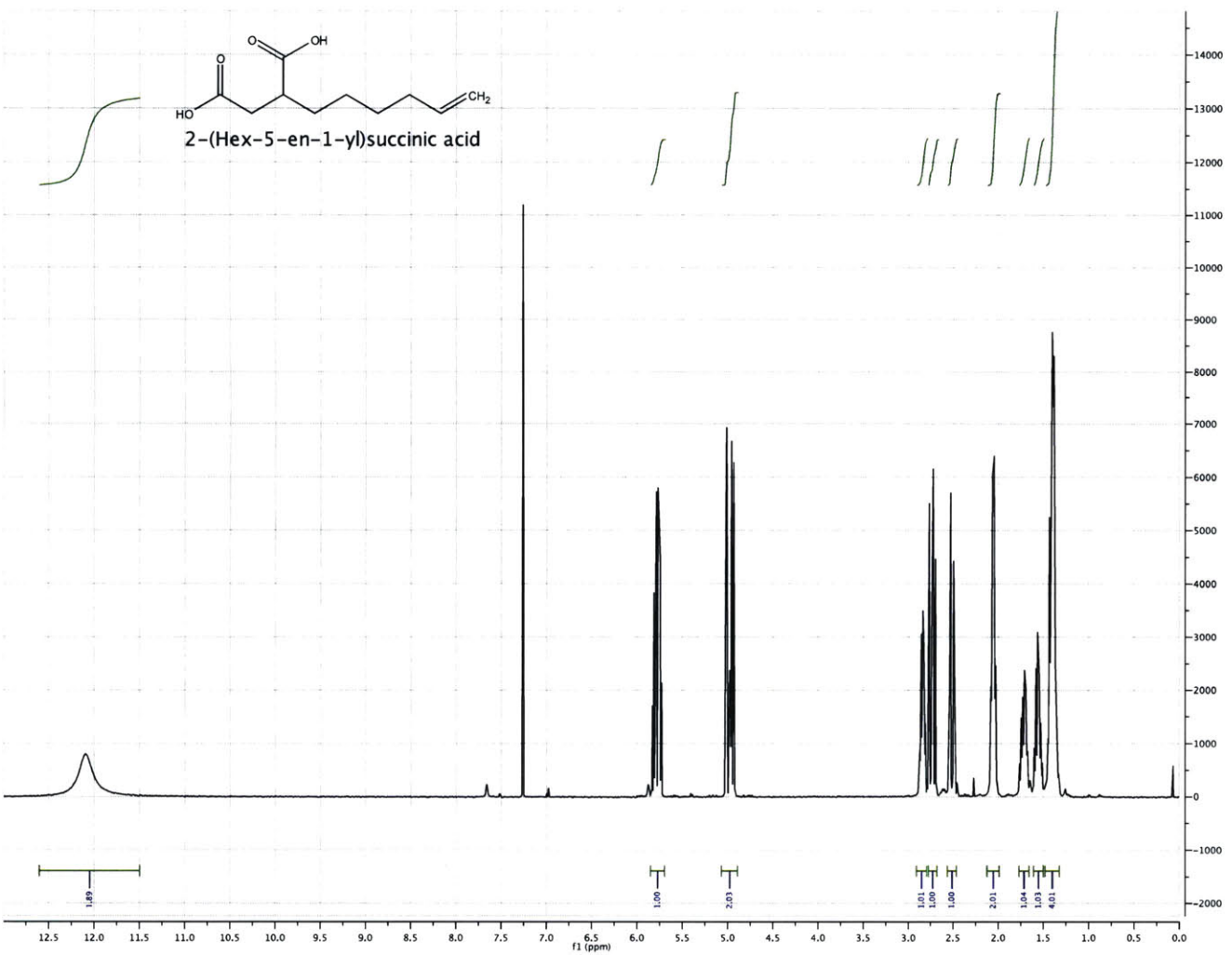
	Control	Monodentate	Bidentate	
	25°C	100°C		
Average fluorescence Lifetime $\bar{\tau}$ (ns)	22.2	23.7	20.8	29.2
Average Radiative Rate \bar{k}_r (ns ⁻¹)	0.043	0.022	0.029	0.031
Average Non-Radiative Rate \bar{k}_{nr} (ns ⁻¹)	0.002	0.020	0.020	0.003

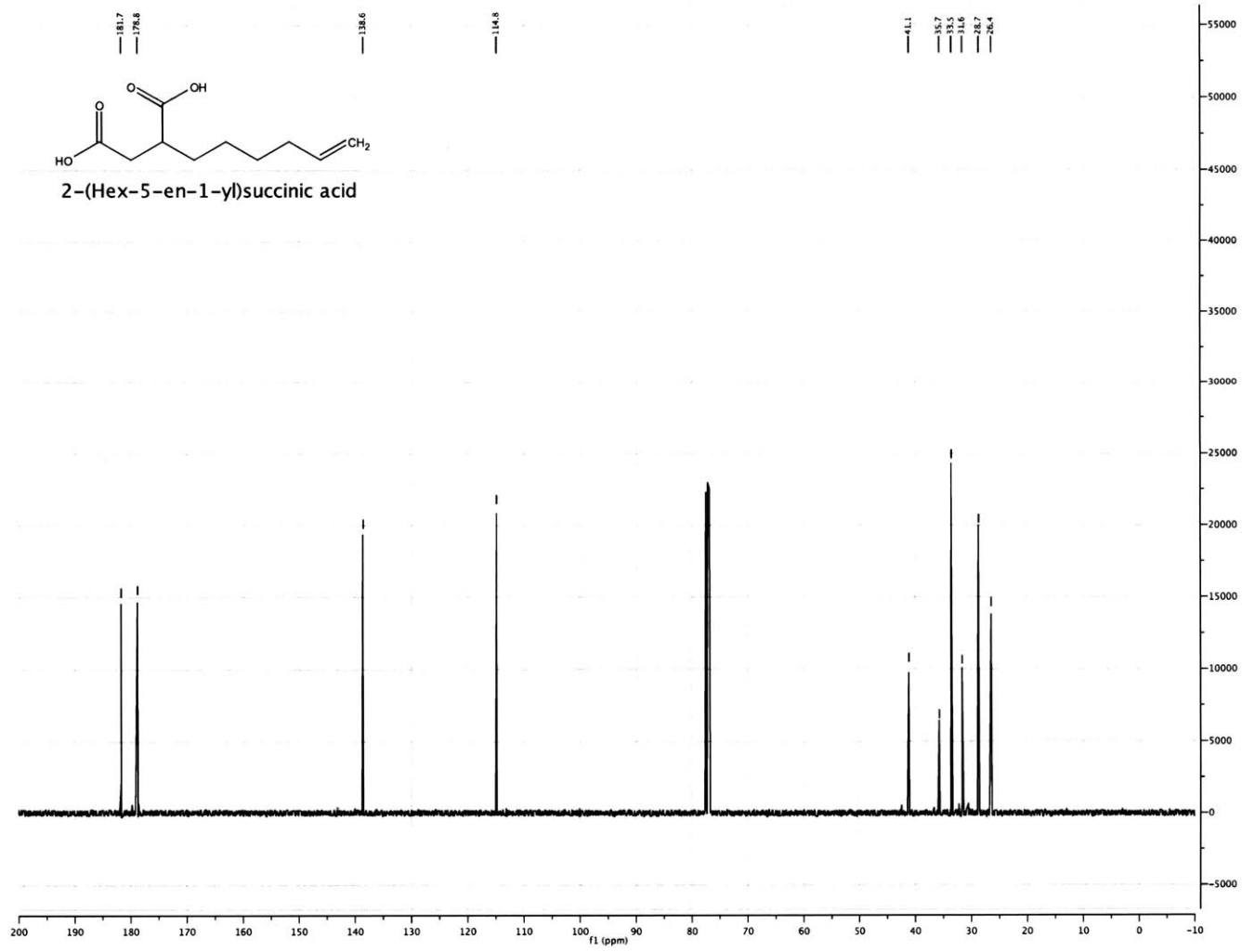
Table 3.6: A detailed description of the photoluminescence lifetime after one hour of ligand exchange at 100°C for various ligands.

	Control	Monodentate	Bidentate	
	Not Heated	After Heating		
Average fluorescence Lifetime $\bar{\tau}$ (ns)	22.2	21.6	19.6	23.1
Average Radiative Rate \bar{k}_r (ns^{-1})	0.043	0.040	0.041	0.035
Average Non-Radiative Rate \bar{k}_{nr} (ns^{-1})	0.002	0.006	0.010	0.009

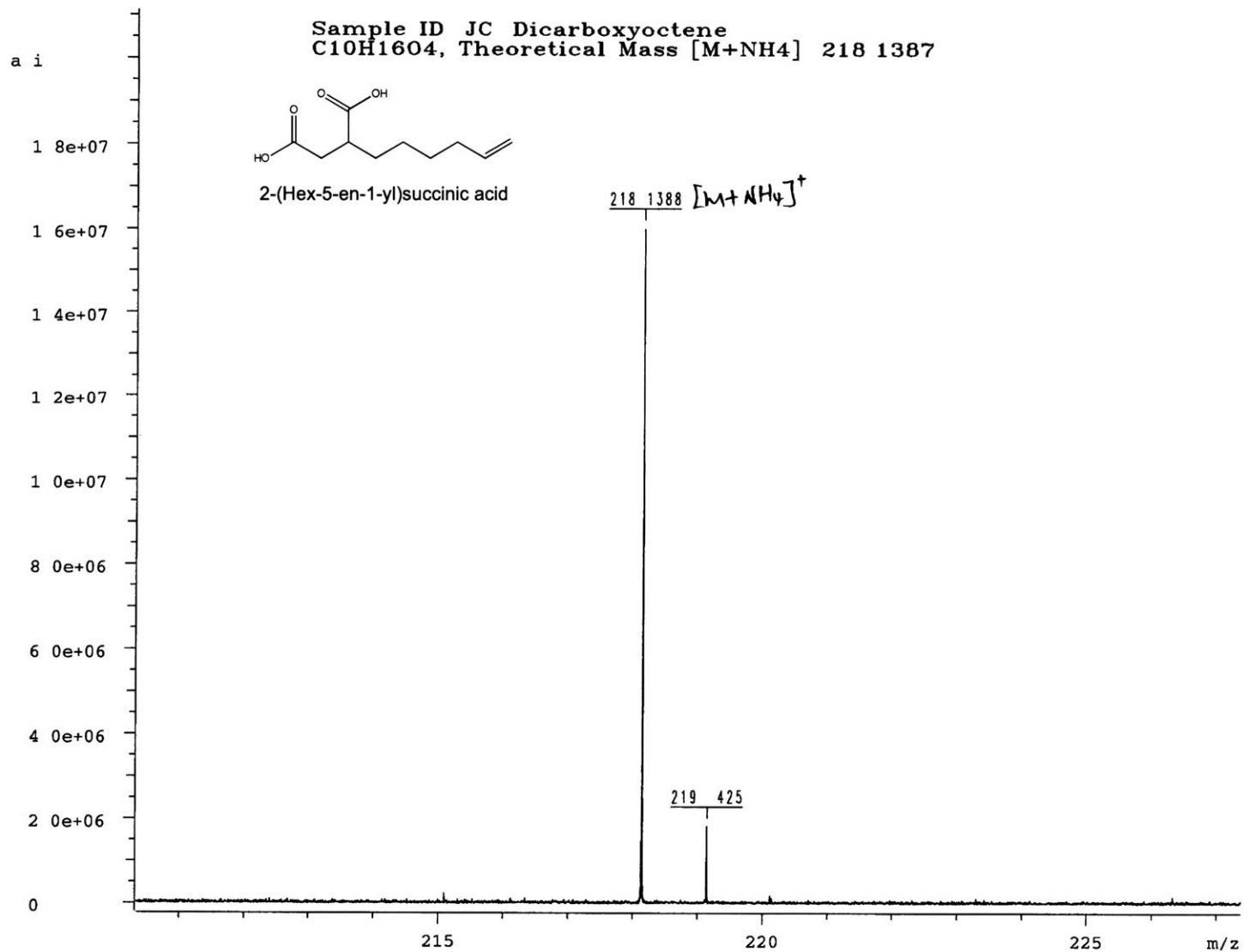
Table 3.7: A detailed description of the photoluminescence lifetime at room temperature after ligand exchange for various ligands.

3.7 Appendix II: ^1H NMR, $^{13}\text{C}\{^1\text{H}\}$ NMR, and DART/FT-MS Spectra of Chemical Compounds





06



Chapter 4

The Furan Maleimide Adduct: A New Functional Group for the Polymeric Imidazole Ligand

4.1 Background and Motivation

As discussed in section 1.4, the PIL polymer has led to the development of new water-soluble QDs that satisfy many of the requirements for biological applications, which include a small size, high PLQY, a functional group for derivatization, high stability and low non-specific binding. Unfortunately, the steps required to conjugate targeting and sensing molecules to PIL-coated QDs have been limited to reactions that involve either amines or thiols, which also possess a strong affinity for the surface of QDs. In recent years, new reactive groups, such as the norbornene moiety for “click” chemistry, have been added to the PIL in an effort to make QDs accessible to a broader range of applications and enhance the efficiency of coupling. These improvements, however, did not remove the limitations described above, but instead relied on the post-polymerization modification of amine-containing monomers to generate derivatizable-QDs. Although in theory, new monomers for derivatization can be added to PIL during polymerization, in practice the harsh radical conditions limit

the number of functional groups that can be ultimately used for this purpose. In this chapter, we provide a solution to this challenge with the synthesis of a new functional group for generating derivatizable-QDs that can be easily copolymerized with the rest of the PIL molecules. This new monomer represents a fresh addition to the PIL toolbox that, in concert with the other modules, greatly expands the functionality of QDs.

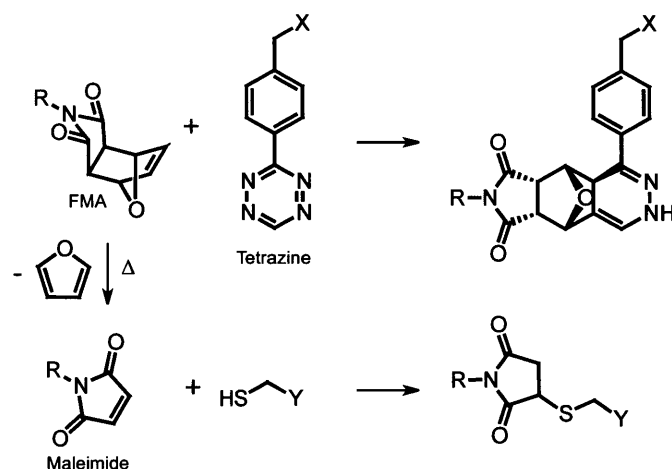
4.2 Results and Discussion

4.2.1 The Furan-Maleimide Adduct Functional Group

The ideal monomer for derivatization must carefully balance two seemingly opposite but deeply essential features, a high level of reactivity towards coupling reactions and sufficient stability to withstand free radical polymerization conditions. The furan-maleimide adduct functional group (FMA)—aka. masked-maleimide—was selected to be the cornerstone of our monomer for its ability to fulfill both of these requirements. With regard to its chemistry of coupling, the FMA group can participate in one of two complementary set of reactions, as will be discussed below.

1. Scheme 4.1 (*vertical arrow*) shows that the FMA can be activated using heat to produce maleimide, a common coupling reagent. The kinetics and, in particular, the activation energy of this rDA reaction vary depending on the stereoisomer under consideration [84, 85]. Nearly all the previous work published on FMA-containing polymers and protein-polymer bioconjugates utilize the more thermodynamically stable *exo* isomer. [86–96] These cases used extreme conditions to unmask the maleimide, such as heating the neat polymer to $>100^{\circ}\text{C}$ under vacuum or refluxing it in toluene (b.p. 111°C) for several hours. In an effort to make this reaction compatible with QDs and with a wide range of solvents, including water, we chose to work exclusively with the more reactive *endo*-FMA isomer, which starts to decompose into maleimide at $\sim 60^{\circ}\text{C}$ —a significantly lower temperature than the $\sim 110^{\circ}\text{C}$ required to decompose the

exo. As shown in scheme 4.1 (*bottom arrow*) maleimide is particularly suited to react with proteins at the cysteine position through a thiol-ene Michael addition [97]. The very low frequency of innate cysteine groups at the surface of proteins, and advances in genetic engineering has enabled researchers to introduce new cysteine groups for conjugation at desirable locations within the structure of proteins. Recent examples of this technique in the literature include proteins, such as streptavidin [98], and IgG-based biopharmaceuticals (e.g. trastuzumab) [99–101], which were later conjugated to maleimide-functionalized fluorescent dye molecules, and chemotherapeutic drugs, respectively, without disrupting their critical function. In section 4.2.5, we will use a similar approach to prepare a QD-bioconjugate construct using the Tt H-NOX(Heme Nitric oxide / Oxygen binding) protein *Thermoanaerobacter tengcongensis*—obtained as a gift from the Marletta’s Lab at UC Berkeley—equipped with a Cys-tag for conjugating to QDs and a phosphorescent Pd-containing porphyrin for oxygen sensing.



Scheme 4.1: Reactivity of the FMA functional group.

- Also, as shown in scheme 4.1 (*top arrow*), FMA can act as a dienophile in the iDA reaction with Tz; a role that is analogous to that of norbornene, as previously described in section 1.5. To the best of our knowledge, we were

the first group to explore the chemical kinetics of this particular reaction. As shown in figure 4-1 and table 4.1, we measured the second-order rate constant ($k_2 = 27.55 \pm 0.01 \text{ mM}^{-1} * \text{s}^{-1}$) for the model reaction between FMA and amino-Tz, using a 20-50X molar excess of FMA and assuming the pseudo-first order approximation. Under these conditions, all tested reactions reached their half-life in < 3.5 hours, which although useful to ourselves, is not sufficiently quick to qualify this reaction as a member of the “click” chemistry repertoire—for reference, the iDA “click” cycloaddition reaction between norbornene and tetrazine occurs at a rate that is $\sim 69\text{X}$ faster ($k_2 = 1.9 \text{ M}^{-1} * \text{s}^{-1}$) than the one reported here [67]. It is worth noting that the FMA displays a high level of versatility, which rivals that of other functional groups, including norbornene, and makes it compatible with the PIL polymerization conditions, as we will see in the next section.

4.2.2 Synthesis of the BromoFMA Monomer

The PIL is crafted using RAFT (Radical Addition-Fragmentation Chain Transfer), a living radical polymerization technique that allows us to control the degree of polymerization and, in turn, the average molecular weight (M_n) of the polymer, and to achieve low polydispersity indexes (PDI) and high reaction yields. Much of the binding strength of the PIL depends on the total number of imidazole groups per chain and, consequently, on the final length of the polymer. Nevertheless, the PIL works best when its size is $\sim 14\text{kDa}$, and each polymer chain contains, on average, 15 imidazole and 15 PEG repeating units. If instead a very large polymer is used for ligand exchange, the QD’s hydrodynamic diameter would likewise increase as a result of the volume of the polymer and for biological processes, the same large polymer may also cross-link the nanoparticles with each other causing aggregation.

Unfortunately, the FMA functional group is not compatible with radical polymerizations, as its internal double bond is known to react to form branched-polymers that are unsuitable for ligand exchange. Additionally, the high temperatures that are typically used to synthesize PIL activates the rDA pathway and produces maleimide,

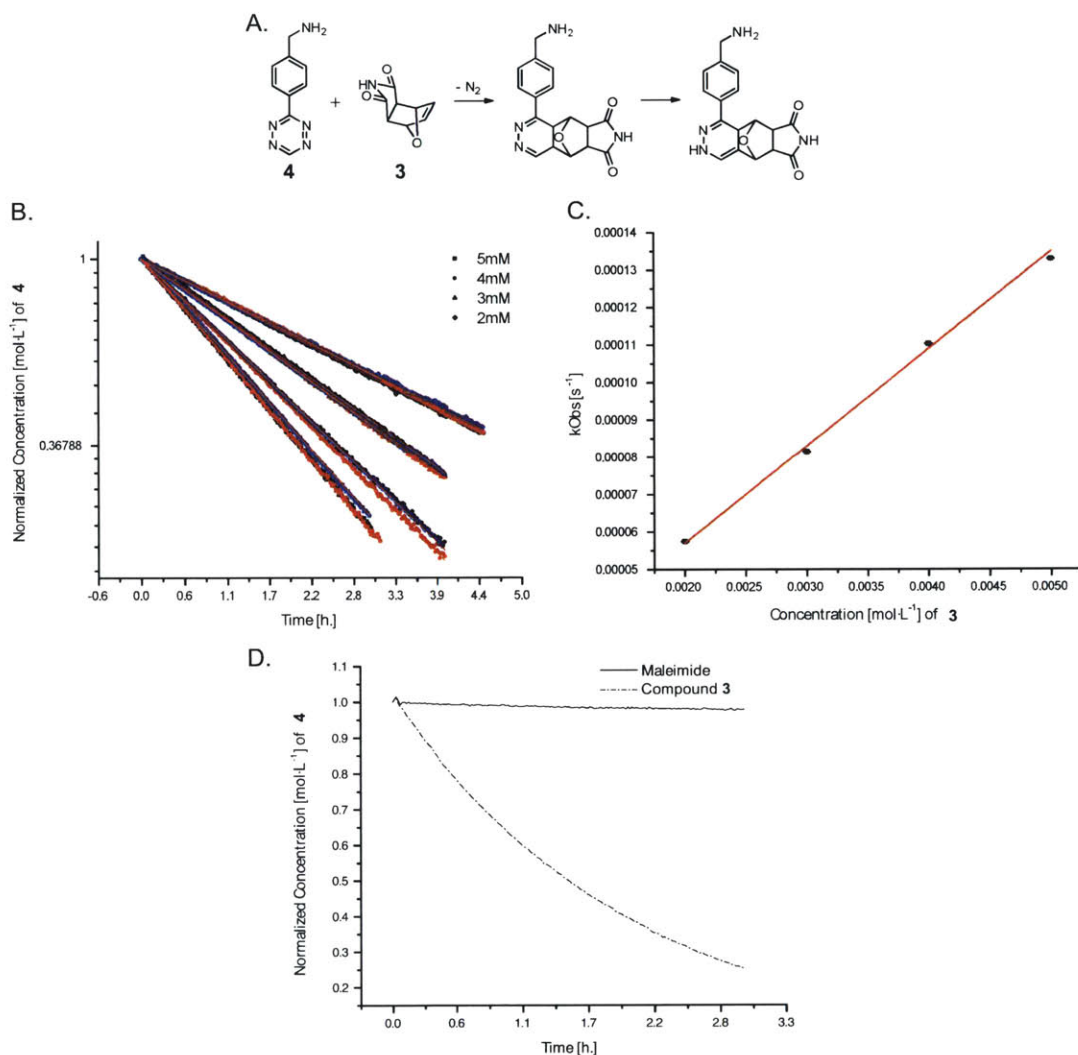
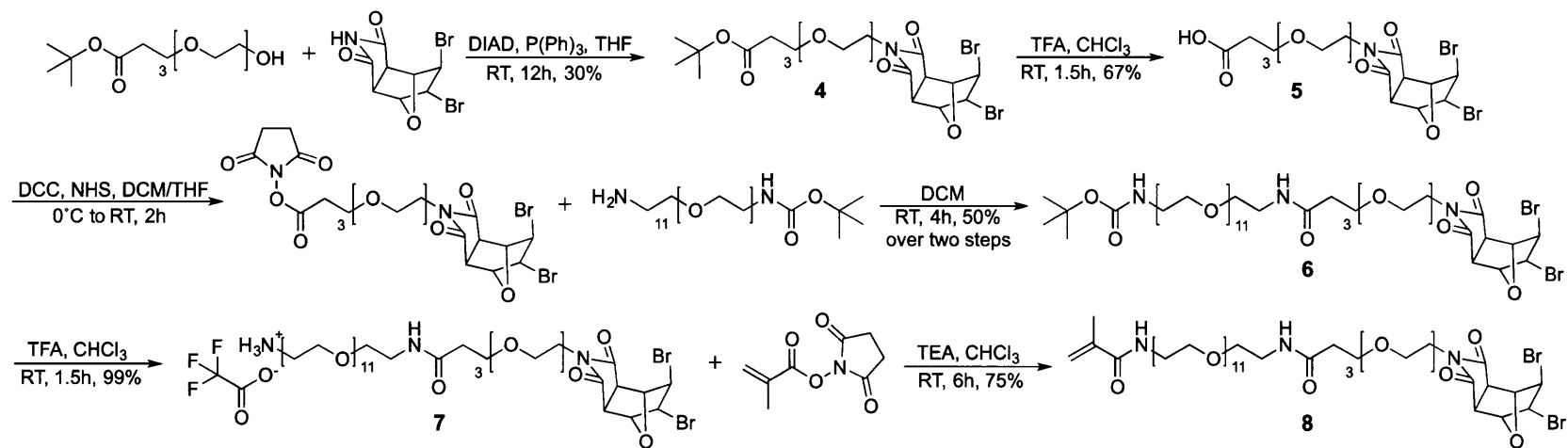


Figure 4-1: A model inverse electron-demand Diels-Alder cycloaddition between amino-Tz (**4**) and FMA (**3**). Chemical Kinetics: (*middle and bottom panels* Plot of the concentration of **4** (Initial $[4] = 1.0 \times 10^{-4}$ M) as it reacts with excess **3** (Initial $[3] = 20.0 \times 10^{-4} - 50.0 \times 10^{-4}$ M) in PBS, exhibiting a pseudo-first-order decay in time. (C) Plot of k_{obs} vs. the concentration of **3** from which a second order rate constant (k_2) value of $27.55 \pm 0.01 \text{ mM}^{-1} * \text{s}^{-1}$. (D) Plot of the concentration of **4** in the presence of equimolar amounts of **3** (----) and maleimide (—) in PBS, showing the specificity of **4** for electron-rich alkenes.



Scheme 4.2: Synthesis of the BromoFMA monomer.

which also partakes in the polymerization. In order to protect the FMA from RAFT, bromine was added to the double bond to produce vicinal dibromides. After polymerization, the olefin can be recovered in quantitative yield following a β -elimination reaction in the presence of elemental zinc. Scheme 4.2 shows the synthetic strategy to produce the BromoFMA monomer.

4.2.3 Synthesis and Characterization of the BromoFMA Homopolymer

We began our analysis of the new functional group by studying the BromoFMA homopolymer, which was synthesized according to a modified procedure based on the work of Liu, *et al.* [47] and originally designed for the synthesis of PIL. Figure

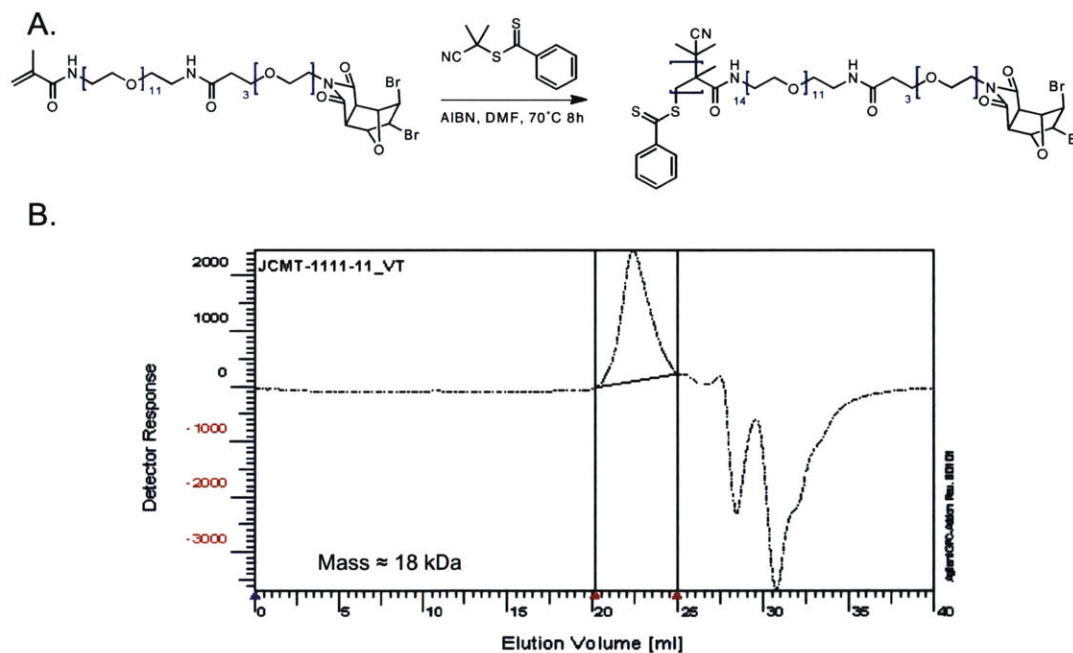


Figure 4-2: (A) Homopolymerization of the BromoFMA monomer. (B) Representative GPC chromatogram depicting a FMA homopolymer with an average molecular weight (M_n) of approximately 18kDa and a PDI ≤ 1.2 .

4-2A shows the proposed RAFT polymerization scheme, and figure 4-2B shows a representative GPC chromatogram of the resulting homopolymer. The GPC data

clearly demonstrates that the polymerization step generates a single distribution of linear polymers with $PDI \leq 1.2$ and an average molecular weight of 18kDa, which corresponds to approximately 16 repeating units per polymer chain. Overall, the physical properties of this homopolymer closely match those exhibited by PIL, which suggests that our monomer might work well with PIL. In order to regenerate the FMA functional group, the polymer was treated with elemental zinc to remove the vicinal dibromides through a reductive elimination reaction. Figure 4-3A depicts the reductive elimination reaction scheme, and figure 4-3B shows a representative ^1H NMR spectra of the homopolymer before and after treatment with zinc. These results clearly demonstrate that the de-protection step proceeds smoothly and reaches completion in under four hours.

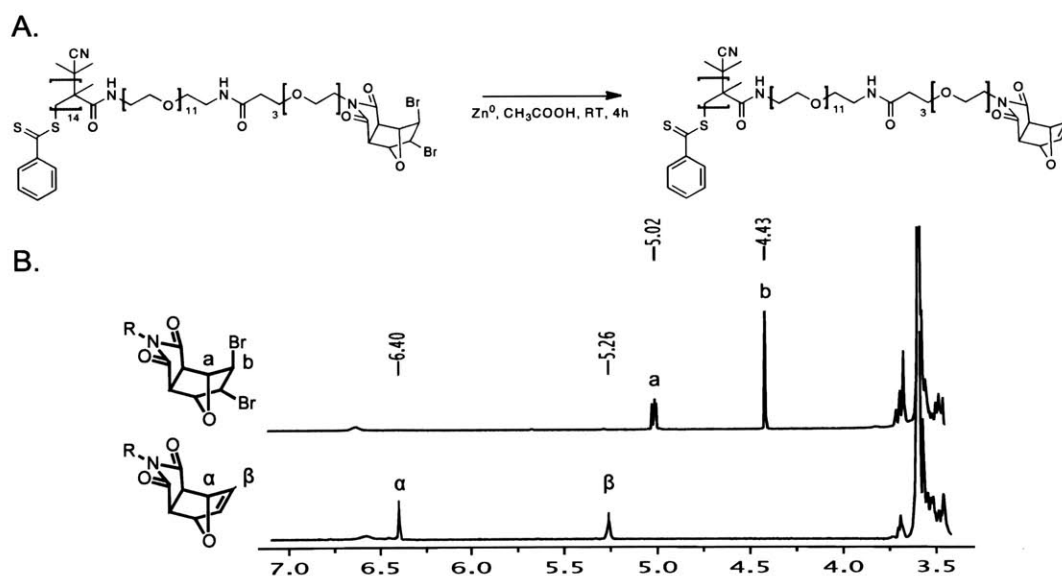


Figure 4-3: (A) Activation of the FMA functional group via a reductive elimination reaction. (B) ^1H NMR spectra showing complete conversion of BromoFMA into FMA in a polymer setting.

4.2.4 The rDA Reaction Kinetics

The next step in our analysis was focused on understanding the rDA reaction in the homopolymer (figure 4-5A). Figure 4-4 presents a series of NMR spectra taken

at different time points throughout the maleimide activation process. Interestingly, this technique, if allowed to proceed partway, can be used to prepare polymers that, on average, contain both the FMA and the maleimide functionalities, (Figure 4-4 *middle*). Using ^1H NMR spectroscopy, we measured the kinetics of this reaction at different temperatures by following the intensity of the FMA's allyl proton (5.25ppm) over time. A summary of this work is presented in table 4.2 and figure 4-5. These results suggest that, at 70°C, 50% of all the FMA groups in the polymer react in ~ 42 minutes, and 95% of the groups in ~ 3 hours.

4.2.5 Derivatization of FMA-coated QDs

After integrating the BromoFMA monomer into the PIL polymer, as shown in figure 4-6, we proceeded to test the reactivity of each of the two possible functional groups. We built a Tz-RhodamineX dye (Figure 4-7) to test the reactivity of the FMA-coated QDs. We used the FRET between the QD and dye pair to access the coupling efficiency between of the reaction. The results are shown in figure 4-8. Even though the QDs exhibit some level of non-specific binding towards the dye (upper panel, the presence of the FMA functional group, significantly enhances the amount of FRET between the pair (lower panel).

Next, in order to test the activity of the maleimide functional group we coupled a Cys-tagged *Tt* H-NOX(Heme Nitric oxide / Oxygen binding) protein *Thermoanaerobacter tengcongensis* obtained from the Marletta's group to the surface of the QDs—the protein contains a synthetic porphyrin with a high phosphorescent quantum yield that is sensitive to the presence of O_2 . As shown in figure 4-9, we see increasing conjugation is observed with increasing heating times (0, 20, 40 min.) with a deviation occurring at 60 min. as a result of maleimide hydrolysis. The absorption spectra were taken after repeated dialysis and gel filtration chromatography (GFC) to remove any unreacted starting materials.

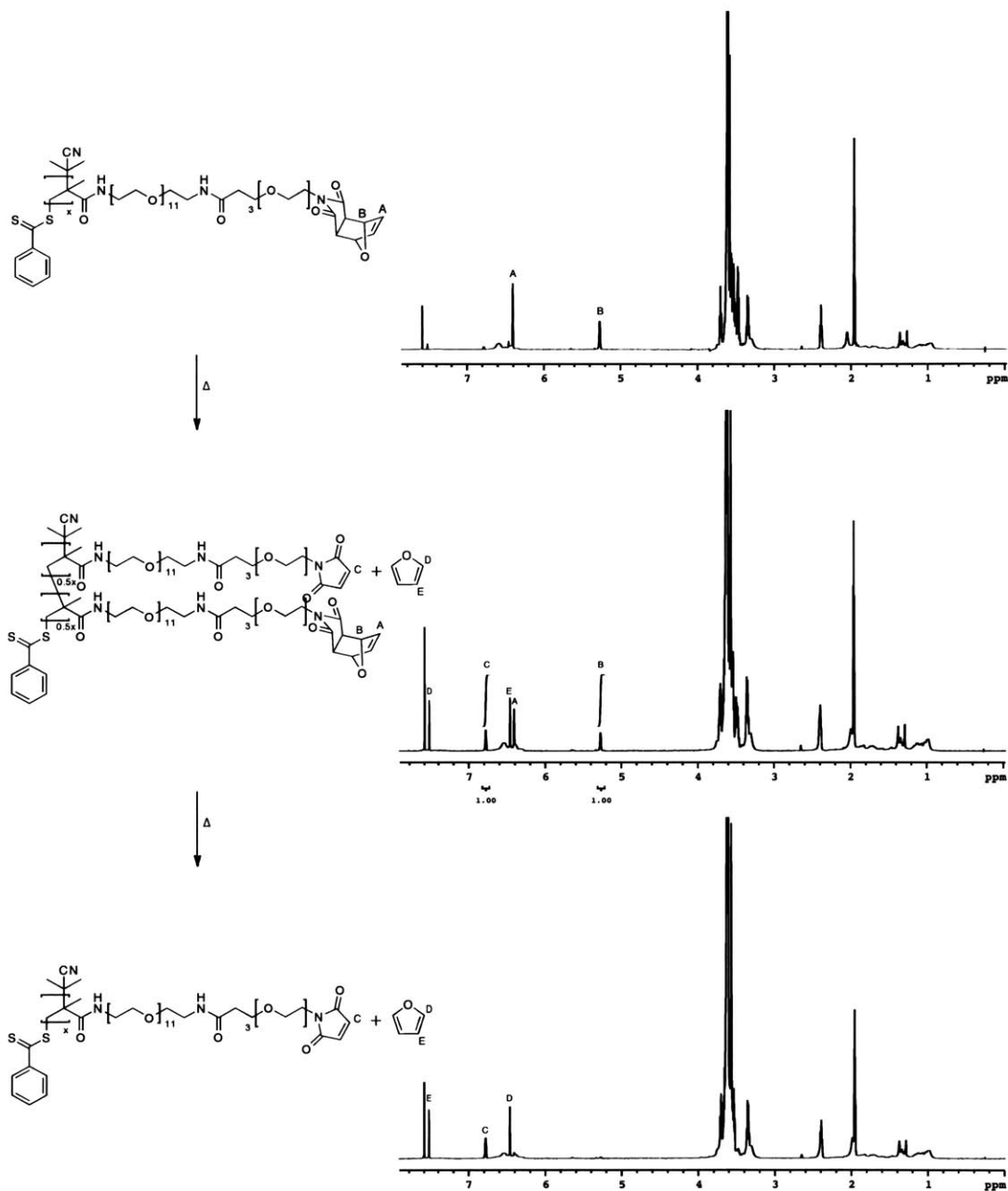


Figure 4-4: A series of ^1H NMR spectra showing the FMA homopolymer at three different points in the maleimide activation process. From *top* to *bottom*, the ratio of FMA to maleimide functional groups are 1:0, 1:1, and 0:1, respectively.

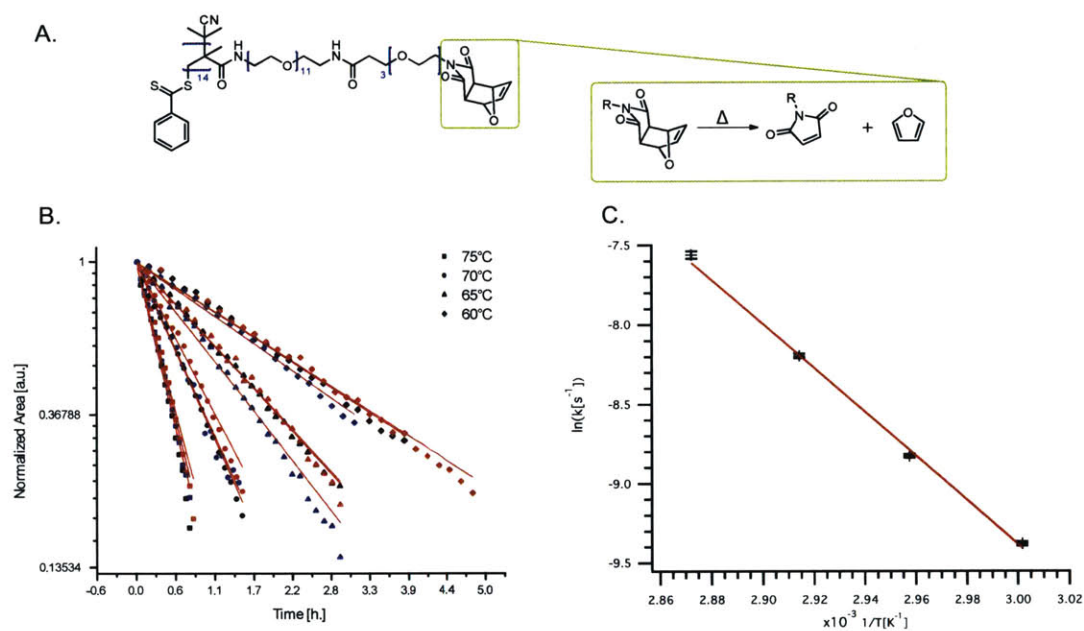


Figure 4-5: (A) Activation of the maleimide functional group via a retro-Diels-Alder reaction. Chemical Kinetics: (*bottom panel*) (B) Plot of the FMA concentration as a function of reaction time with its characteristic first-order chemical rate, at various temperatures. (C) The Arrhenius plot for this reaction, from which an activation energy (E_a) value of $-115.5 \pm 1.4 \text{ kJ} \cdot \text{mol}^{-1}$ and a pre-exponential factor (A) value of $1.05(53) \times 10^{14} \text{ s}^{-1}$ were calculated.

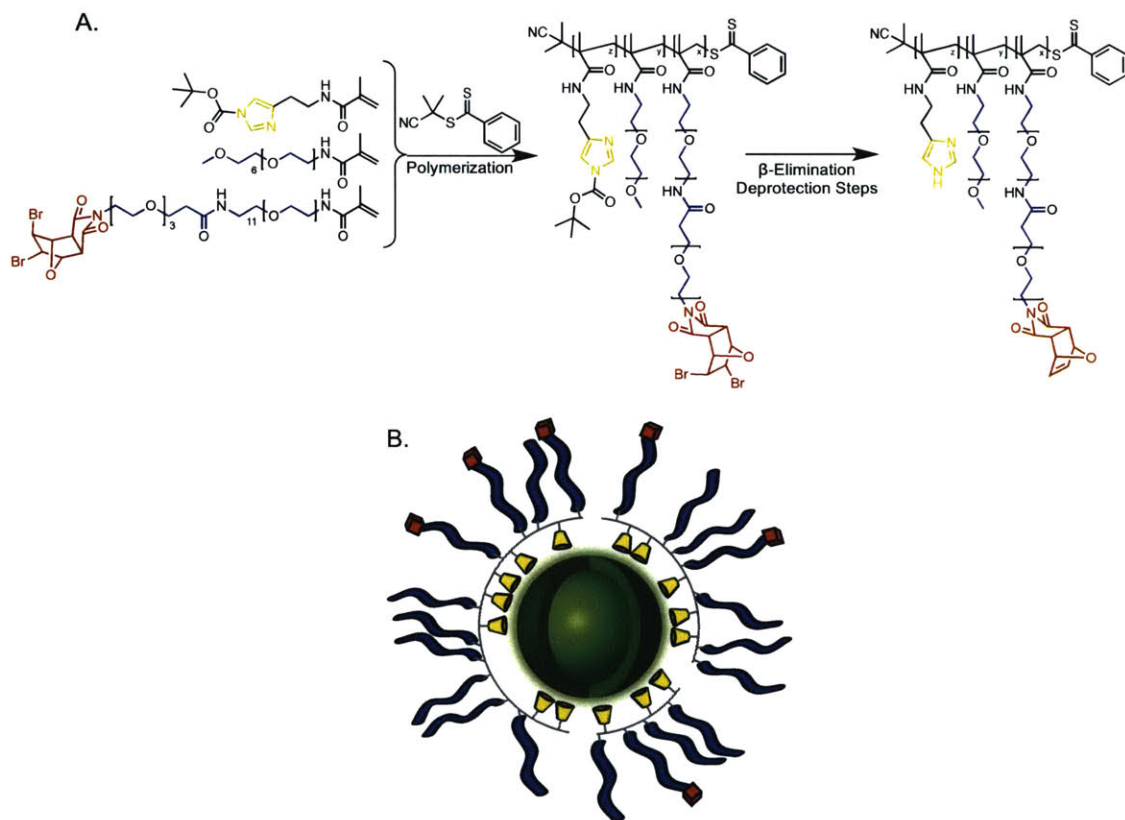


Figure 4-6: (A) Synthesis of PIL terpolymer containing the FMA functional group. (B) A schematic representation of PIL-coated QDs. The FMA functional groups are denoted by red squares.

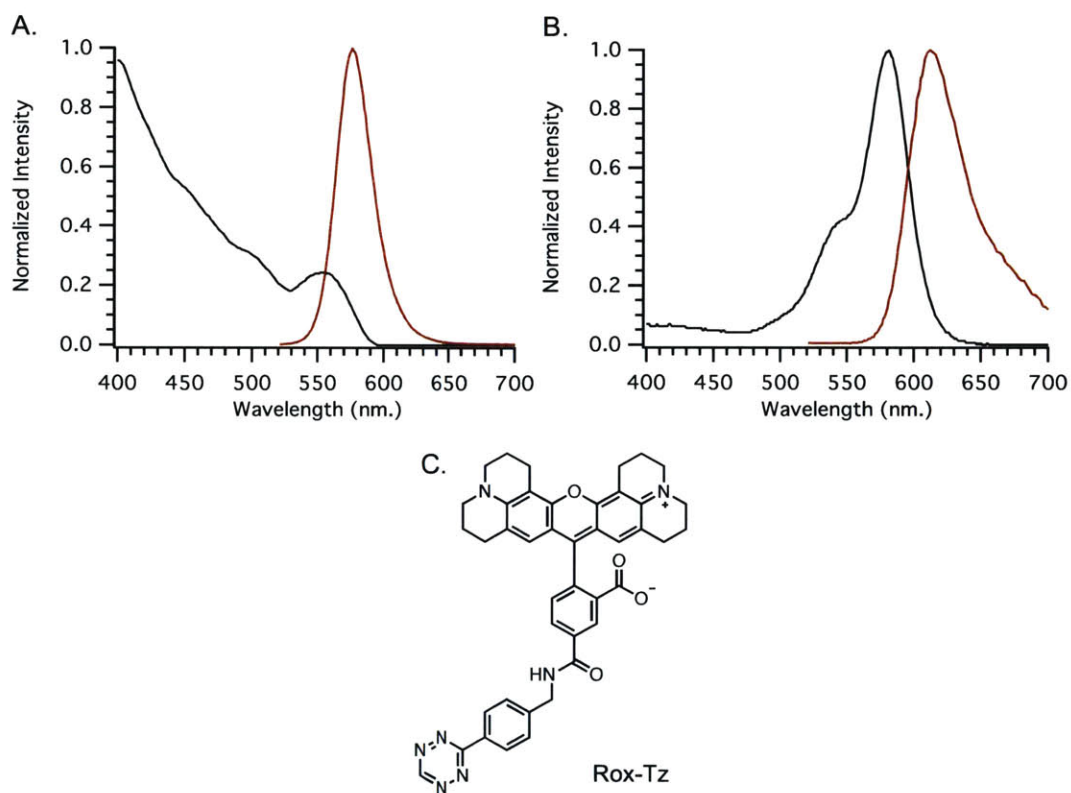


Figure 4-7: (A) Absorption (black) and emission (red) spectra of PIL-coated CdSe-CdZnS QDs in PBS. (B) Absorption (black) and emission (red) spectra of the Rox-Tz conjugate in PBS. (C) The chemical structure of Rox-Tz.

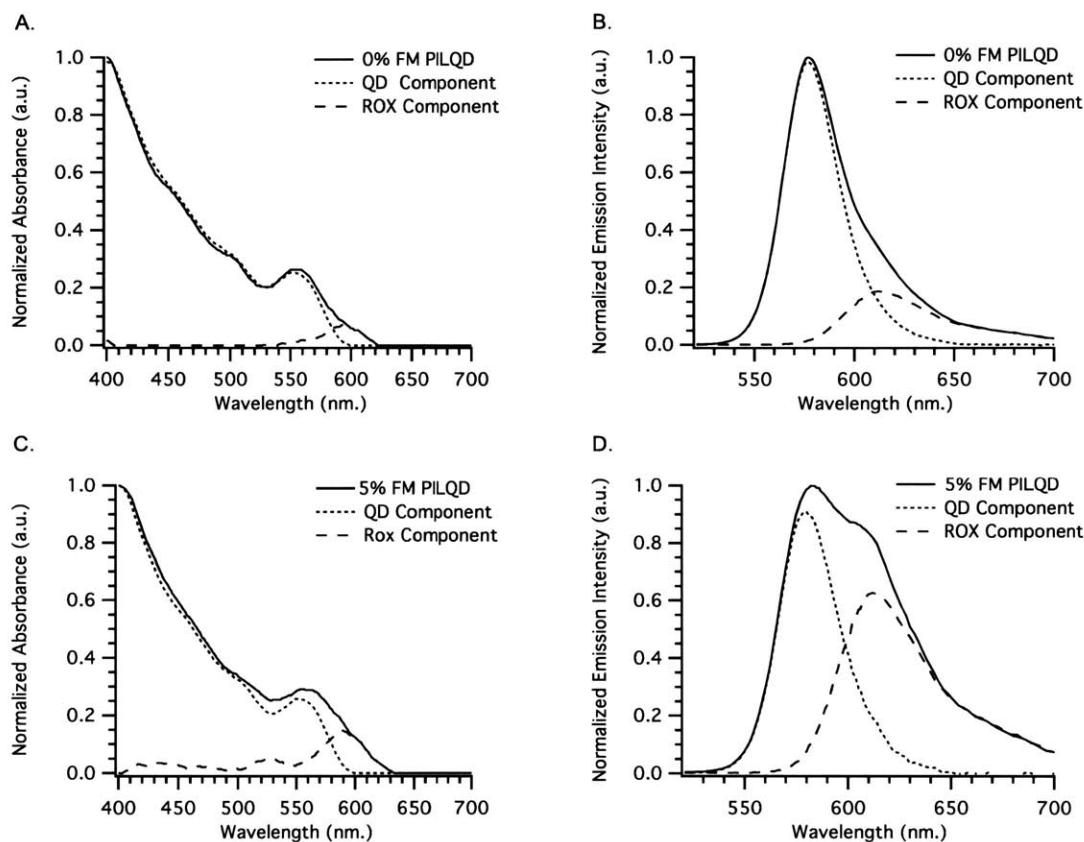


Figure 4-8: (*top panel*) Non-specific binding of Rox-Tz to PIL-coated QDs after incubation in PBS for one hour —the PIL was composed of PEG and imidazole side chains in a 1:1 molar ratio. (A) The absorption spectrum of the purified constructs (—) and of its two fundamental components: QD (- - - - -), and Rox-Tz (- - -). The QD’s contribution was calculated from the absorption spectrum of an unreacted QD control sample. The dye’s contribution was determined from the main results after subtracting the QD’s contribution. (B) The emission spectrum of the purified constructs (—) and of its two fundamental components: QD (- - - - -), and Rox-Tz (- - -). The dye’s contribution was calculated from the emission spectrum of the original unconjugated sample. The QD’s contribution was determined from the main results after subtracting the dye’s contribution. (*bottom panel*) Covalent conjugation of RoxTz to PIL-coated QDs after incubation in PBS for one hour —the PIL was composed of FMA, PEG and imidazole side chains in a 5:45:50 molar ratio. (C) Absorption and (D) emission spectra of the purified constructs. The the two characteristic components of the spectra were calculated as described above.

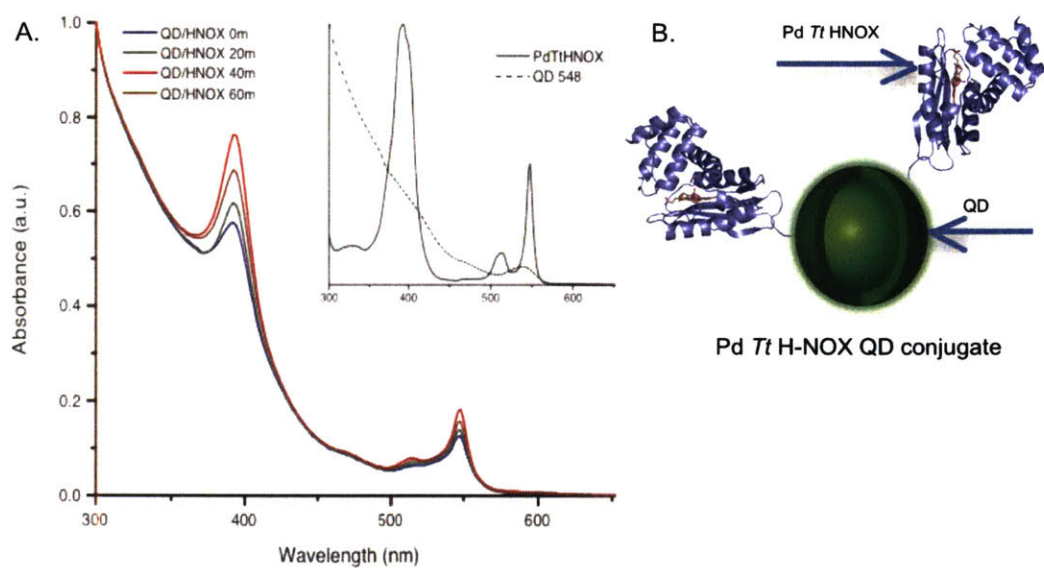


Figure 4-9: (A) Normalized absorption spectra of the purified QD-Pd *Tt*HNOX bioconjugates, each prepared from QDs with varying degrees of activated maleimide. Inset: Normalized absorption spectra of the individual species in PBS before thiol-ene coupling. (B) Schematic representation of the Pd-*Tt*HNOX-QD bioconjugate.

4.3 Conclusion

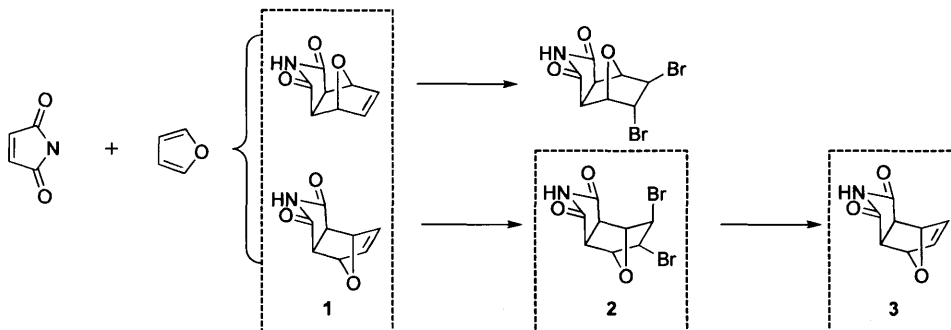
We have developed a new monomer for the derivatization of PIL-coated QDs. The monomer possesses the FMA functional group that is reactive towards tetrazine groups and, upon thermal activation, towards thiols. We also have demonstrated its utility after conjugating a tetrazine-functionalized dye molecule and a Cys-tagged protein to the surface of QDs.

4.4 Chapter-Specific Acknowledgements

Michael Winter from the Marletta Lab at UC Berkeley generously provided the Pd-*Tt* H-NOX protein. Dr. Elizabeth Karnas from the Nocera Lab at MIT helped with the synthesis and characterization of the QD-Pd-*Tt* H-NOX bioconjugate.

4.5 Experimental Details

Materials and Instrumentation: All chemicals unless otherwise noted were obtained from Sigma Aldrich and used as received. All solvents were spectrophotometric grade and purchased from EMD Millipore. Absolute ethanol (200° Proof) was purchased from Koptec. Flash column chromatography was performed using a Teledyne Isco CombiFlash Companion. ^1H NMR spectra, and ^{13}C NMR spectra with complete proton decoupling were recorded on a Bruker DRX 400 NMR spectrometer. Chemical shifts are reported in ppm from tetramethylsilane, and using the solvent resonance as the internal standard (CDCl_3 : ^1H NMR δ 7.26, ^{13}C NMR δ 77.16; and d_6 -DMSO: ^1H NMR δ 2.50, ^{13}C NMR δ 39.52).



Scheme 4.3: Synthesis of the *endo*-BromoFMA and the *endo*-FMA. Major differences in solubility between the two BromoFMA stereoisomers permit the exclusive separation of the *endo*-BromoFMA.

Compounds **1** and **2** were prepared using a method based on the works of Berson, et al. [102], and Rulisek, et al. [85]. The ^1H NMR spectra of these compounds matched the previously reported values.

Compound 1 Chilled furan (100mL, 1.38mol) was added to maleimide (13.38g, 0.138mol) and the resulting solution stirred at room temperature for 12 hours. Compound **1** was obtained as a white solid precipitate, which was collected, using a fritted glass filter funnel, washed with ethyl acetate (10mL, 2X), and, finally, dried under high vacuum. (20.99g, 0.127mol, 92% yield): mixture of *exo* and *endo* (3:5, respectively) ^1H NMR (400MHz, d_6 -DMSO) MAJOR ISOMER (*endo*) δ (ppm) 10.96 (br, 1H), 6.49 (m, 2H), 5.25 (m, 2H), 3.48 (m, 2H).

Compound 2 Compound **1** (20.94g, 0.127mol) was dissolved in ethyl acetate (1.4L). The sample was protected from light and kept under constant stirring. Bromine (7.51mL, 23.30g, 0.146mol, 1.15eq) was added drop-wise, and left to react at room temperature for 18 hours. The resulting crystals were collected, washed with excess ethyl acetate and diethyl ether, and dried under high vacuum to yield **2** as a white solid. (17.33g, 0.053mol, 42% yield): *endo* isomer ^1H NMR (400MHz, d_6 -DMSO) δ (ppm) 11.32 (br, 1H), 5.00 (m, 2H), 4.63 (s, 2H), 3.54 (m, 2H).

Compound 3 Zinc powder (22.13g, 0.34mol) was added over the course of 30 minutes to a suspension of **2** (11.0g, 33.9mmol) in glacial acetic acid (90mL), and the resulting mixture was kept under constant stirring for 2 hours at room temperature. The solid side-products were filtered using a fritted glass filter funnel, and washed with excess methanol. The filtrate was collected, and the solvent was evaporated under reduced pressure. The resulting solid was washed with copious amounts diethyl ether to obtain **3** as a white solid (4.30g, 0.026mol, 77% yield).

Compound 4 A freshly prepared mixture of diisopropyl azodicarboxylate (DIAD) (2.42mL, 2.49g, 12.3mmol), and triphenylphosphine (2.42g, 9.2mmol) in anhydrous THF (10mL) was added to a stirring solution of tert-butyl 12-hydroxy-4,7,10-trioxadodecanoate (2.04mL, 2.15g, 7.7mmol), and **2** (5.00g, 15.4mmol) in anhydrous THF (175mL). The reaction mixture was kept at room temperature for 12 hours, under constant stirring. The solvent was then evaporated under reduced pressure, and the resulting oil was dissolved in a mixture of ethyl acetate (12.5mL) and hexanes (12.5mL). Newly formed crystals were filtered using a fritted glass filter funnel, and washed with excess solvent. The filtrate was collected, and the solvent was evaporated *in vacuo*. The resulting oil was then purified using silica gel chromatography (ethyl acetate/hexanes gradient 1:1 to 4:1) to obtain **4** as a white semi-solid. (1.35g, 2.31mmol, 30% yield): ^1H NMR (400MHz, CDCl_3) δ (ppm) 5.04 (m, 2H), 4.45 (s, 2H), 3.71 (m, 6H), 3.60 (m, 8H), 3.50 (m, 2H), 2.49 (t, $J = 6.6$ Hz, 2H), 1.43 (s, 9H); $^{13}\text{C}\{^1\text{H}\}$ (100MHz, CDCl_3) δ (ppm) 173.3, 171.0, 86.6, 80.6, 70.7, 70.6, 70.5, 70.3, 67.0, 66.6, 50.7, 50.1, 38.4, 36.4, 28.2; HRMS (ESI/FT-MS): m/z $[\text{M} - \text{H}]^-$ Calcd for $\text{C}_{21}\text{H}_{31}\text{Br}_2\text{NO}_8$ 584.0333; Found 584.0318

Compound 5 Trifluoroacetic acid (TFA) (2mL) was added drop-wise to a solution of **4** (1.35g, 2.31mmol) in CHCl₃ (2mL), and stirred for 1.5 hours at room temperature. The solvent was then evaporated under reduced pressure, and the resulting oil was dried under high vacuum. In order to completely remove all trace of TFA, the sample was re-dissolved in CHCl₃, and dried under high vacuum for a second time. This process was repeated twice. Finally, the sample was dissolved in ethyl acetate, and placed in the freezer (-20°C) for a period of 4 hours. The solids were separated using centrifugation, the supernatant was decanted, and the pellet was collected and dried one last time to obtain **5** as a white solid. (0.83g, 1.57mmol 68% yield): ¹H NMR (400MHz, CDCl₃) δ (ppm) 5.06 (m, 2H), 4.46 (s, 2H), 3.78 (t, *J* = 6.1 Hz, 2H), 3.72 (br, 4H), 3.65 (br, 4H), 3.60 (m, 4H), 3.52 (m, 2H), 2.65 (t, *J* = 6.1 Hz, 2H); ¹³C{¹H} (100MHz, CDCl₃) δ (ppm) 175.2, 173.5, 86.6, 70.6, 70.5, 70.5, 70.4, 66.7, 66.4, 50.7, 50.1, 38.5, 34.9; HRMS (ESI/FT-MS): *m/z* [M - H]⁻ Calcd for C₁₇H₂₃Br₂NO₈ 527.9706; Found 527.9719

Compound 6 Compound **5** (0.821mg, 1.6mmol), NHS (0.21mg, 1.9mmol), DCM (6mL), and anhydrous THF (2mL) were mixed, cooled to 0°C using an ice bath, and kept under constant stirring. A solution of DCC (0.38mg, 1.9mmol) in DCM (2mL) and anhydrous THF (1mL) was added drop-wise, and the resulting solution was allowed to reach room temperature and to react for two hours. Crystals of N,N'-dicyclohexylurea that formed throughout the course of the reaction were collected and washed with DCM. The filtrate was collected and concentrated under reduce pressure to a volume of 3mL, which was added to a solution of O-(2-aminoethyl)-O'-[2-(Boc-amino)ethyl]decaethylene glycol in DCM (10mL), and allowed to react at room temperature for 4h. The solution was again filtered, the filtrate collected, the solvent evaporated *in vacuo* and the resulting oil dissolved in CHCl₃ (10mL). The organic phase was then washed thrice with water (5mL) and dried over Na₂SO₄. The solvent was evaporated *in vacuo* and the resulting solid was purified using silica gel chromatography (dichloromethane/methanol gradient 98:2 to 93:7, v/v), to obtain **6** as a clear viscous oil. (0.89mg, 0.77mmol, 50% yield) HRMS (ESI/FT-MS): *m/z* [M + H]⁺ Calcd for C₄₆H₈₁Br₂N₃O₂₀ 1156.3852; Found 1156.3881.

Compound 7 Trifluoroacetic acid (TFA) (2mL) was added drop-wise to a solution of **6** (0.89g, 0.8mmol) in CHCl₃ (2mL), and stirred for 1.5 hours at room temperature. The solvent was then evaporated under reduced pressure, and the resulting oil was dried under high vacuum. In order to completely remove all trace of TFA, the sample was re-dissolved in CHCl₃, and dried under high vacuum for a second time. This process was repeated twice to obtain **7** as a white semi-solid. The TFA salt was obtained. (0.90mg, 0.8mmol, 99% yield) HRMS (ESI/FT-MS): m/z [M + H]⁺ Calcd for C₄₁H₇₃Br₂N₃O₁₈ 1056.3326; Found 1056.3461.

Compound 8. A solution of methacrylic acid N-hydroxysuccinimide ester (167.5mg, 0.9mmol) in anhydrous THF (2mL) was added drop-wise to a stirring solution of **7** (972.4mg, 0.8mmol) and triethylamine (139uL, 1.0mmol) in anhydrous THF (10mL) and allowed to react at room temperature for five hours. The solvent was evaporated *in vacuo* and the resulting oil dissolved in CHCl₃ (10mL). The organic phase was then washed thrice with water (5mL) and dried over Na₂SO₄. The solvent was evaporated *in vacuo* and the resulting solid was purified using silica gel chromatography (dichloromethane/methanol gradient 98:2 to 93:7, v/v), to obtain **8** as a clear viscous oil. (0.70g, 0.62mmol, 75% yield) HRMS (ESI/FT-MS): m/z [M + H]⁺ Calcd for C₄₅H₇₇Br₂N₃O₁₉ 1124.3589; Found 1124.3597.

Polymerization The RAFT agent, 2-Cyanoprop-2-yl-dithiobenzoate, was purchased from Strem Chemicals, Inc. and used as received. The RAFT polymerization followed a modified procedure described by Liu, *et al.* [47] Briefly, all the monomers were kept in solution between 50-150 mg/mL in either CHCl₃ or methanol. Stock solutions of the RAFT agent and 2,2'-Azobis(2-methylpropionitrile) (AIBN) were prepared at 100 mg/mL in DMF. All reagents were weighed out volumetrically. In a typical polymerization, **8** (0.19mmol) was added to an 8 mL vial and the solvent removed *in vacuo*. Dry DMF (122uL) along with the RAFT agent (2.75 mg, 0.012mmol), and AIBN (3.05mg, 0.019mmol) were added. The resulting solution was transferred to a 1 mL ampule, which was subjected to four freeze-pump-thaw cycles and then was sealed under vacuum using a butane torch. The vial was heated to 70°C on an oil bath and the reaction left to proceed overnight. After synthesis, the contents

of the vial were transferred to an 8mL vial and diluted with methanol (250uL). The polymer was precipitated using excess diethyl ether and separated from the mother liquor using centrifugation.

Reductive Elimination The Bromo-FMA polymer (~100mg) was dissolved in glacial acetic acid (500uL). To this solution zinc powder (58mg, 0.89mmol) was added and the resulting suspension was allowed to react at room temperature for 4h under constant stirring. The solvent was evaporated *in vacuo* and the resulting solids were dispersed in H₂O (1mL). The mixture was filtered, using a 0.45um PTFE syringe filter, and the filtrate loaded onto a PD-10 desalting column, in order to remove excess zinc ions. The fractions containing the polymer were combined and the solvent evaporated under reduced pressure.

3-(*p*-Benzylamino)-1,2,4,5-tetrazine (Amino-Tz) (4) The amino-tetrazine was prepared according to the method described by Devaraj *et al.* [67].

Gel Filtration Chromatography GFC was performed on an ÄKTAprime Plus chromatography system from Amersham Biosciences equipped with a Superose 6 10/300 GL column. PBS (pH 7.4) was used as the mobile phase with a flow rate of 0.5mL/min. A single point detector working at 280nm was used for detection.

4.6 Appendix I: Tables

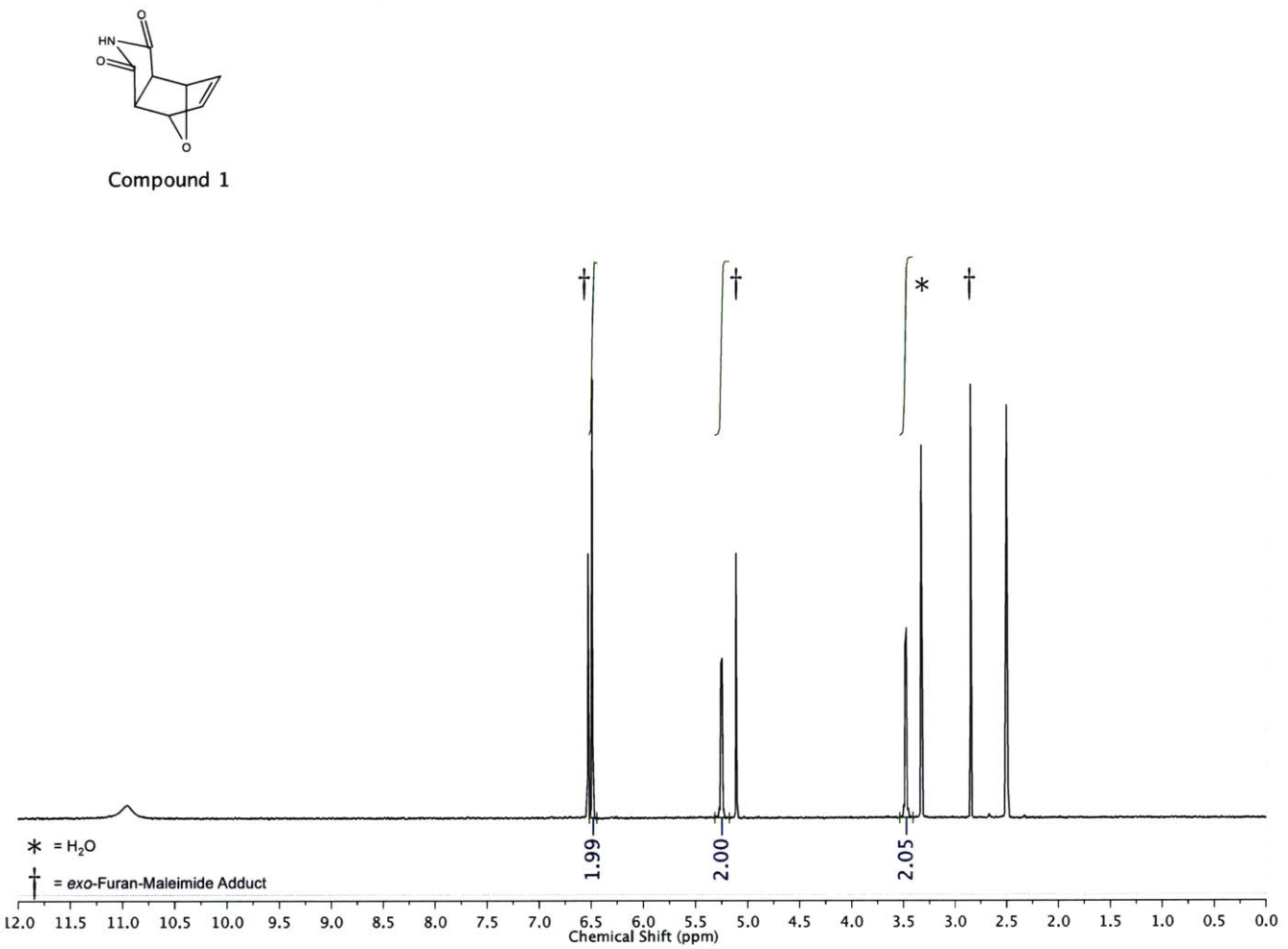
Concentration of 3 (mM)	Pseudo-First-Order Observed Reaction Rate			
	1 st Trial	2 nd Trial	3 rd Trial	Mean
2	$-5.8203(59) \times 10^{-5}$	$-5.7239(34) \times 10^{-5}$	$-5.6645(64) \times 10^{-5}$	$-5.7462(54) \times 10^{-5}$
3	$-8.0072(76) \times 10^{-5}$	$-8.2537(61) \times 10^{-5}$	$-8.1757(57) \times 10^{-5}$	$-8.1455(65) \times 10^{-5}$
4	$-1.089\,09(81) \times 10^{-4}$	$-1.128\,39(70) \times 10^{-4}$	$-1.089\,99(53) \times 10^{-4}$	$-1.102\,49(69) \times 10^{-4}$
5	$-1.3545(11) \times 10^{-4}$	$-1.3479(16) \times 10^{-4}$	$-1.2825(23) \times 10^{-4}$	$-1.3283(17) \times 10^{-4}$

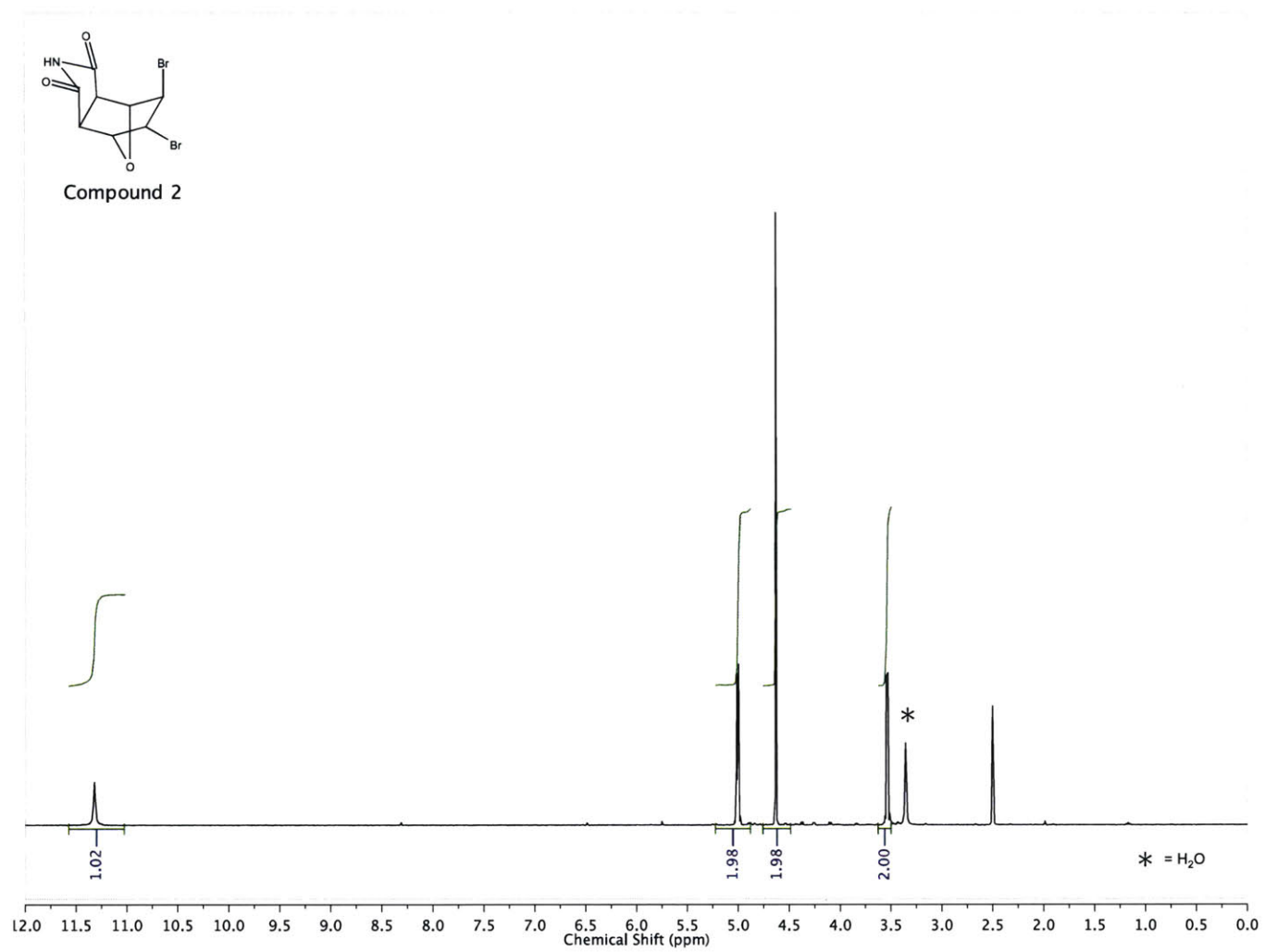
Table 4.1: The FMA and amino-Tz iDA reaction kinetics

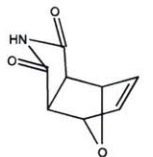
Temperature (°C)	First Order Reaction Rate (s ⁻¹)			
	1 st Trial	2 nd Trial	3 rd Trial	Mean
60	$-8.25(13) \times 10^{-5}$	$-8.153(82) \times 10^{-5}$	$-8.93(11) \times 10^{-5}$	$-8.45(11) \times 10^{-5}$
65	$-1.390(10) \times 10^{-4}$	$-1.376(15) \times 10^{-4}$	$-1.633(24) \times 10^{-4}$	$-1.466(18) \times 10^{-4}$
70	$-2.922(30) \times 10^{-4}$	$-2.498(48) \times 10^{-4}$	$-2.866(42) \times 10^{-4}$	$-2.762(40) \times 10^{-4}$
75	$-5.48(13) \times 10^{-4}$	$-4.93(13) \times 10^{-4}$	$-5.211(90) \times 10^{-4}$	$-5.21(12) \times 10^{-4}$

Table 4.2: The FMA rDA reaction kinetics

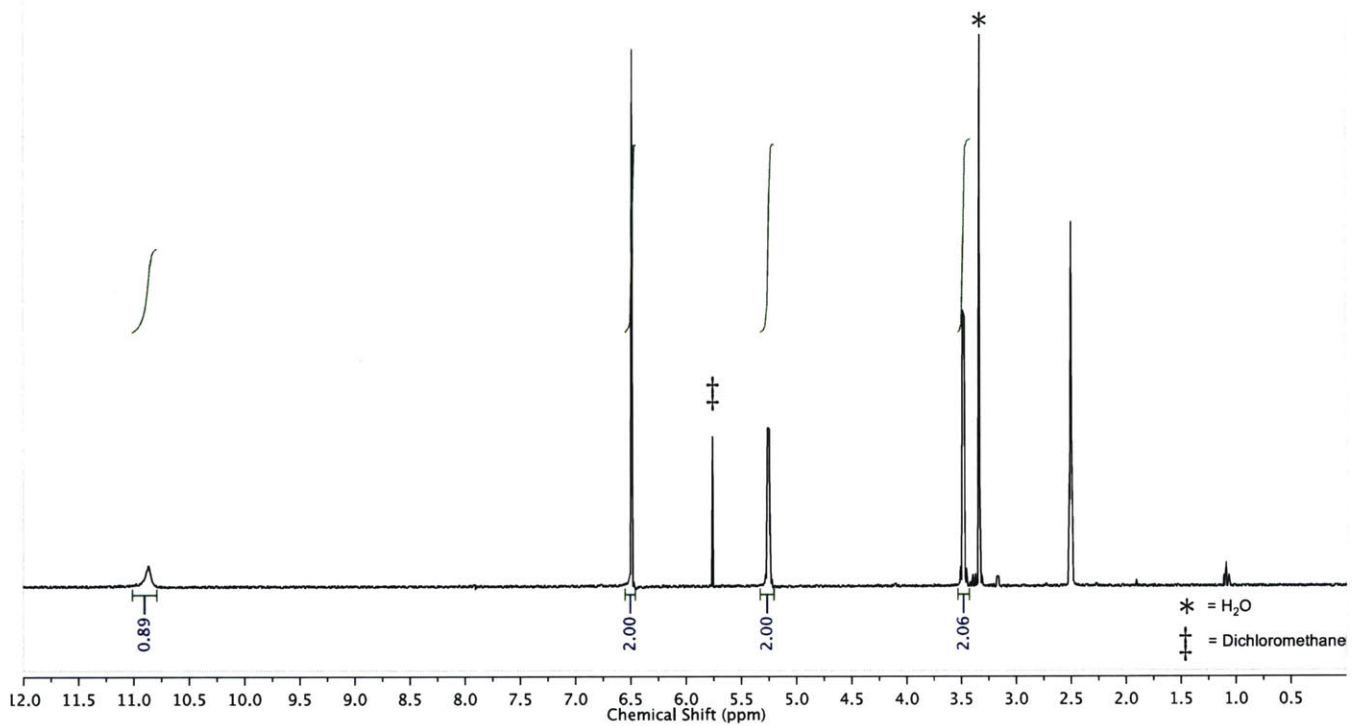
4.7 Appendix II: ^1H NMR, $^{13}\text{C}\{^1\text{H}\}$ NMR, and DART/FT-MS Spectra of Chemical Compounds

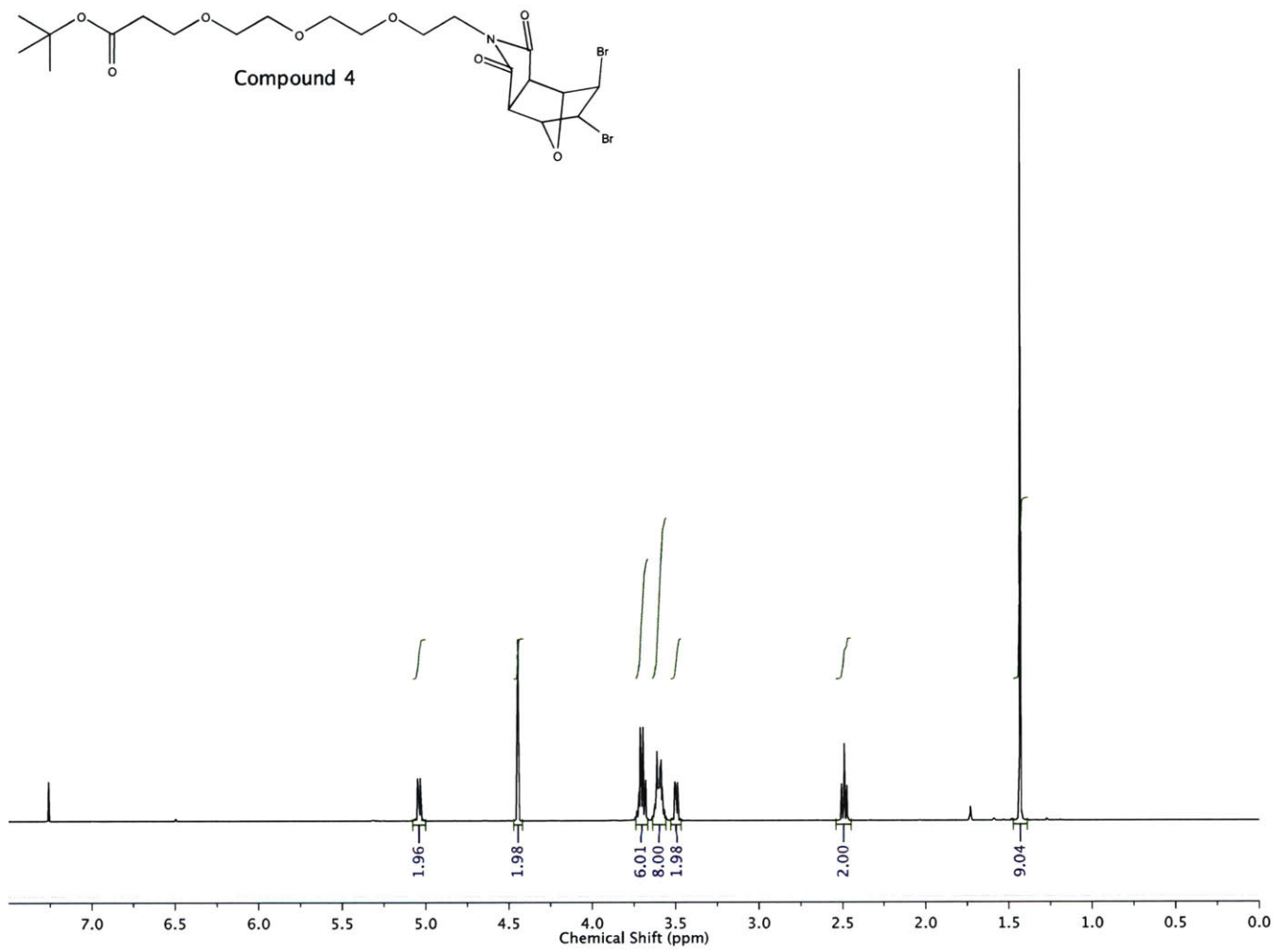


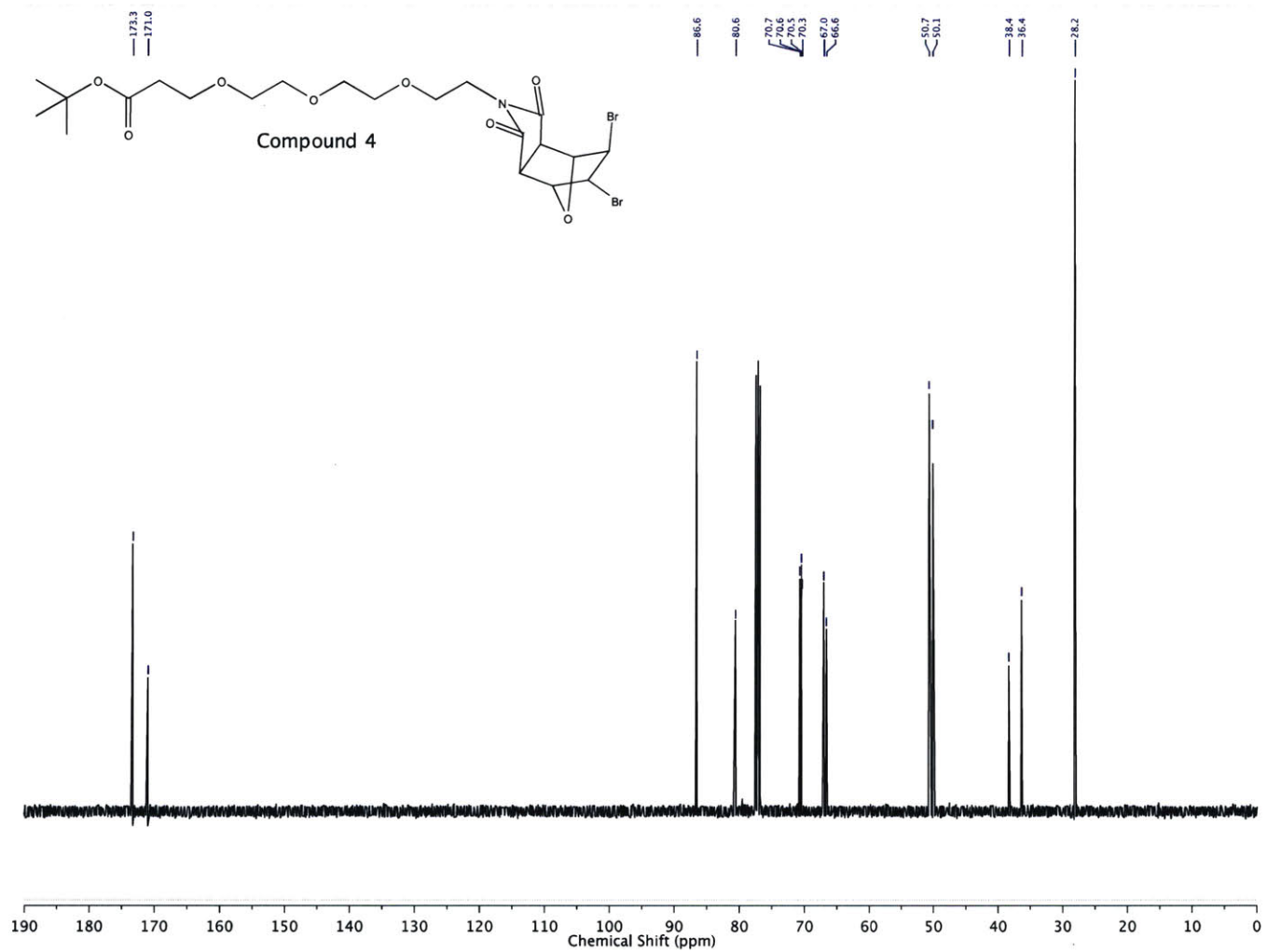


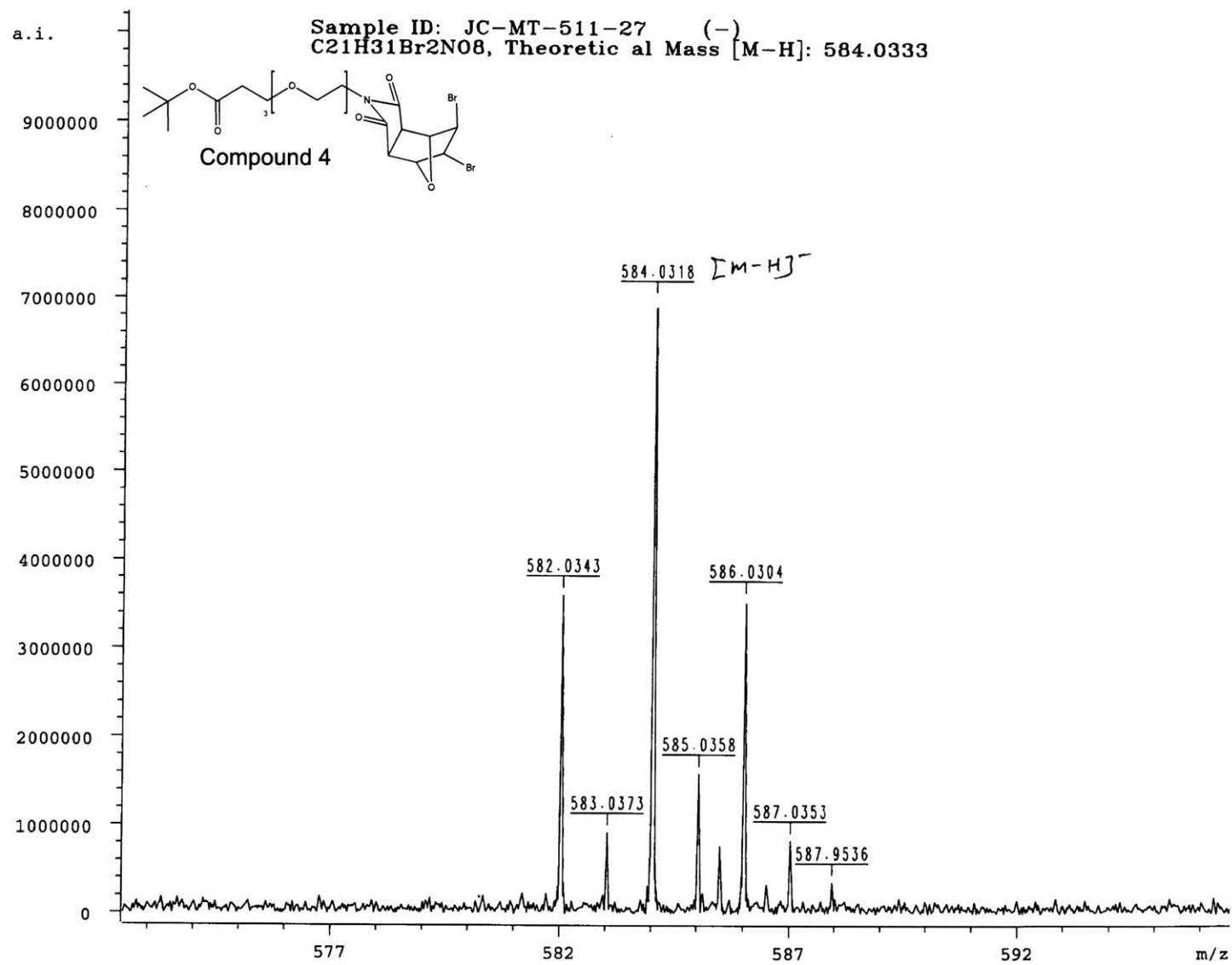


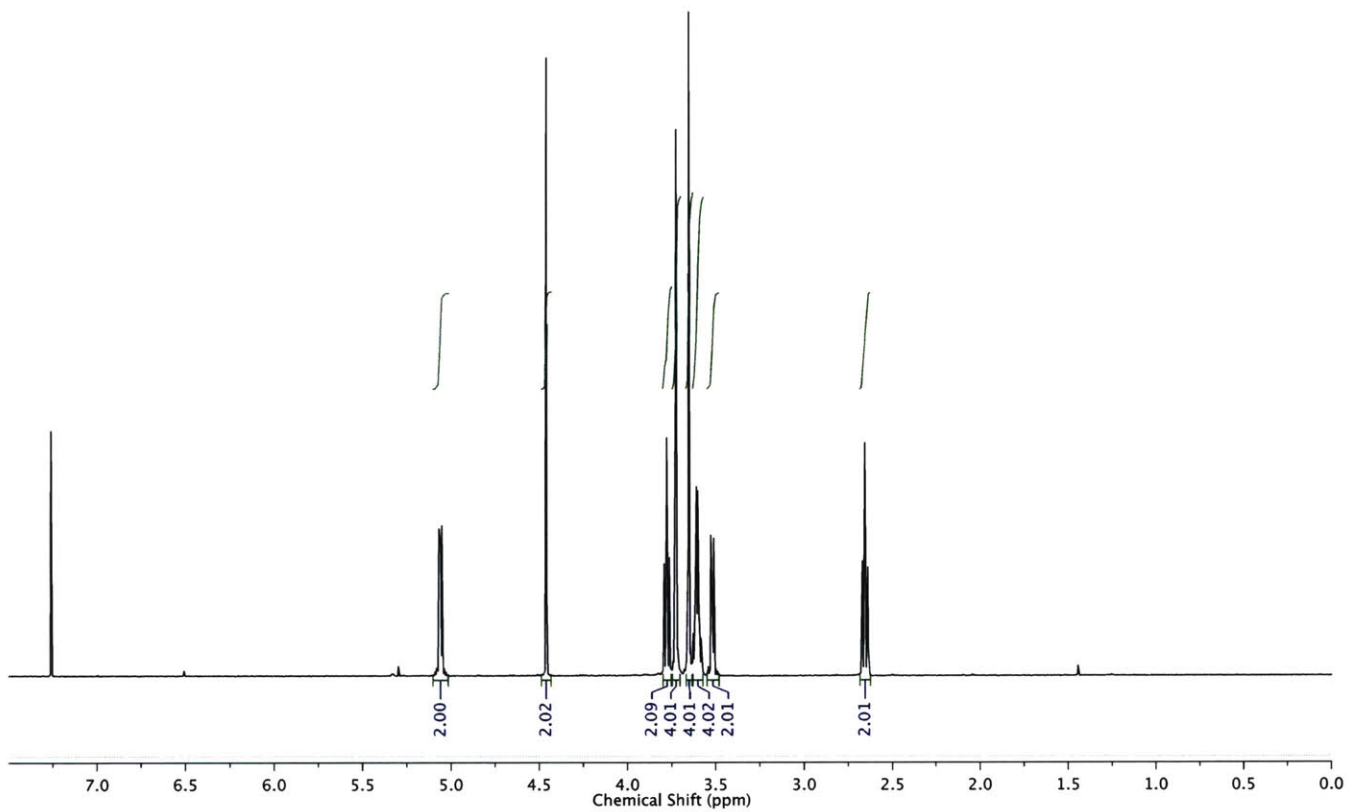
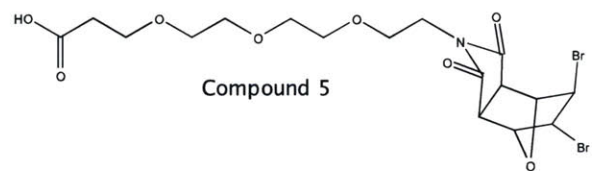
Compound 3

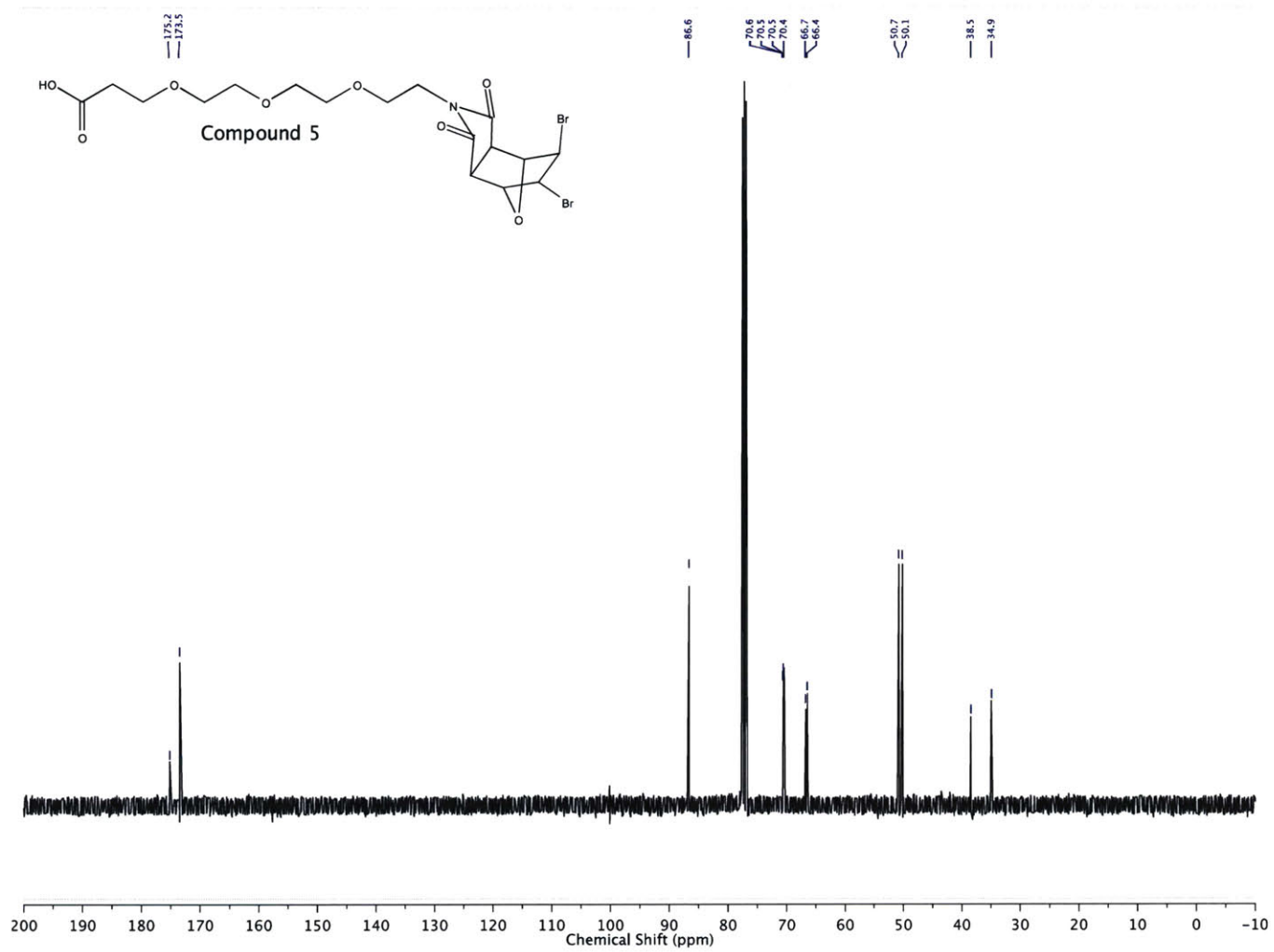


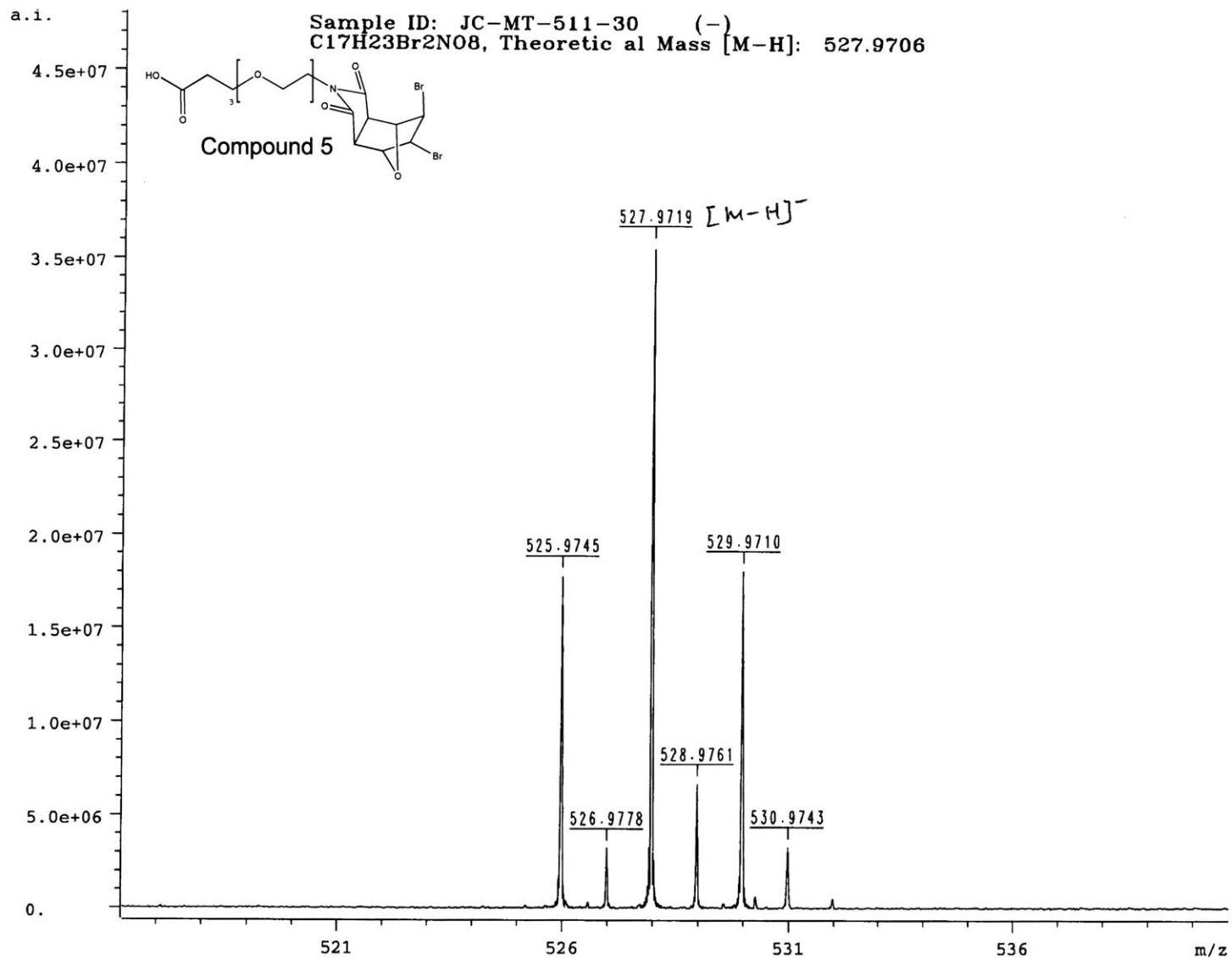


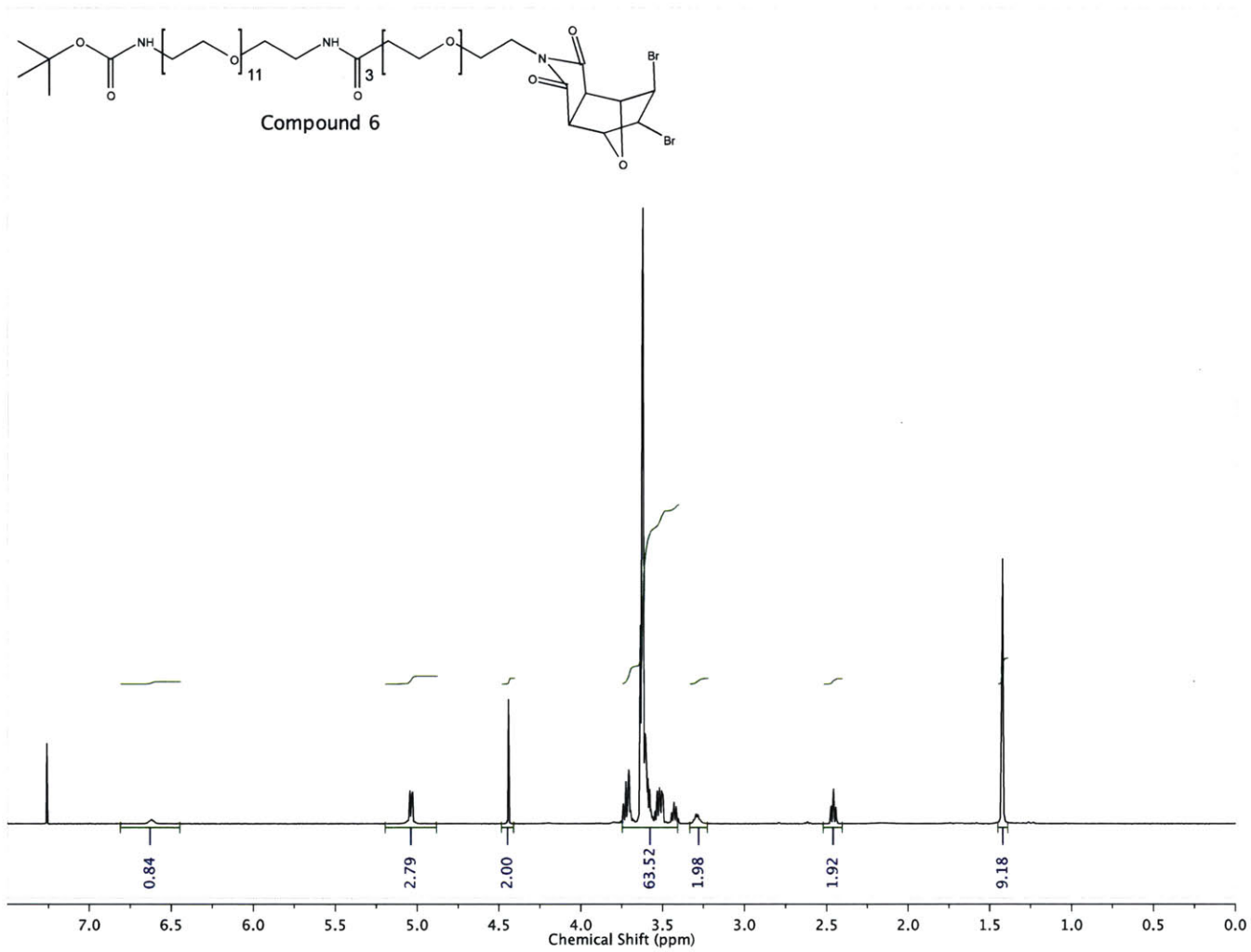


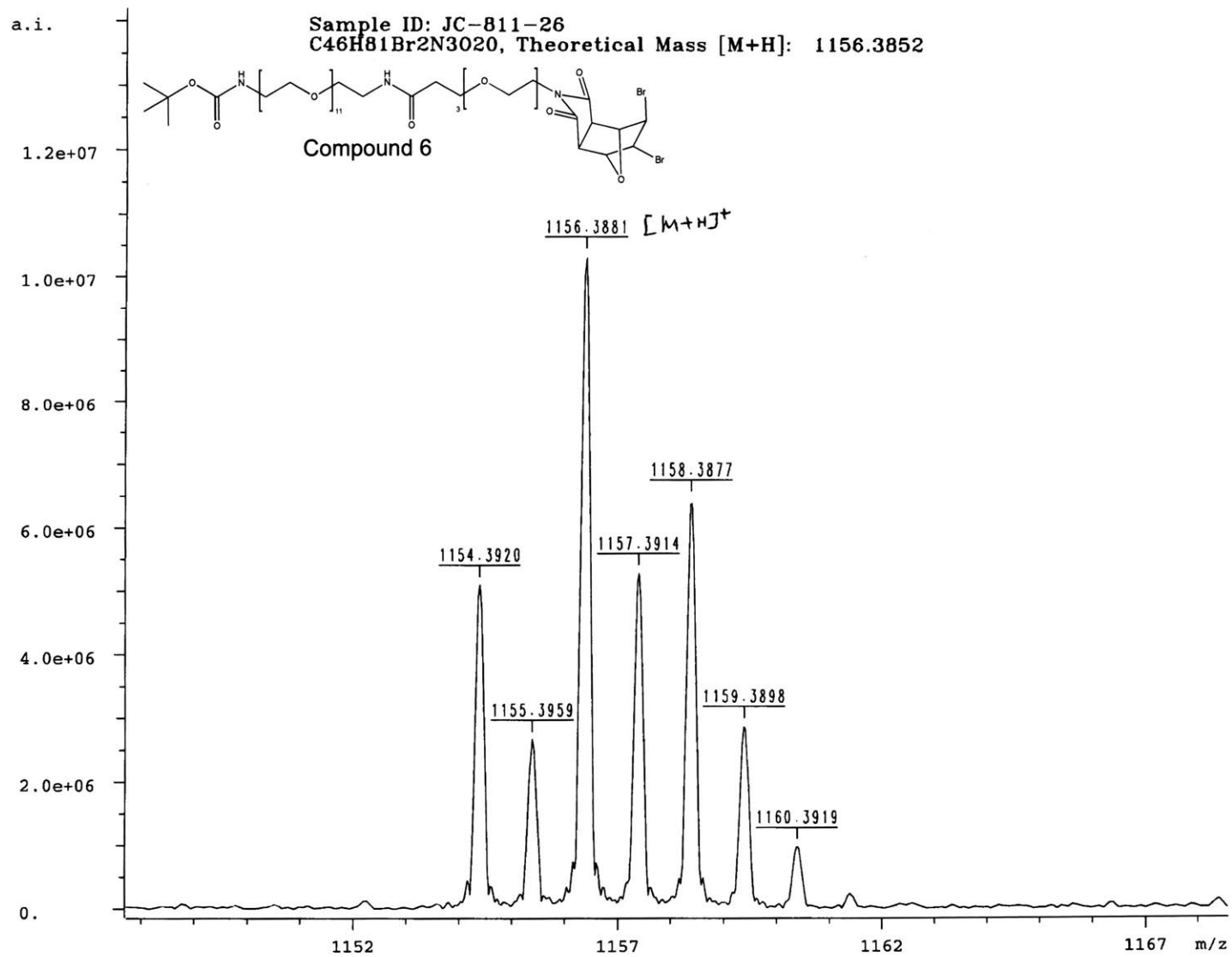


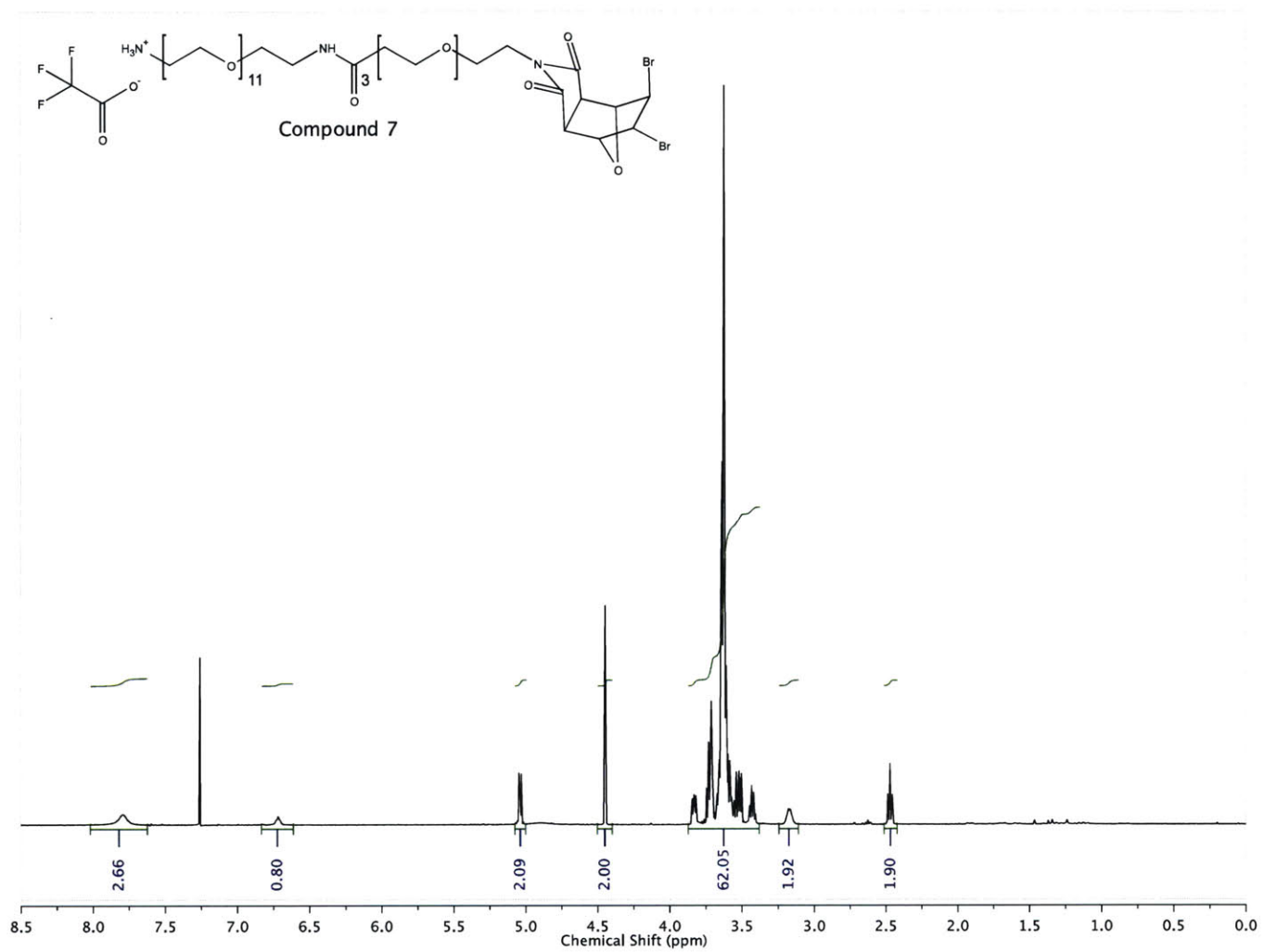


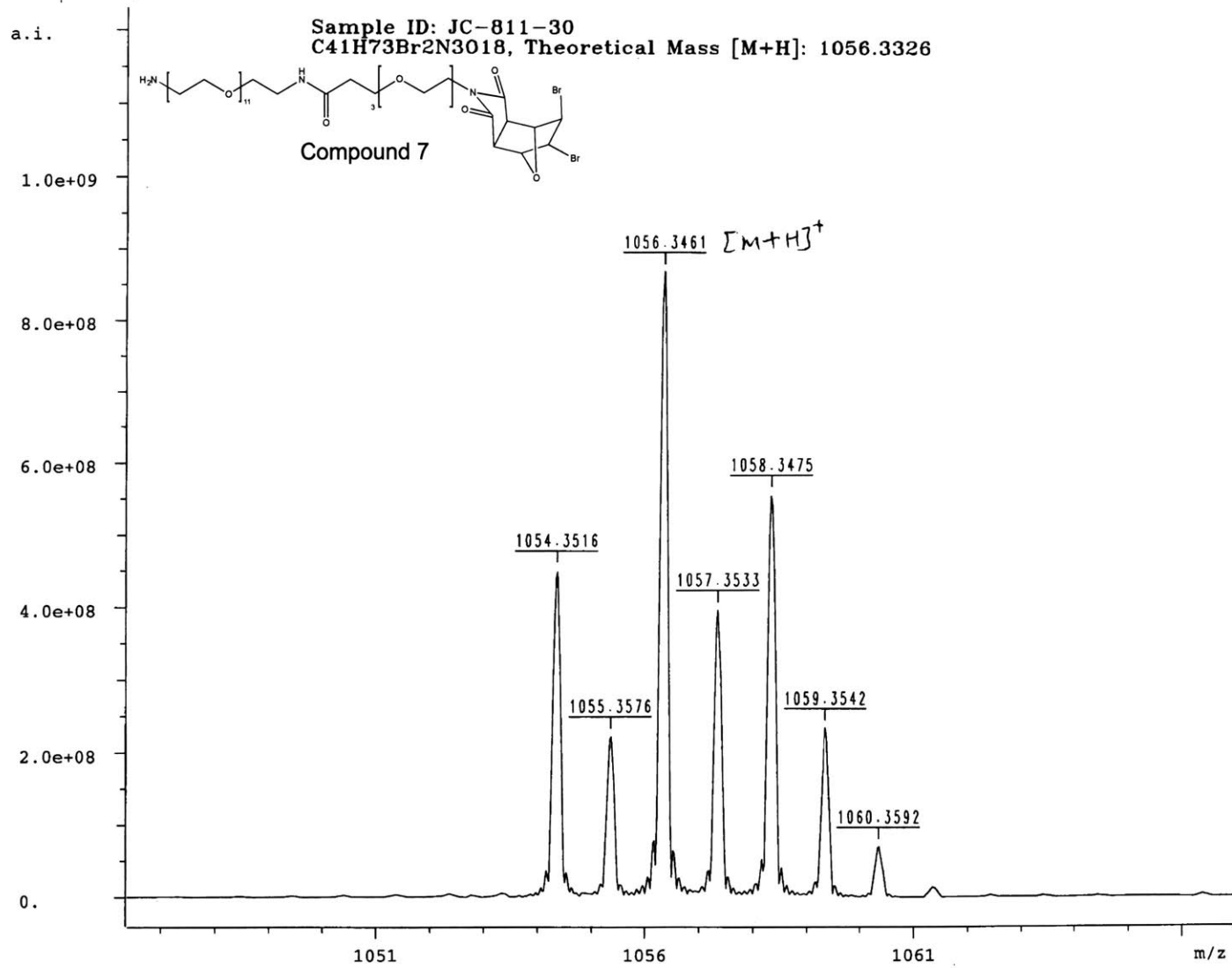


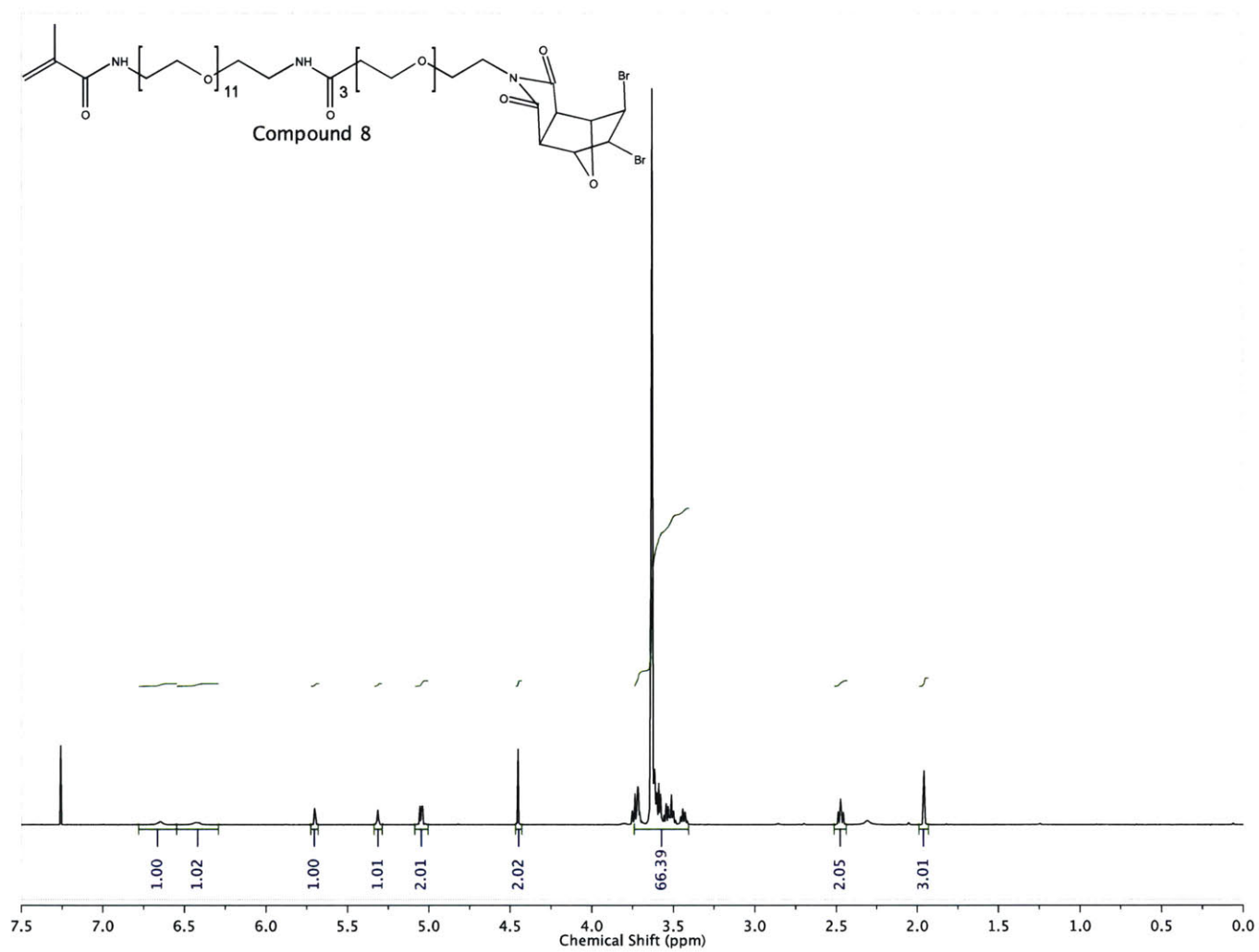


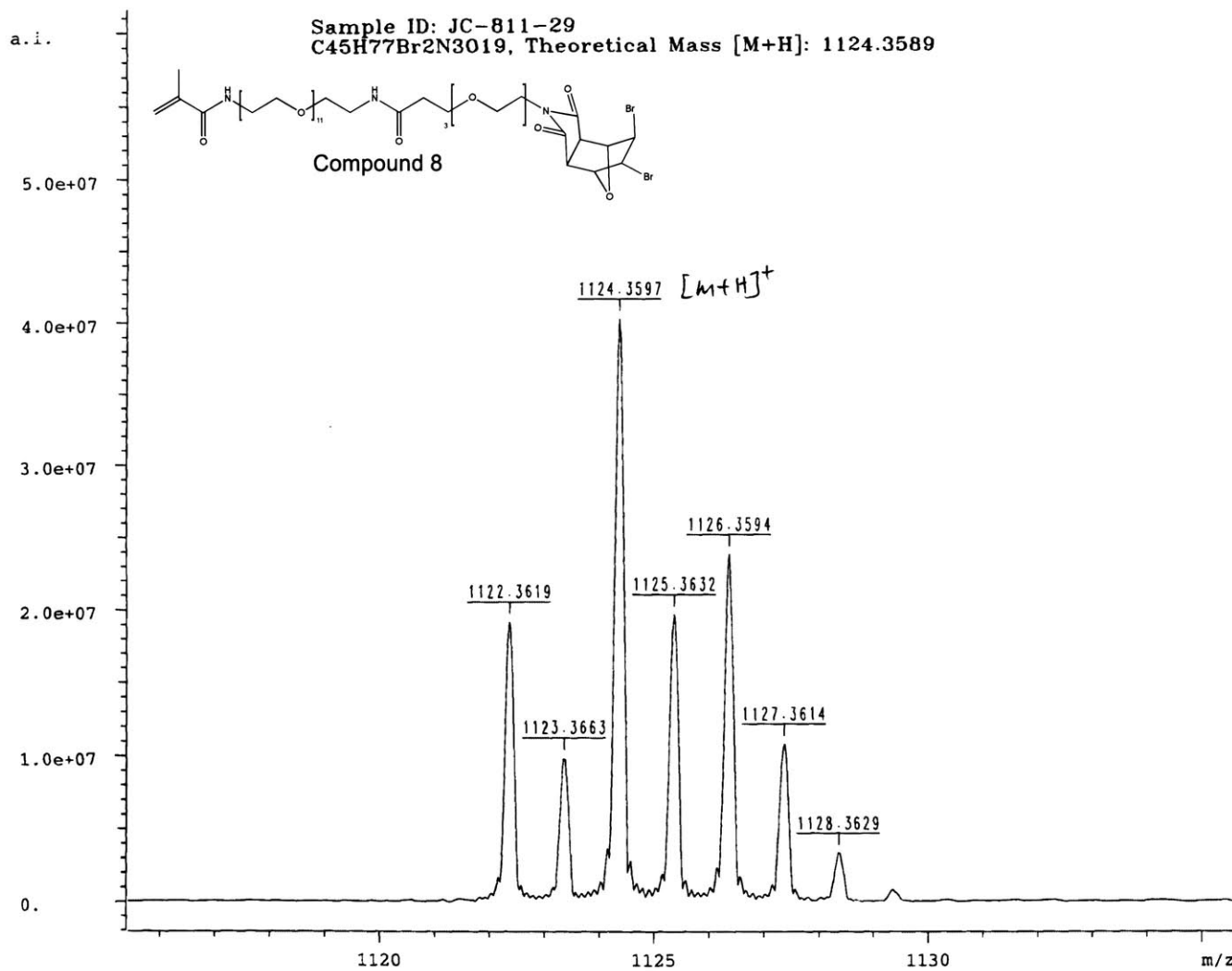


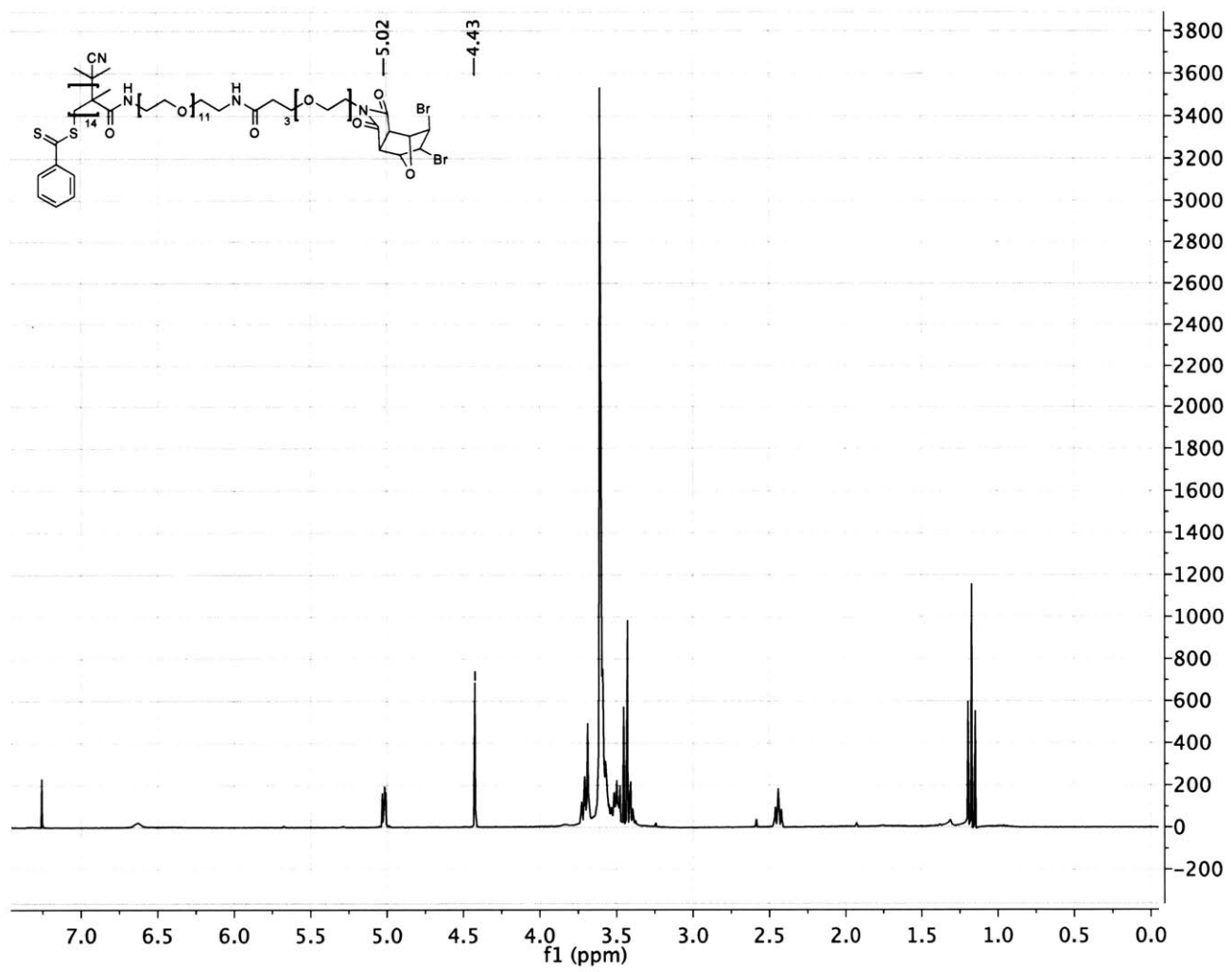


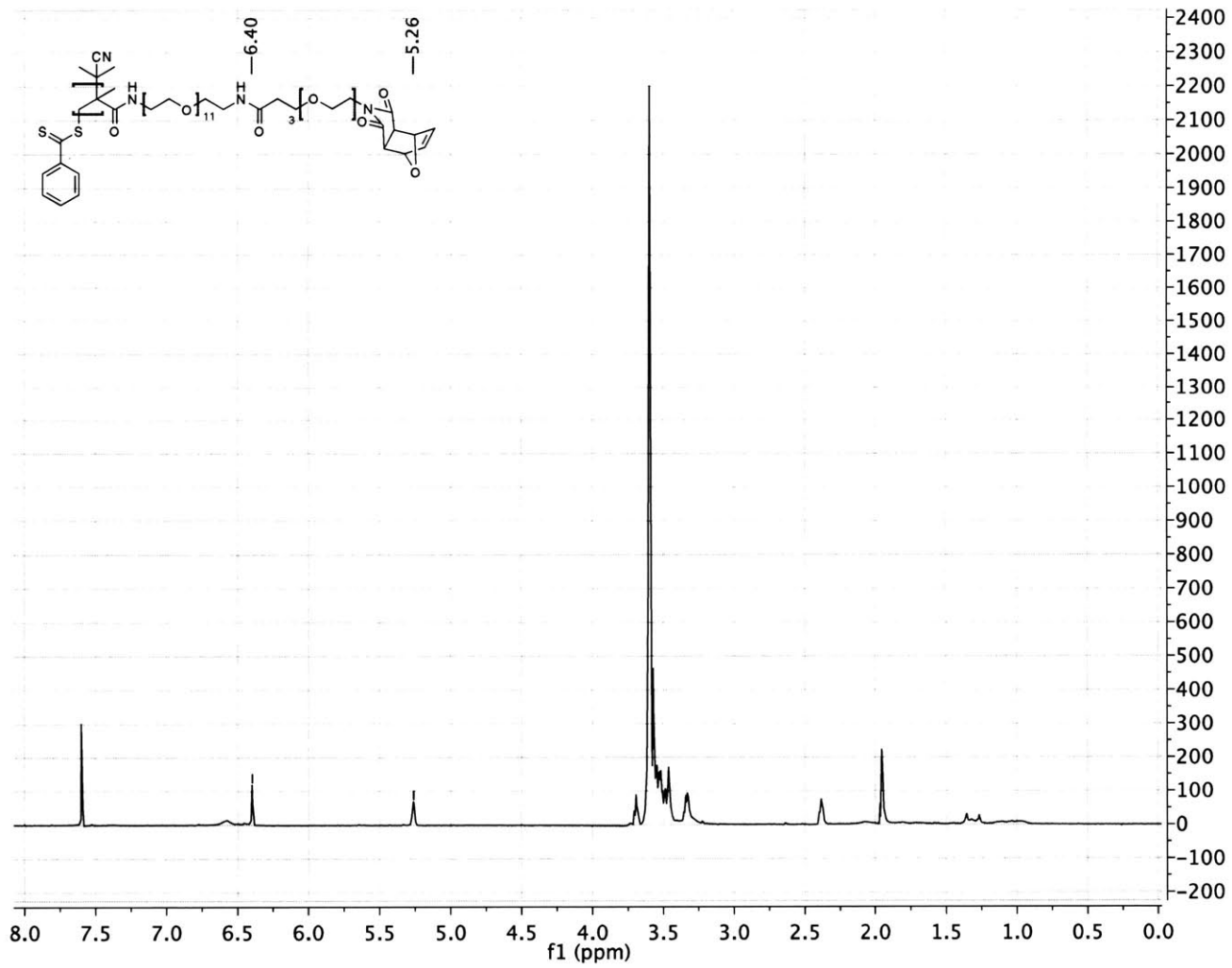


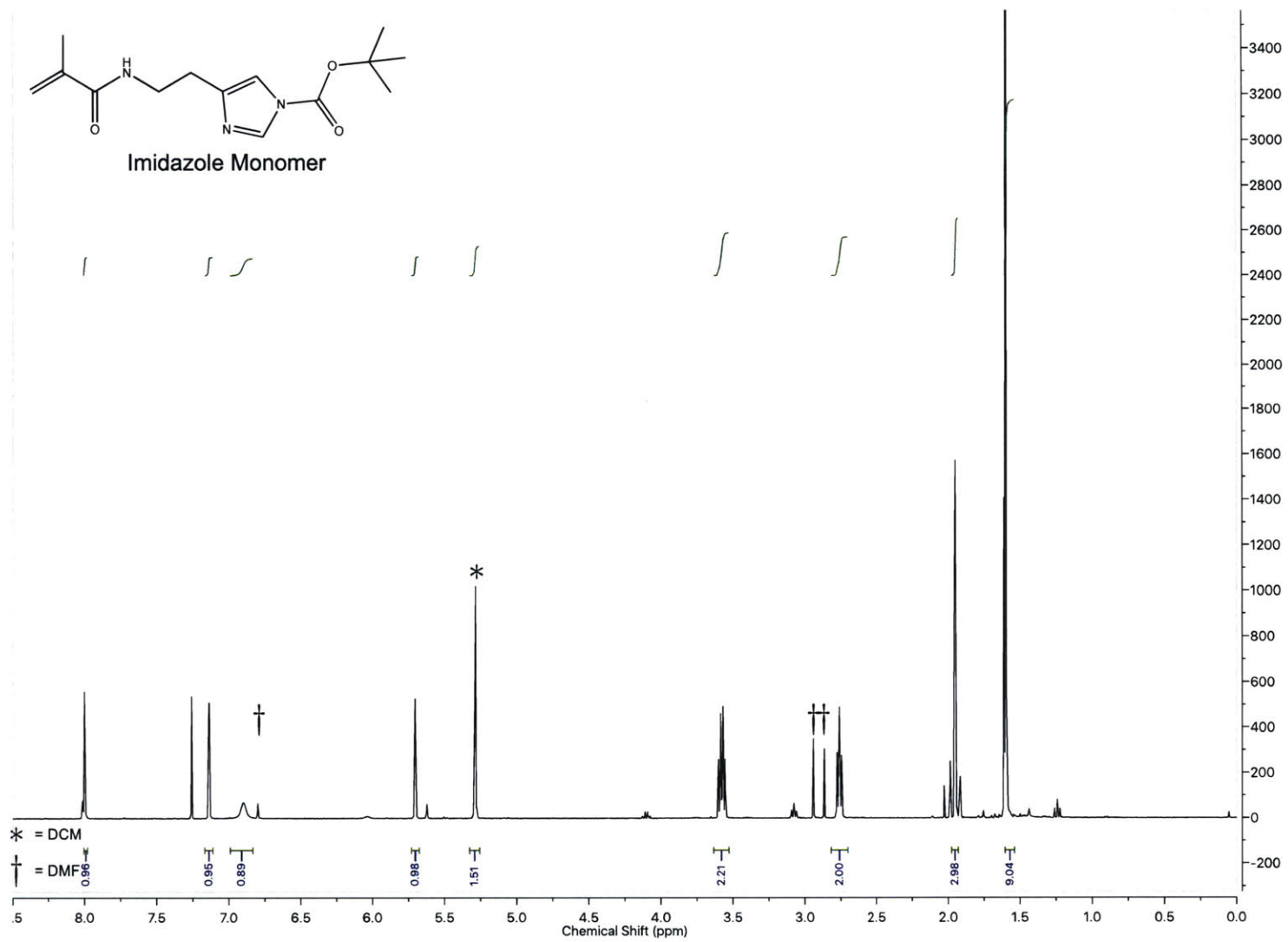


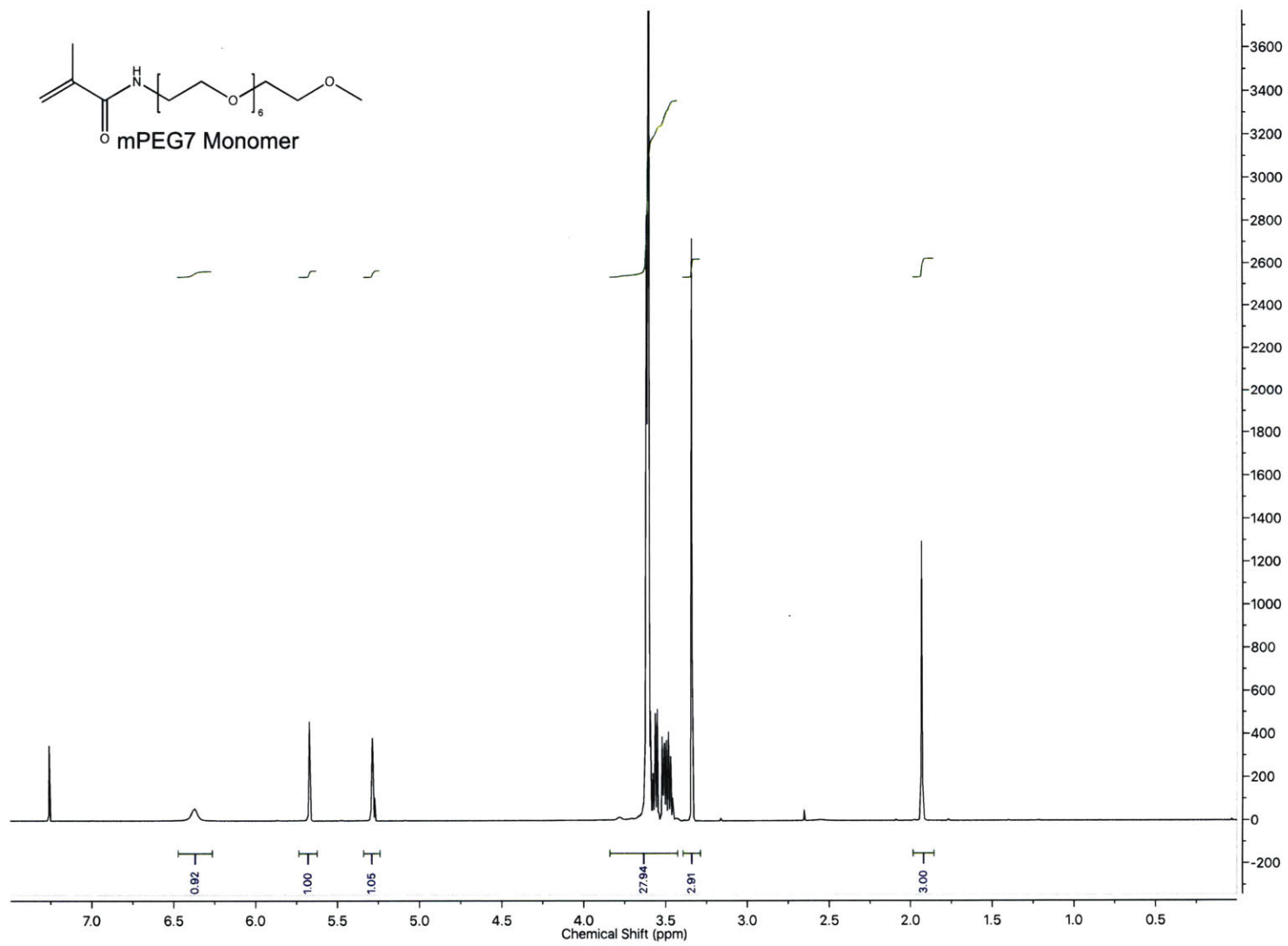


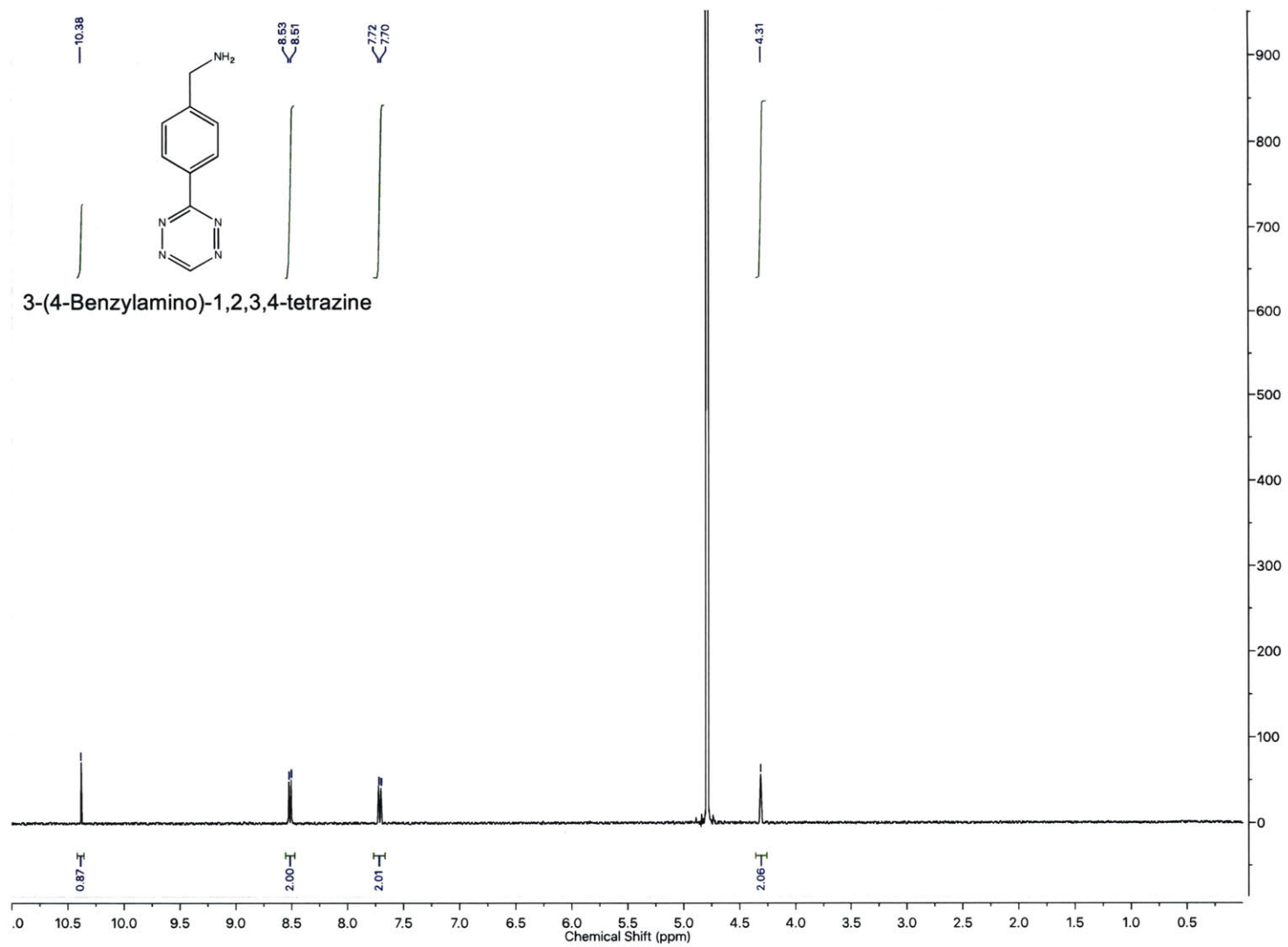


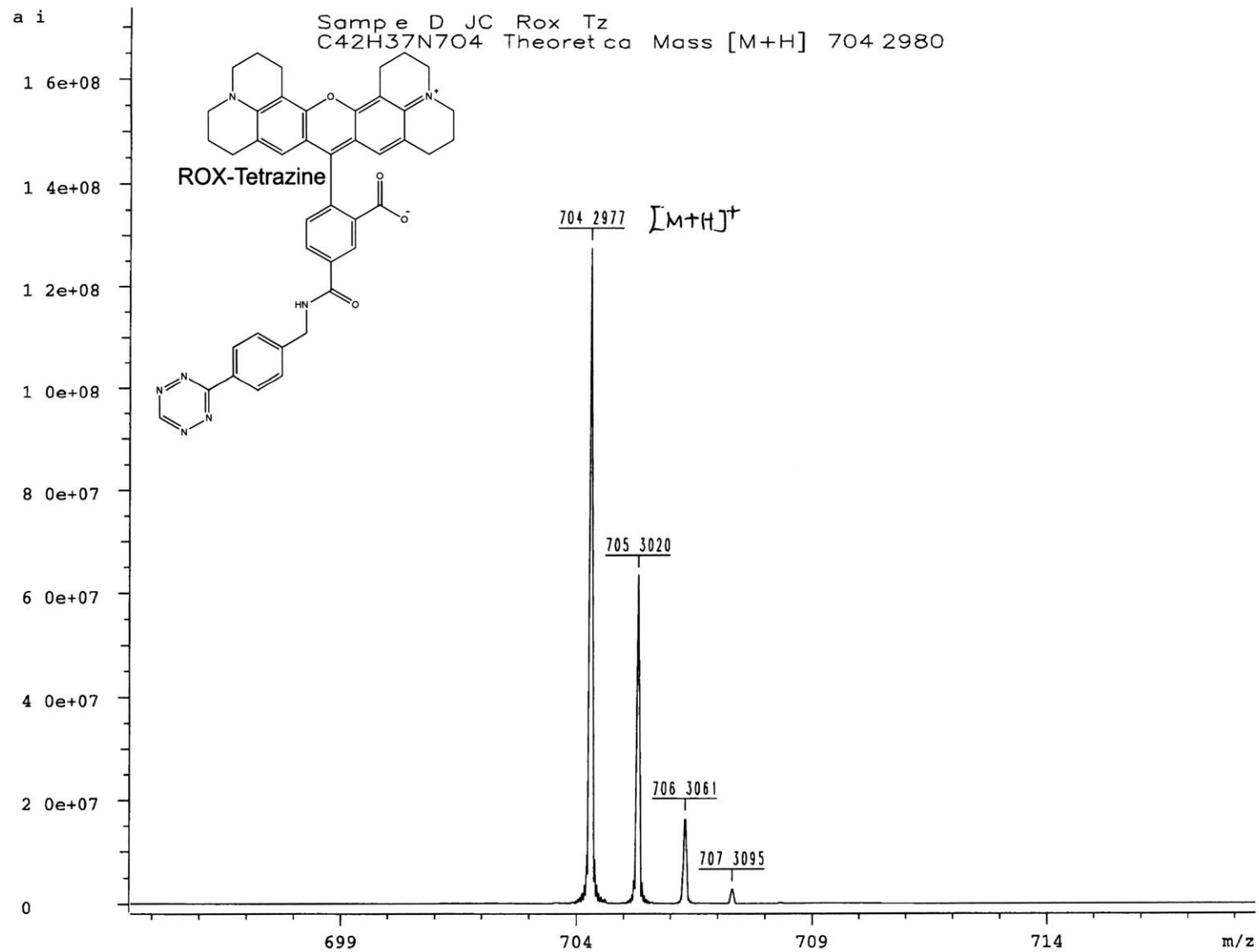












Bibliography

- [1] Murray, C. B., Norris, D. J., and Bawendi, M. G. Synthesis and characterization of nearly monodisperse CdE (E = sulfur, selenium, tellurium) semiconductor nanocrystallites. *Journal of the American Chemical Society*, 115(19):8706–8715 (1993).
- [2] Peng, Z. Adam and Peng, Xiaogang. Formation of High-Quality CdTe, CdSe, and CdS Nanocrystals Using CdO as Precursor. *Journal of the American Chemical Society*, 123(1):183–184 (2001).
- [3] Carbone, Luigi, Nobile, Concetta, De Giorgi, Milena, Sala, Fabio Della, Morello, Giovanni, Pompa, Pierpaolo, Hytch, Martin, Snoeck, Etienne, Fiore, Angela, Franchini, Isabella R., Nadasan, Monica, Silvestre, Albert F., Chiodo, Letizia, Kudera, Stefan, Cingolani, Roberto, Krahne, Roman, and Manna, Liberato. Synthesis and Micrometer-Scale Assembly of Colloidal CdSe/CdS Nanorods Prepared by a Seeded Growth Approach. *Nano Letters*, 7(10):2942–2950 (2007).
- [4] Chen, Ou, Zhao, Jing, Chauhan, Vikash P., Cui, Jian, Wong, Cliff, Harris, Daniel K., Wei, He, Han, Hee-Sun, Fukumura, Dai, Jain, Rakesh K., and Bawendi, Mounqi G. Compact high-quality CdSe–CdS core–shell nanocrystals with narrow emission linewidths and suppressed blinking. *Nat Mater*, 12(5):445–451 (2013).
- [5] Peng, Xiaogang, Manna, Liberato, Yang, Weidong, Wickham, Juanita, Scher, Erik, Kadavanich, Andreas, and Alivisatos, A. P. Shape control of CdSe nanocrystals. *Nature*, 404(6773):59–61 (2000).
- [6] Manna, Liberato, Milliron, Delia J., Meisel, Andreas, Scher, Erik C., and Alivisatos, A. Paul. Controlled growth of tetrapod-branched inorganic nanocrystals. *Nat Mater*, 2(6):382–385 (2003).
- [7] Ithurria, Sandrine and Dubertret, Benoit. Quasi 2D Colloidal CdSe Platelets with Thicknesses Controlled at the Atomic Level. *Journal of the American Chemical Society*, 130(49):16504–16505 (2008).
- [8] Yu, W. William and Peng, Xiaogang. Formation of High-Quality CdS and Other II–VI Semiconductor Nanocrystals in Noncoordinating Solvents: Tunable Reactivity of Monomers. *Angewandte Chemie International Edition*, 41(13):2368–2371 (2002).

- [9] Hines, M. A. and Scholes, G. D. Colloidal PbS Nanocrystals with Size-Tunable Near-Infrared Emission: Observation of Post-Synthesis Self-Narrowing of the Particle Size Distribution. *Advanced Materials*, 15(21):1844–1849 (2003).
- [10] Dannhauser, T., O’Neil, M., Johansson, K., Whitten, D., and McLendon, G. Photophysics of quantized colloidal semiconductors. Dramatic luminescence enhancement by binding of simple amines. *The Journal of Physical Chemistry*, 90(23):6074–6076 (1986).
- [11] Kuno, M., Lee, J. K., Dabbousi, B. O., Mikulec, F. V., and Bawendi, M. G. The band edge luminescence of surface modified CdSe nanocrystallites: Probing the luminescing state. *The Journal of Chemical Physics*, 106(23):9869–9882 (1997).
- [12] Klimov, V. I., McBranch, D. W., Leatherdale, C. A., and Bawendi, M. G. Electron and hole relaxation pathways in semiconductor quantum dots. *Physical Review B*, 60(19):13740–13749 (1999).
- [13] Munro, Andrea M., Jen-La Plante, Ilan, Ng, Marsha S., and Ginger, David S. Quantitative Study of the Effects of Surface Ligand Concentration on CdSe Nanocrystal Photoluminescence. *The Journal of Physical Chemistry C*, 111(17):6220–6227 (2007).
- [14] Garrett, Maria Danielle, Bowers, Michael J., McBride, James R., Orndorff, Rebecca L., Pennycook, Stephen J., and Rosenthal, Sandra J. Band Edge Dynamics in CdSe Nanocrystals Observed by Ultrafast Fluorescence Upconversion. *The Journal of Physical Chemistry C*, 112(2):436–442 (2008).
- [15] Cossairt, Brandi M., Juhas, Pavol, Billinge, Simon J. L., and Owen, Jonathan S. Tuning the Surface Structure and Optical Properties of CdSe Clusters Using Coordination Chemistry. *The Journal of Physical Chemistry Letters*, 2(24):3075–3080 (2011).
- [16] Voznyy, Oleksandr, Zhitomirsky, David, Stadler, Philipp, Ning, Zhijun, Hoogland, Sjoerd, and Sargent, Edward H. A Charge-Orbital Balance Picture of Doping in Colloidal Quantum Dot Solids. *ACS Nano*, 6(9):8448–8455 (2012).
- [17] Fomenko, Vasiliy and Nesbitt, David J. Solution Control of Radiative and Nonradiative Lifetimes: A Novel Contribution to Quantum Dot Blinking Suppression. *Nano Letters*, 8(1):287–293 (2008).
- [18] Michalet, X., Pinaud, F. F., Bentolila, L. A., Tsay, J. M., Doose, S., Li, J. J., Sundaresan, G., Wu, A. M., Gambhir, S. S., and Weiss, S. Quantum Dots for Live Cells, in Vivo Imaging, and Diagnostics. *Science*, 307(5709):538–544 (2005).
- [19] Medintz, Igor L., Uyeda, H. Tetsuo, Goldman, Ellen R., and Mattoussi, Hedi. Quantum dot bioconjugates for imaging, labelling and sensing. *Nat Mater*, 4(6):435–446 (2005).

- [20] Chuang, Chia-Hao M., Brown, Patrick R., Bulović, Vladimir, and Bawendi, Moungi G. Improved performance and stability in quantum dot solar cells through band alignment engineering. *Nat Mater*, 13(8):796–801 (2014).
- [21] Green, M. L. H. A new approach to the formal classification of covalent compounds of the elements. *Journal of Organometallic Chemistry*, 500(1):127–148 (1995).
- [22] Crabtree, Robert H. *General Properties of Organometallic Complexes*, pp. 29–52. John Wiley & Sons, Inc. (2005).
- [23] Owen, Jonathan. The coordination chemistry of nanocrystal surfaces. *Science*, 347(6222):615–616 (2015).
- [24] Owen, Jonathan S., Park, Jungwon, Trudeau, Paul-Emile, and Alivisatos, A. Paul. Reaction Chemistry and Ligand Exchange at Cadmium–Selenide Nanocrystal Surfaces. *Journal of the American Chemical Society*, 130(37):12279–12281 (2008).
- [25] Morris-Cohen, Adam J., Donakowski, Martin D., Knowles, Kathryn E., and Weiss, Emily A. The Effect of a Common Purification Procedure on the Chemical Composition of the Surfaces of CdSe Quantum Dots Synthesized with Trioctylphosphine Oxide. *The Journal of Physical Chemistry C*, 114(2):897–906 (2010).
- [26] Fritzing, Bernd, Capek, Richard K., Lambert, Karel, Martins, José C., and Hens, Zeger. Utilizing Self-Exchange To Address the Binding of Carboxylic Acid Ligands to CdSe Quantum Dots. *Journal of the American Chemical Society*, 132(29):10195–10201 (2010).
- [27] Chen, Ou, Yang, Yongan, Wang, Tie, Wu, Huimeng, Niu, Chenggang, Yang, Jianhui, and Cao, Y. Charles. Surface-Functionalization-Dependent Optical Properties of II–VI Semiconductor Nanocrystals. *Journal of the American Chemical Society*, 133(43):17504–17512 (2011).
- [28] Anderson, Nicholas C., Hendricks, Mark P., Choi, Joshua J., and Owen, Jonathan S. Ligand Exchange and the Stoichiometry of Metal Chalcogenide Nanocrystals: Spectroscopic Observation of Facile Metal-Carboxylate Displacement and Binding. *Journal of the American Chemical Society*, 135(49):18536–18548 (2013).
- [29] Qu, Lianhua and Peng, Xiaogang. Control of Photoluminescence Properties of CdSe Nanocrystals in Growth. *Journal of the American Chemical Society*, 124(9):2049–2055 (2002).
- [30] Gomes, Raquel, Hassinen, Antti, Szczygiel, Agnieszka, Zhao, Qiang, Van-tomme, André, Martins, José C., and Hens, Zeger. Binding of Phosphonic Acids to CdSe Quantum Dots: A Solution NMR Study. *The Journal of Physical Chemistry Letters*, 2(3):145–152 (2011).

- [31] Fritzing, Bernd, Moreels, Iwan, Lommens, Petra, Koole, Rolf, Hens, Zeger, and Martins, JoséC. In Situ Observation of Rapid Ligand Exchange in Colloidal Nanocrystal Suspensions Using Transfer NOE Nuclear Magnetic Resonance Spectroscopy. *Journal of the American Chemical Society*, 131(8):3024–3032 (2009).
- [32] Kim, Donghun, Kim, Dong-Ho, Lee, Joo-Hyoung, and Grossman, Jeffrey C. Impact of Stoichiometry on the Electronic Structure of PbS Quantum Dots. *Physical Review Letters*, 110(19):196802– (2013).
- [33] Hwang, Gyu Weon, Kim, Donghun, Cordero, Jose M., Wilson, Mark W. B., Chuang, Chia-Hao M., Grossman, Jeffrey C., and Bawendi, Mounqi G. Identifying and Eliminating Emissive Sub-bandgap States in Thin Films of PbS Nanocrystals. *Advanced Materials*, 27(30):4481–4486 (2015).
- [34] Moreels, Iwan, Fritzing, Bernd, Martins, JoséC., and Hens, Zeger. Surface Chemistry of Colloidal PbSe Nanocrystals. *Journal of the American Chemical Society*, 130(45):15081–15086 (2008).
- [35] Allen, Peter M., Liu, Wenhao, Chauhan, Vikash P., Lee, Jungmin, Ting, Alice Y., Fukumura, Dai, Jain, Rakesh K., and Bawendi, Mounqi G. InAs(ZnCdS) Quantum Dots Optimized for Biological Imaging in the Near-Infrared. *Journal of the American Chemical Society*, 132(2):470–471 (2010).
- [36] Bruchez, Marcel, Moronne, Mario, Gin, Peter, Weiss, Shimon, and Alivisatos, A. Paul. Semiconductor Nanocrystals as Fluorescent Biological Labels. *Science*, 281(5385):2013–2016 (1998).
- [37] Larson, Daniel R., Zipfel, Warren R., Williams, Rebecca M., Clark, Stephen W., Bruchez, Marcel P., Wise, Frank W., and Webb, Watt W. Water-Soluble Quantum Dots for Multiphoton Fluorescence Imaging in Vivo. *Science*, 300(5624):1434–1436 (2003).
- [38] Gao, Xiaohu, Cui, Yuanyuan, Levenson, Richard M, Chung, Leland W K, and Nie, Shuming. In vivo cancer targeting and imaging with semiconductor quantum dots. *Nat Biotech*, 22(8):969–976 (2004).
- [39] Kim, Sungjee, Lim, Yong Taik, Soltesz, Edward G, De Grand, Alec M, Lee, Jaihyoung, Nakayama, Akira, Parker, J Anthony, Mihaljevic, Tomislav, Lawrence, Rita G, Dor, Delphine M, Cohn, Lawrence H, Bawendi, Mounqi G, and Frangioni, John V. Near-infrared fluorescent type II quantum dots for sentinel lymph node mapping. *Nat Biotech*, 22(1):93–97 (2004).
- [40] Choi, Hak Soo, Ipe, Binil Itty, Misra, Preeti, Lee, Jeong Heon, Bawendi, Mounqi G., and Frangioni, John V. Tissue- and Organ-Selective Biodistribution of NIR Fluorescent Quantum Dots. *Nano Letters*, 9(6):2354–2359 (2009).

- [41] Wu, Xingyong, Liu, Hongjian, Liu, Jianquan, Haley, Kari N., Treadway, Joseph A., Larson, J Peter, Ge, Nianfeng, Peale, Frank, and Bruchez, Marcel P. Immunofluorescent labeling of cancer marker Her2 and other cellular targets with semiconductor quantum dots. *Nat Biotech*, 21(1):41–46 (2003).
- [42] Dubertret, Benoit, Skourides, Paris, Norris, David J., Noireaux, Vincent, Brivanlou, Ali H., and Libchaber, Albert. In Vivo Imaging of Quantum Dots Encapsulated in Phospholipid Micelles. *Science*, 298(5599):1759–1762 (2002).
- [43] Dahan, Maxime, Lévi, Sabine, Luccardini, Camilla, Rostaing, Philippe, Riveau, Béatrice, and Triller, Antoine. Diffusion Dynamics of Glycine Receptors Revealed by Single-Quantum Dot Tracking. *Science*, 302(5644):442–445 (2003).
- [44] Groc, Laurent, Heine, Martin, Cognet, Laurent, Brickley, Kieran, Stephenson, F Anne, Lounis, Brahim, and Choquet, Daniel. Differential activity-dependent regulation of the lateral mobilities of AMPA and NMDA receptors. *Nat Neurosci*, 7(7):695–696 (2004).
- [45] Howarth, Mark, Liu, Wenhao, Puthenveetil, Sujiet, Zheng, Yi, Marshall, Lisa F, Schmidt, Michael M, Wittrup, K Dane, Bawendi, Mounqi G, and Ting, Alice Y. Monovalent, reduced-size quantum dots for imaging receptors on living cells. *Nat Meth*, 5(5):397–399 (2008).
- [46] Ballou, Byron, Lagerholm, B. Christoffer, Ernst, Lauren A., Bruchez, Marcel P., and Waggoner, Alan S. Noninvasive Imaging of Quantum Dots in Mice. *Bioconjugate Chemistry*, 15(1):79–86 (2004).
- [47] Liu, Wenhao, Greytak, Andrew B., Lee, Jungmin, Wong, Cliff R., Park, Jongnam, Marshall, Lisa F., Jiang, Wen, Curtin, Peter N., Ting, Alice Y., Nocera, Daniel G., Fukumura, Dai, Jain, Rakesh K., and Bawendi, Mounqi G. Compact Biocompatible Quantum Dots via RAFT-Mediated Synthesis of Imidazole-Based Random Copolymer Ligand. *Journal of the American Chemical Society*, 132(2):472–483 (2010).
- [48] Clapp, Aaron R., Medintz, Igor L., Uyeda, H. Tetsuo, Fisher, Brent R., Goldman, Ellen R., Bawendi, Mounqi G., and Mattoussi, Hedi. Quantum Dot-Based Multiplexed Fluorescence Resonance Energy Transfer. *Journal of the American Chemical Society*, 127(51):18212–18221 (2005).
- [49] Han, Hee-Sun, Niemeyer, Elisabeth, Huang, Yuhui, Kamoun, Walid S., Martin, John D., Bhaumik, Jayeeta, Chen, Yunching, Roberge, Sylvie, Cui, Jian, Martin, Margaret R., Fukumura, Dai, Jain, Rakesh K., Bawendi, Mounqi G., and Duda, Dan G. Quantum dot/antibody conjugates for in vivo cytometric imaging in mice. *Proceedings of the National Academy of Sciences*, 112(5):1350–1355 (2015).
- [50] Bentzen, Elizabeth L., Tomlinson, Ian D., Mason, John, Gresch, Paul, Warneiment, Michael R., Wright, David, Sanders-Bush, Elaine, Blakely, Randy, and

- Rosenthal, Sandra J. Surface Modification To Reduce Nonspecific Binding of Quantum Dots in Live Cell Assays. *Bioconjugate Chemistry*, 16(6):1488–1494 (2005).
- [51] Soo Choi, Hak, Liu, Wenhao, Misra, Preeti, Tanaka, Eiichi, Zimmer, John P, Itty Ipe, Binil, Bawendi, Mounqi G, and Frangioni, John V. Renal clearance of quantum dots. *Nat Biotech*, 25(10):1165–1170 (2007).
- [52] Aldana, Jose, Wang, Y. Andrew, and Peng, Xiaogang. Photochemical Instability of CdSe Nanocrystals Coated by Hydrophilic Thiols. *Journal of the American Chemical Society*, 123(36):8844–8850 (2001).
- [53] Mattoussi, Hedi, Mauro, J. Matthew, Goldman, Ellen R., Anderson, George P., Sundar, Vikram C., Mikulec, Frederic V., and Bawendi, Mounqi G. Self-Assembly of CdSe/ZnS Quantum Dot Bioconjugates Using an Engineered Recombinant Protein. *Journal of the American Chemical Society*, 122(49):12142–12150 (2000).
- [54] Uyeda, H. Tetsuo, Medintz, Igor L., Jaiswal, Jyoti K., Simon, Sanford M., and Mattoussi, Hedi. Synthesis of Compact Multidentate Ligands to Prepare Stable Hydrophilic Quantum Dot Fluorophores. *Journal of the American Chemical Society*, 127(11):3870–3878 (2005).
- [55] Liu, Wenhao, Howarth, Mark, Greytak, Andrew B., Zheng, Yi, Nocera, Daniel G., Ting, Alice Y., and Bawendi, Mounqi G. Compact Biocompatible Quantum Dots Functionalized for Cellular Imaging. *Journal of the American Chemical Society*, 130(4):1274–1284 (2008).
- [56] Liu, Wenhao, Choi, Hak Soo, Zimmer, John P., Tanaka, Eiichi, Frangioni, John V., and Bawendi, Mounqi. Compact Cysteine-Coated CdSe(ZnCdS) Quantum Dots for in Vivo Applications. *Journal of the American Chemical Society*, 129(47):14530–14531 (2007).
- [57] Lee, Jungmin, Sharei, Armon, Sim, Woo Young, Adamo, Andrea, Langer, Robert, Jensen, Klavs F., and Bawendi, Mounqi G. Nonendocytic Delivery of Functional Engineered Nanoparticles into the Cytoplasm of Live Cells Using a Novel, High-Throughput Microfluidic Device. *Nano Letters*, 12(12):6322–6327 (2012).
- [58] Kay, Euan R., Lee, Jungmin, Nocera, Daniel G., and Bawendi, Mounqi G. Conformational Control of Energy Transfer: A Mechanism for Biocompatible Nanocrystal-Based Sensors. *Angewandte Chemie International Edition*, 52(4):1165–1169 (2013).
- [59] Han, Hee-Sun, Devaraj, Neal K., Lee, Jungmin, Hilderbrand, Scott A., Weissleder, Ralph, and Bawendi, Mounqi G. Development of a Bioorthogonal and Highly Efficient Conjugation Method for Quantum Dots Using

Tetrazine–Norbornene Cycloaddition. *Journal of the American Chemical Society*, 132(23):7838–7839 (2010).

- [60] Snee, Preston T., Somers, Rebecca C., Nair, Gautham, Zimmer, John P., Bawendi, Moungi G., and Nocera, Daniel G. A Ratiometric CdSe/ZnS Nanocrystal pH Sensor. *Journal of the American Chemical Society*, 128(41):13320–13321 (2006).
- [61] Somers, Rebecca C., Lanning, Ryan M., Snee, Preston T., Greytak, Andrew B., Jain, Rakesh K., Bawendi, Moungi G., and Nocera, Daniel G. A nanocrystal-based ratiometric pH sensor for natural pH ranges. *Chemical Science*, 3(10):2980–2985 (2012).
- [62] Lemon, Christopher M., Curtin, Peter N., Somers, Rebecca C., Greytak, Andrew B., Lanning, Ryan M., Jain, Rakesh K., Bawendi, Moungi G., and Nocera, Daniel G. Metabolic Tumor Profiling with pH, Oxygen, and Glucose Chemosensors on a Quantum Dot Scaffold. *Inorganic Chemistry*, 53(4):1900–1915 (2014).
- [63] McLaurin, Emily J., Greytak, Andrew B., Bawendi, Moungi G., and Nocera, Daniel G. Two-Photon Absorbing Nanocrystal Sensors for Ratiometric Detection of Oxygen. *Journal of the American Chemical Society*, 131(36):12994–13001 (2009).
- [64] Lemon, Christopher M., Karnas, Elizabeth, Han, Xiaoxing, Bruns, Oliver T., Kempa, Thomas J., Fukumura, Dai, Bawendi, Moungi G., Jain, Rakesh K., Duda, Dan G., and Nocera, Daniel G. Micelle-Encapsulated Quantum Dot-Porphyrin Assemblies as in Vivo Two-Photon Oxygen Sensors. *Journal of the American Chemical Society*, 137(31):9832–9842 (2015).
- [65] Haun, Jered B., Devaraj, Neal K., Hilderbrand, Scott A., Lee, Hakho, and Weissleder, Ralph. Bioorthogonal chemistry amplifies nanoparticle binding and enhances the sensitivity of cell detection. *Nat Nano*, 5(9):660–665 (2010).
- [66] Kolb, Hartmuth C., Finn, M. G., and Sharpless, K. Barry. Click Chemistry: Diverse Chemical Function from a Few Good Reactions. *Angewandte Chemie International Edition*, 40(11):2004–2021 (2001).
- [67] Devaraj, Neal K., Weissleder, Ralph, and Hilderbrand, Scott A. Tetrazine-Based Cycloadditions: Application to Pretargeted Live Cell Imaging. *Bioconjugate Chemistry*, 19(12):2297–2299 (2008).
- [68] Lee, Sang-Min, Jun, Young-wook, Cho, Sung-Nam, and Cheon, Jinwoo. Single-Crystalline Star-Shaped Nanocrystals and Their Evolution: Programming the Geometry of Nano-Building Blocks. *Journal of the American Chemical Society*, 124(38):11244–11245 (2002).
- [69] Hendricks, Mark P., Campos, Michael P., Cleveland, Gregory T., Jen-La Plante, Ilan, and Owen, Jonathan S. A tunable library of substituted thiourea precursors to metal sulfide nanocrystals. *Science*, 348(6240):1226–1230 (2015).

- [70] Jellicoe, Tom C., Richter, Johannes M., Glass, Hugh F. J., Tabachnyk, Maxim, Brady, Ryan, Dutton, Siân E., Rao, Akshay, Friend, Richard H., Credgington, Dan, Greenham, Neil C., and Böhm, Marcus L. Synthesis and Optical Properties of Lead-Free Cesium Tin Halide Perovskite Nanocrystals. *Journal of the American Chemical Society*, 138(9):2941–2944 (2016).
- [71] Protesescu, Loredana, Yakunin, Sergii, Bodnarchuk, Maryna I., Krieg, Franziska, Caputo, Riccarda, Hendon, Christopher H., Yang, Ruo Xi, Walsh, Aron, and Kovalenko, Maksym V. Nanocrystals of Cesium Lead Halide Perovskites (CsPbX₃, X = Cl, Br, and I): Novel Optoelectronic Materials Showing Bright Emission with Wide Color Gamut. *Nano Letters*, 15(6):3692–3696 (2015).
- [72] Zhang, Dandan, Yang, Yiming, Bekenstein, Yehonadav, Yu, Yi, Gibson, Natalie A., Wong, Andrew B., Eaton, Samuel W., Kornienko, Nikolay, Kong, Qiao, Lai, Minliang, Alivisatos, A. Paul, Leone, Stephen R., and Yang, Peidong. Synthesis of Composition Tunable and Highly Luminescent Cesium Lead Halide Nanowires through Anion-Exchange Reactions. *Journal of the American Chemical Society*, 138(23):7236–7239 (2016).
- [73] Akkerman, Quinten A., Motti, Silvia Genaro, Srimath Kandada, Ajay Ram, Mosconi, Edoardo, D’Innocenzo, Valerio, Bertoni, Giovanni, Marras, Sergio, Kamino, Brett A., Miranda, Laura, De Angelis, Filippo, Petrozza, Annamaria, Prato, Mirko, and Manna, Liberato. Solution Synthesis Approach to Colloidal Cesium Lead Halide Perovskite Nanoplatelets with Monolayer-Level Thickness Control. *Journal of the American Chemical Society*, 138(3):1010–1016 (2016).
- [74] Shamsi, Javad, Dang, Zhiya, Bianchini, Paolo, Canale, Claudio, Stasio, Francesco Di, Brescia, Rosaria, Prato, Mirko, and Manna, Liberato. Colloidal Synthesis of Quantum Confined Single Crystal CsPbBr₃ Nanosheets with Lateral Size Control up to the Micrometer Range. *Journal of the American Chemical Society*, 138(23):7240–7243 (2016).
- [75] Yang, Jun, Karver, Mark R., Li, Weilong, Sahu, Swagat, and Devaraj, Neal K. Metal-Catalyzed One-Pot Synthesis of Tetrazines Directly from Aliphatic Nitriles and Hydrazine. *Angewandte Chemie International Edition*, 51(21):5222–5225 (2012).
- [76] Zhao, Ni, Osedach, Tim P., Chang, Liang-Yi, Geyer, Scott M., Wanger, Darcy, Binda, Maddalena T., Arango, Alexi C., Bawendi, Mounqi G., and Bulovic, Vladimir. Colloidal PbS Quantum Dot Solar Cells with High Fill Factor. *ACS Nano*, 4(7):3743–3752 (2010).
- [77] Franke, Daniel, Harris, Daniel K., Chen, Ou, Bruns, Oliver T., Carr, Jessica A., Wilson, Mark W. B., and Bawendi, Mounqi G. Continuous Injection Synthesis of Indium Arsenide Quantum Dots for Short-Wavelength Infrared Imaging. *Nat Communications* (Accepted In Principle).

- [78] Leatherdale, C. A., Woo, W. K., Mikulec, F. V., and Bawendi, M. G. On the Absorption Cross Section of CdSe Nanocrystal Quantum Dots. *The Journal of Physical Chemistry B*, 106(31):7619–7622 (2002).
- [79] Zhao, Yiming, Riemersma, Charl, Pietra, Francesca, Koole, Rolf, de Mello Donegá, Celso, and Meijerink, Andries. High-Temperature Luminescence Quenching of Colloidal Quantum Dots. *ACS Nano*, 6(10):9058–9067 (2012).
- [80] Li, Xin, Nichols, Valerie M., Zhou, Dapeng, Lim, Cynthia, Pau, George Shu Heng, Bardeen, Christopher J., and Tang, Ming L. Observation of Multiple, Identical Binding Sites in the Exchange of Carboxylic Acid Ligands with CdS Nanocrystals. *Nano Letters*, 14(6):3382–3387 (2014).
- [81] Ji, Xiaohui, Copenhaver, Danis, Sichmeller, Christopher, and Peng, Xiaogang. Ligand Bonding and Dynamics on Colloidal Nanocrystals at Room Temperature: The Case of Alkylamines on CdSe Nanocrystals. *Journal of the American Chemical Society*, 130(17):5726–5735 (2008).
- [82] Santillán, Moisés. *Chemical kinetics, stochastic processes, and irreversible thermodynamics*. Springer, 2014. (2014).
- [83] Munro, Andrea M. and Ginger, David S. Photoluminescence Quenching of Single CdSe Nanocrystals by Ligand Adsorption. *Nano Letters*, 8(8):2585–2590 (2008).
- [84] Boutelle, Robert C. and Northrop, Brian H. Substituent Effects on the Reversibility of Furan–Maleimide Cycloadditions. *The Journal of Organic Chemistry*, 76(19):7994–8002 (2011).
- [85] Rulíšek, Lubomír, Šebek, Pavel, Havlas, Zdeněk, Hrabal, Richard, Čapek, Pavel, and Svatoš, Aleš. An Experimental and Theoretical Study of Stereoselectivity of Furan–Maleic Anhydride and Furan–Maleimide Diels–Alder Reactions. *The Journal of Organic Chemistry*, 70(16):6295–6302 (2005).
- [86] Subramani, Chandramouleeswaran, Cengiz, Nergiz, Saha, Krishnendu, Gevrek, Tugce Nihal, Yu, Xi, Jeong, Youngdo, Bajaj, Avinash, Sanyal, Amitav, and Rotello, Vincent M. Direct Fabrication of Functional and Biofunctional Nanostructures Through Reactive Imprinting. *Advanced Materials*, 23(28):3165–3169 (2011).
- [87] Tolstyka, Zachary P., Kopping, Jordan T., and Maynard, Heather D. Straightforward Synthesis of Cysteine-Reactive Telechelic Polystyrene. *Macromolecules*, 41(3):599–606 (2008).
- [88] Dispinar, Tugba, Sanyal, Rana, and Sanyal, Amitav. A Diels–Alder/retro Diels–Alder strategy to synthesize polymers bearing maleimide side chains. *Journal of Polymer Science Part A: Polymer Chemistry*, 45(20):4545–4551 (2007).

- [89] Onbulak, Sebla, Tempelaar, Sarah, Pounder, Ryan J., Gok, Ozgul, Sanyal, Rana, Dove, Andrew P., and Sanyal, Amitav. Synthesis and Functionalization of Thiol-Reactive Biodegradable Polymers. *Macromolecules*, 45(3):1715–1722 (2012).
- [90] Yilmaz, Idil Ipek, Arslan, Mehmet, and Sanyal, Amitav. Design and Synthesis of Novel “Orthogonally”Functionalizable Maleimide-Based Styrenic Copolymers. *Macromolecular Rapid Communications*, 33(9):856–862 (2012).
- [91] Kosif, Irem, Park, Eun-Ju, Sanyal, Rana, and Sanyal, Amitav. Fabrication of Maleimide Containing Thiol Reactive Hydrogels via Diels–Alder/Retro-Diels–Alder Strategy. *Macromolecules*, 43(9):4140–4148 (2010).
- [92] Bailey, Ghislaine C. and Swager, Timothy M. Masked Michael Acceptors in Poly(phenyleneethynylene)s for Facile Conjugation. *Macromolecules*, 39(8):2815–2818 (2006).
- [93] Da Pieve, Chiara, Williams, Paul, Haddleton, David M., Palmer, Richard M. J., and Missailidis, Sotiris. Modification of Thiol Functionalized Aptamers by Conjugation of Synthetic Polymers. *Bioconjugate Chemistry*, 21(1):169–174 (2010).
- [94] Mantovani, Giuseppe, Lecolley, François, Tao, Lei, Haddleton, David M., Clerx, Joost, Cornelissen, Jeroen J. L. M., and Velonia, Kelly. Design and Synthesis of N-Maleimido-Functionalized Hydrophilic Polymers via Copper-Mediated Living Radical Polymerization: A Suitable Alternative to PEGylation Chemistry. *Journal of the American Chemical Society*, 127(9):2966–2973 (2005).
- [95] Geng, Jin, Mantovani, Giuseppe, Tao, Lei, Nicolas, Julien, Chen, Gaojian, Wallis, Russell, Mitchell, Daniel A., Johnson, Benjamin R. G., Evans, Stephen D., and Haddleton, David M. Site-Directed Conjugation of “Clicked”Glycopolymers To Form Glycoprotein Mimics: Binding to Mammalian Lectin and Induction of Immunological Function. *Journal of the American Chemical Society*, 129(49):15156–15163 (2007).
- [96] Thomas, Carla S., Glassman, Matthew J., and Olsen, Bradley D. Solid-State Nanostructured Materials from Self-Assembly of a Globular Protein–Polymer Diblock Copolymer. *ACS Nano*, 5(7):5697–5707 (2011).
- [97] Smyth, DG, Blumenfeld, OO, and Konigsberg, W. Reactions of N-ethylmaleimide with peptides and amino acids. *Biochemical Journal*, 91(3):589–595 (1964).
- [98] Sano, Takeshi, Smith, Cassandra L., and Cantor, Charles R. A Streptavidin Mutant Containing a Cysteine Stretch That Facilitates Production of a Variety of Specific Streptavidin Conjugates. *Nat Biotech*, 11(2):201–206 (1993).
- [99] Shen, Ben-Quan, Xu, Keyang, Liu, Luna, Raab, Helga, Bhakta, Sunil, Kenrick, Margaret, Parsons-Reponete, Kathryn L, Tien, Janet, Yu, Shang-Fan, Mai,

- Elaine, Li, Dongwei, Tibbitts, Jay, Baudys, Jakub, Saad, Ola M, Scales, Suzie J, McDonald, Paul J, Hass, Philip E, Eigenbrot, Charles, Nguyen, Trung, Solis, Willy A, Fuji, Reina N, Flagella, Kelly M, Patel, Darshana, Spencer, Susan D, Khawli, Leslie A, Ebens, Allen, Wong, Wai Lee, Vandlen, Richard, Kaur, Surinder, Sliwkowski, Mark X, Scheller, Richard H, Polakis, Paul, and Junutula, Jagath R. Conjugation site modulates the in vivo stability and therapeutic activity of antibody-drug conjugates. *Nat Biotech*, 30(2):184–189 (2012).
- [100] Junutula, Jagath R, Flagella, Kelly M, Graham, Richard A, Parsons, Kathryn L, Ha, Edward, Raab, Helga, Bhakta, Sunil, Nguyen, Trung, Dugger, Debra L, Li, Guangmin, Mai, Elaine, Lewis Phillips, Gail D, Hilaragi, Hajime, Fuji, Reina N, Tibbitts, Jay, Vandlen, Richard, Spencer, Susan D, Scheller, Richard H, Polakis, Paul, and Sliwkowski, Mark X. Engineered thio-trastuzumab-DM1 conjugate with an improved therapeutic index to target human epidermal growth factor receptor 2-positive breast cancer. *Clinical Cancer Research*, 16(19):4769–4778 (2010).
- [101] Junutula, Jagath R, Raab, Helga, Clark, Suzanna, Bhakta, Sunil, Leipold, Douglas D, Weir, Sylvia, Chen, Yvonne, Simpson, Michelle, Tsai, Siao Ping, Dennis, Mark S, Lu, Yanmei, Meng, Y Gloria, Ng, Carl, Yang, Jihong, Lee, Chien C, Duenas, Eileen, Gorrell, Jeffrey, Katta, Viswanatham, Kim, Amy, McDorman, Kevin, Flagella, Kelly, Venook, Rayna, Ross, Sarajane, Spencer, Susan D, Lee Wong, Wai, Lowman, Henry B, Vandlen, Richard, Sliwkowski, Mark X, Scheller, Richard H, Polakis, Paul, and Mallet, William. Site-specific conjugation of a cytotoxic drug to an antibody improves the therapeutic index. *Nat Biotech*, 26(8):925–932 (2008).
- [102] Berson, Jerome A. and Swidler, Ronald. cis-Addition in the Bromination of Bicyclic Olefins. The Structure and Stereochemistry of the Dibromides of exo-cis-3,6-Endoxo- Δ^4 -tetrahydrophthalic Anhydride and endo-cis-3,6-Endomethylene- Δ^4 -tetrahydrophthalic Anhydride1. *Journal of the American Chemical Society*, 76(16):4060–4069 (1954).